**Bruno Galelli Chieregatti**

# Optimization based on the Adjoint Method for Adsorbed Natural Gas Storage Systems

Thesis presented to the Polytechnic School of the University of São Paulo to obtain the title of Doctor of Sciences

São Paulo
2020

**Bruno Galelli Chieregatti**

# Optimization based on the Adjoint Method for Adsorbed Natural Gas Storage Systems

Versão Corrigida

Thesis presented to the Polytechnic School of the University of São Paulo to obtain the title of Doctor of Sciences

Concentration area:
Mechanical Engineering

Supervisor:
Prof. Dr. Ernani Vitillo Volpe

São Paulo
2020

Este exemplar foi revisado e corrigido em relação à versão original, sob responsabilidade única do autor e com a anuência de seu orientador.

São Paulo, _____ de _____ de _____

Assinatura do autor: _____

Assinatura do orientador: _____

Catalogação-na-publicação

Chieregatti, Bruno Galelli
Optimization based on the Adjoint Method for Adsorbed Natural Gas Storage Systems / B. G. Chieregatti -- versão corr. -- São Paulo, 2020.
164 p.

Tese (Doutorado) - Escola Politécnica da Universidade de São Paulo. Departamento de Engenharia Mecânica.

1.GÁS NATURAL (SISTEMAS DE ARMAZENAGEM) 2.DINÂMICA DOS FLUÍDOS COMPUTACIONAL 3.GESTÃO POR PROCESSOS (OTIMIZAÇÃO ) 4.MÉTODO ADJUNTO I.Universidade de São Paulo. Escola Politécnica. Departamento de Engenharia Mecânica II.t.

May the force be with you - Star Wars

# Acknowledgments[1]

Esta tese de doutorado é fruto de uma vida dedicada ao estudo. Desde os 4 anos e meio, quando entrei no ensino infantil, minha mente sempre foi ligada a curiosidade de se aprender algo. Chegando ao ensino fundamental, já era o aluno mais aplicado, o famoso 'CDF'. No ensino médio, a confiança era tanta que acabei negligenciando um pouco o estudo e não passei no vestibular, o que foi um grande golpe. Mas como sempre falou Sylvester Stallone na franquia *Rocky*: "Não importa o quanto você bata, mas sim o quanto consegue apanhar e seguir em frente", segui a vida, tracei um plano e fiz cursinho estudando 48 horas semanais de segunda a sábado!

De volta ao caminho planejado, chego a Poli-USP em 2004, totalmente vislumbrado, querendo aproveitar tudo o que é oferecido. O resultado disso foi um 4.5 na prova de Cálculo I, outra porrada no orgulho! Percebi que precisava alinhar a vontade de querer aprender com o caminho formal do curso. Ao longo da graduação, peguei 'o jeito' e mesmo com algumas notas vermelhas pelo caminho, tive uma boa graduação sem nenhuma dependência. Além disso, participei do Aerodesign, competição onde as equipes de estudantes tinham que desenvolver um projeto aeronáutico completo. Uma experiência que lembro com grande nostalgia até hoje, pois além da parte técnica, aprendi valores importantes de confiança, organização, trabalho em equipe e defesa de pontos de vista em arguições. Agradeço de coração a todos os amigos que fiz na graduação, os quais mantenho contato com a grande maioria até hoje: André Marguti, Suyami Maruyama, Diego Carreras, Felipe Langellotti, Adriano Axel Pliopas, Newton Fukumasu, Enrico Aleixo, Paulo Abraham, Sinjin Yano, Gabriel do Prado, Eduardo Simões, Fábio Castelli, André de Oliveira, Guilherme Peresi e o Prof. Antônio Luiz de Campos Mariani.

Ainda na graduação, iniciei minha vida acadêmica e não tem como destacar o grande apoio de meu orientador, Prof. Ernani Volpe. Sempre propondo temas desafiadores desde a iniciação científica até este doutorado. Foram inúmeros artigos escritos e espero que continuemos assim, agora ambos como doutores. Agradeço também o apoio do professor Marcelo Tanaka Hayashi, a quem pude auxiliar, através do meu trabalho de formatura, a finalizar o seu mestrado.

[1]Writen in my language, Portuguese

Depois isso, veio uma vontade de conhecer o mundo além academia e ir para o mercado de trabalho. Foram 6 anos trabalhados em projetos de engenharia, que me trouxeram incrível experiência no gerenciamento de prazos, definição de soluções, cobrança de clientes, montagem de relatórios técnicos, comportamento em reuniões, etc. Aqueles que focam apenas na vida acadêmica, aconselho ao menos ir ao mercado de trabalho por alguns anos, pois garanto que fará toda a diferença na sua vida, principalmente quando você conhece engenheiros com muita experiência. Tive a sorte ao conhecer dois deles: José Luiz Prado e Hildebrando Vasconcellos. Agradeço de coração os conselhos e as frases icônicas.

Agora, neste final de doutorado, uma nova fase se iniciou na minha carreira, como docente no Instituto Mauá de Tecnologia e assim cumpri meu sonho de poder abraçar a academia de vez! Espero ler estes agradecimentos daqui a alguns anos e refletir que foi aqui que começou tudo. E para chegar aqui, não tem como dedicar um agradecimento especial a meu grande amigo, Prof. João Brasil, companheiro de laboratório, de videoaulas para concursos públicos e agora colega de profissão! Desejo que a gente mantenha essa amizade para sempre e fique falando dos títulos do nosso Palmeiras!

Mas obviamente, um homem que se preze precisa ter sucesso tanto no pessoal como no profissional (já diria Fausto Silva). Aqui, dedico este parágrafo aos meus pais, Alcidio e Maria Alice, além da minha irmã Bianca que sempre acreditaram no meu potencial e me apoiaram em todos os momentos. Os sacrificios que fizeram por mim jamais serão esquecidos!

Também não posso esquecer dos meus primos irmãos, Luis Fernando Marcopito e João Marcopito que foram sempre uma referência em estilo de vida e me fizeram conhecer muitas pessoas além do mundo acadêmico.

E uma dessas pessoas que conheci simplesmente transformou a minha vida por completo. Ela conseguiu me tornar um homem melhor e que por consequência me fez tornar um ótimo marido e também recentemente um excelente pai. Minha esposa, Talita Chieregatti, às vezes não encontro palavras para descrever o turbilhão de coisas novas que aprendo com você. Se não estivesse comigo, certamente eu seria um rato de laboratório e não teria aproveitado quase nada da vida. E agora temos muito mais a curtir com nossos tesouros: Lucas e Sofia.

Com essas pessoas especiais, vieram outras tantas, que se enumerar uma por uma, esses agradecimentos ficarão maiores que a própria tese! Assim, encerro por aqui, com meu sincero muito obrigado a todos que me ajudaram a completar esta etapa da minha vida!

# Abstract

This PhD thesis aims to develop and investigate the application of the so-called Adjoint Method in flows through porous media. Its main focus is on the Adsorbed Natural Gas (ANG) Storage Systems, a growing concept in Natural Gas equipments, but the formulation developed is applied in all porous media flows, considering (or not) the Adsorption Phenomena. The primary objective is to optimize their filling process performance which consists an adsorption process. To that end, it shall consider controlling not only geometry parameters, as the tank dimensions, but also the non geometric parameters, such as filling flow curves, temperature fields and heat transfer coefficients. These kinds of control devices and strategies have their niche in small and specially in large scale systems that can be found in power and industrial plants. Owing to their strong dependence on both the system geometry and on the thermodynamics of the adsorption processes, this class of applications could greatly benefit from parametric and form optimization techniques. That is precisely the rationale behind the choice of the Adjoint Method, which can in principle serve both purposes. In that regard, it should be added that, although the physics of the adsorption processes is well documented in the literature, there seems to be very few references that consider their optimization, and none that make use of the Adjoint Method. Under such circumstances, this thesis developed a strong mathematical formulation, starting from the basic equations of fluid mechanics, where applying the suitable hypothesis, the physics flow were been modeled and validated. The Adjoint Equations received the same treatment, starting from the Lagrange Multipliers until the study of the Adjoint Contour Problem. The results, not only produces values of the sensitivity gradients of some objective functions but also present a dramatically reduction of computational cost, in compassion between a classic method, called Central Finite Difference. A study of an optimization of a filling flow curve is done in the end of the work, showing the possibity of the use this tool in engineering problems.

**Key words:** Optimization, Adjoint Method, CFD, Adsorbed Natural Gas.

# Contents

# List of Figures

# List of Tables

# 1 Introduction

Worldwide, the energy market is going through a phase of intense research and development efforts. In several countries, the energy matrices are undergoing progressive changes, so as to adapt to more stringent environmental laws and to the global economy instabilities. In this scenario, the Natural Gas appears as a source of energy of growing relevance, owing to both its direct uses and to the possibilities it offers regarding the process of gas reform, for hydrogen production and carbon capture. The growth of its share of the energy market prompts the need to optimize the chain of production, processing and storage of Natural Gas. The search for optimal solutions should allow significant savings in the implementation and operational costs of the Natural Gas industry.

Amongst the most relevant approaches to optimization, the Adjoint Method stands out as it allows an exceptional reduction in the computational costs of design sensitivity derivatives. It makes for a more efficient analysis of design alternatives, without compromising the results accuracy. The method is also attractive for its high fidelity to the flow physics, and for the great diversity of its applications. This project aims to use the Adjoint Method to optimize Natural Gas Adsorption systems for storage. The study focuses on gas flow through porous media that adequately represent those systems. Moreover, it is not limited to the search for optimal geometries for the adsorption beds in reservoirs. As it shall also consider the optimization of the filling and emptying operations of such reservoirs.

## 1.1 Scope and Objectives of the Project

In the last years, extensive studies have been carry out about ANG systems and it has been abundantly reported in the literature (SAHOO; JOHN, 2010; MOTA; SAATDJIAN, 1995; HIRATA; COUTO, 2009; RAHMAN, 2011). There are a consensus that the performance of those systems fundamentally depends upon the thermal and fluid dynamic processes that take place during adsorption and desorption process. Besides, the geometry also contributes significantly to the efficiency of

the storage devices as well as the thermal properties of the adsorbent bed.

Under such circumstances, it seems substantially advantageous to investigate optimum solutions to those systems. In particular, on making use of a method that combines shape and parametric optimization capabilities, one could potentially tackle the full breadth of the problem. In that regard, it is instructive to note that temperature control is paramount to the efficiency of the adsorption process. One means of achieving it is by appropriately managing heat transfer, while the reservoir is filled. The heat transfer, in turn, could be enhanced and controlled by changing geometry and environmental parameters of the installations. As it turns out, geometric features such as internal heat–fins or heat exchangers, and the conditions under which they operate are all interconnected. Whence comes the need for an optimization method that offers a broad spectrum of possibilities.

The Adjoint Method has proven to be a powerful tool for optimizing complex systems, where a high fidelity representation of the physics is essential. It has shown to be particularly suitable to tackle problems with large numbers of control parameters, and several possibilities of optimum criteria. For it only requires two converged solutions to compute sensitivity gradients, regardless of their dimensionality and for any particular measure of merit. Owing to those characteristics, the Adjoint Method has been the subject of intense research activity. It has spawned a wide variety of applications, ranging from nuclear reactor thermo–hydraulics (CACUCI et al., 1980) to aerodynamics (JAMESON; PIERCE; MARTINELLI, 1997) and the design of ship hulls (JAMESON; MARTINELLI, 2007).

In the literature, virtually all of the works on the Adjoint Method involve Euler and Navier–Stokes equations, for compressible and incompressible flows alike. Most of them concern shape optimization. However, in our previous research into the subject, we have developed a novel approach to the Adjoint boundary problem (HAYASHI; CEZE; VOLPE, 2013; VOLPE, 2013), which enables one to compute sensitivity gradients with respect to a broader range of parameters (LIMA et al., 2015; HAYASHI et al., 2016). That approach allows one to compute those derivatives with respect to inflow boundary conditions. It does so within the same framework that is used for shape optimization. So far, it has been successfully adopted for Euler compressible and Navier–Stokes incompressible flows, where it does get geometric and non–geometric sensitivity derivatives from a single solution to the same set of Adjoint Equations (HAYASHI, 2016; LIMA, 2017)

.

These ideas seem to be in line with what is required in a search for optimized ANG systems. In principle, our approach offers the prospect of tackling the thermodynamics of the filling and emptying processes, along with the geometry of the devices involved in it. Besides, the phenomena of adsorption and desorption entail many optimization criteria. There are several measures of merit that could be considered, such as the ratio between the mass of the stored gas and the volume of the storage unit; the rate at which gas leaves that system in the emptying process, and so on.

These kind of applications find relevance and purpose in the niche of large ANG storage units. Those that are used to transport Natural Gas between offshore resevoirs and consumption hubs, and which can also be found in industrial and power plants. Many of them will involve large reservoirs with porous matrices. For them, devices such as internal heat fins and heat exchangers may provide a reliable means of ensuring optimum operation conditions.

Nonetheless, there are significant challenges that must be surmounted. First, differently of the ANG sytems, the literature virtually seems to lack any references to applications of the Adjoint Method to flow in porous media. It clearly implies that the whole set of Adjoint equations and corresponding boundary conditions must be derived from zero. Although the mathematical model for that class of flows is similar to the well–known Navier–Stokes equations, it must include the energy equation and a series of closure terms. Where the latter concern the interactions between gas and porous matrix (WHITAKER, 1997; WHITAKER, 1996; WHITAKER, 1992; WHITAKER, 1967). Moreover, these flows involve compressibility effects that are mostly related to temperature gradients— quite different from those that arise from pressure gradients, which are amply discussed in prevailing applications of the method. Put together, these circumstances make for a considerable research effort and part of the results will be presented in the chapters 3 and 5.

Another important challenge follows as a direct consequence of the first, and it is the need for developing an Adjoint solver that corresponds to the problem in hand, namely the flow in porous media. While there are software packages that can solve for the flow physics, there appears to be none that could be adapted to what the corresponding Adjoint problem is expected to require. As a means of circumventing that difficult, we have turned our attention to some open source codes that are currently available. Such is the case with the so called *FREEFEM* (HECHT, 2012). It allows one to write down the partial differential equations (PDEs) that govern a given problem, and then solve it by using finite element

methods.

On making use of this particular tool, we have succeeded in building our own flow solver. Now, on the basis of the similarity the flow (*i.e. Primal*) and Adjoint (*i.e. Dual*) problems always exhibit (VOLPE, 2013), it is reasonable to expect that the corresponding Adjoint solver should be feasible.

Therefore, the main objective of this work is the development of an algorithm that we call "Adjoint Optimization loop". This software that will be delivered at the end of this project should be used by companies that design and manufacture gas storage systems, as well as by those that operate them. These companies will be capable of improving their operation conditions, regarding the gas storage process and to design better adsorption systems such as reservoirs and adsorption beds. A basic structure of the loop is presented in figure 1.1.

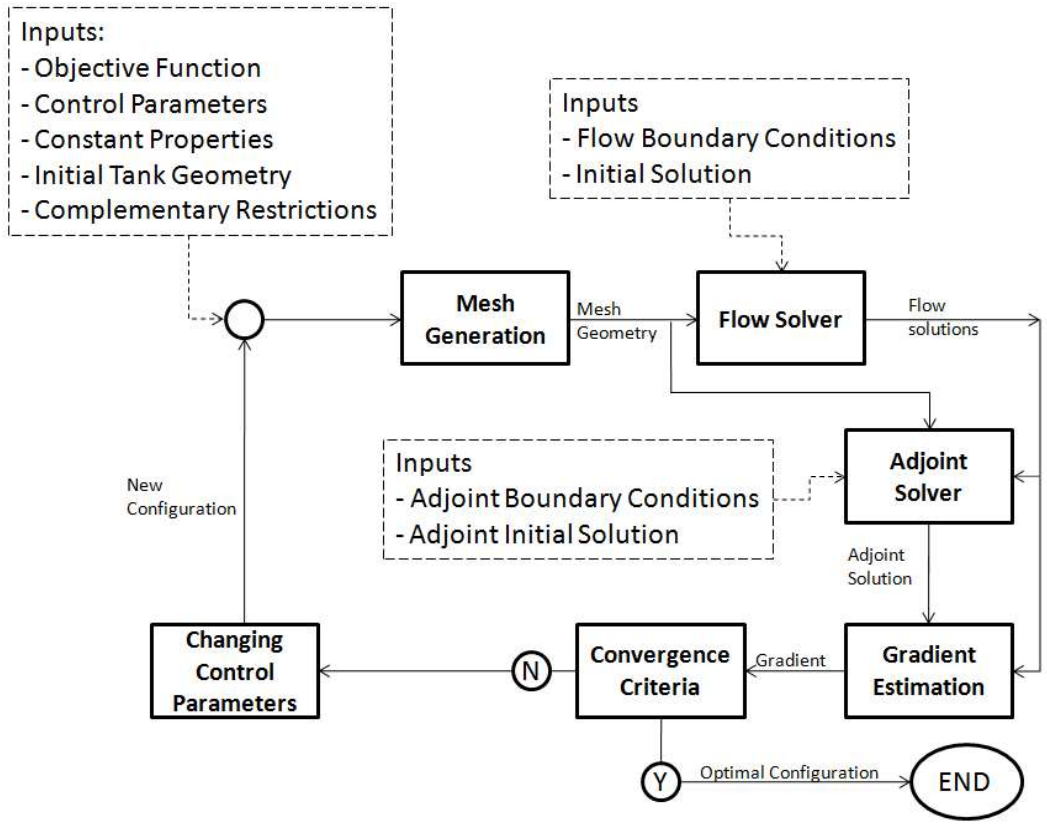


**Figure 1.1:** Schematic diagram of the optimization loop. The flow and adjoint solver are nested in the loop, along with a grid generator, gradient evaluation and search codes, and a parameterized geometry generator.

All the routines will be develop on *FreeFem++* platform (HECHT, 2012). The mesh generator and flow solver are done and will be presented in the next chapters. The pos-processing was developed on *MATLAB* software, due the user friendly platform to generate graphs.

On having defined the scope, objectives and the main aspects of its method-

ology, this thesis now turns its focus to the specific topics it entails. Chapter 2 presents a literature survey on the physics of flow through porous media. It is followed by another that discusses the mathematical model that represents the physics with details of the flow governing equations.

The numerical discretization and the validation results are presented in the chapter 4 followed by exploratory simulations that define some engineering applications. Moreover, it is also presented a scale analysis that corroborates the idea of the ANG use in large scale reservoirs.

The formulation of the Adjoint Method will be presented in the chapter 5 with the Adjoint boundary conditions. The following chapter (6) presents the results of the dual problem validatio, with examples of measure of merit and gradient estimations.

As the subsidies created, the chapter 7 integrates the Primal e Dual problem in an optimization algorithm, presenting tests and some applications to the industry. Then, the concluding remarks fininsh this thesis and presents the suggestions of the research continuity.

# 2 Problem Description

## 2.1 Natural Gas

It is well-known that Natural Gas (NG) is released in the process of decomposition of organic material. It is considered a fossil fuel and can be found in underground reservoirs. These hydrocarbon resources can be exploited economically from offshore and onshore basins.

Because of the different sources, the composition of NG varies significantly. It is considered a hydrocarbons mixture, where the main substance is methane ($CH_4$). The NG is considered pure when its composition is 100% $CH_4$ and it is one of the assumptions that this work used in numerical simulations. Other substances can be ethane ($C_2H_6$), propane ($C_3H_8$) and heavier constitutes, such as Isobutane, Heptane and non-hydrocarbons such as Nytrogen, Carbon Dyoxide and others. The table 2.1 shows an average composition of the NG:

**Table 2.1:** NG average composition (MONTEIRO; SILVA, 2010)

| **Substance** | **Volume, in (%)** |
|---|---|
| Methane | 89.0 |
| Propane | 1.8 |
| Butane, Pentane, Hexane e heaviers | 1.0 |
| Carbon Dyoxide | 1.5 |
| Nytrogen | 0.7 |

## 2.2 The NG Market

In 21st century, the NG is considered one of the most important energy sources in the world. According to most recently published data (CIA, 2016), the reserves are estimated at almost 180 trilions of cubic meters under standard conditions. Figure 2.1 shows the reserves distribution by continents:

The reserves do not have an homogeneous distribution worldwide, and the

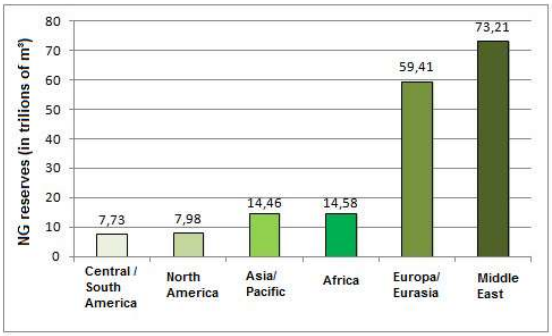


**Figure 2.1:** NG reserves distribution, (MONTEIRO; SILVA, 2010)

consumption shows the same behavior. The demand sustains an important bilionary market around the world and the basic structure of this market involves several stages, presented in the figure 2.2:

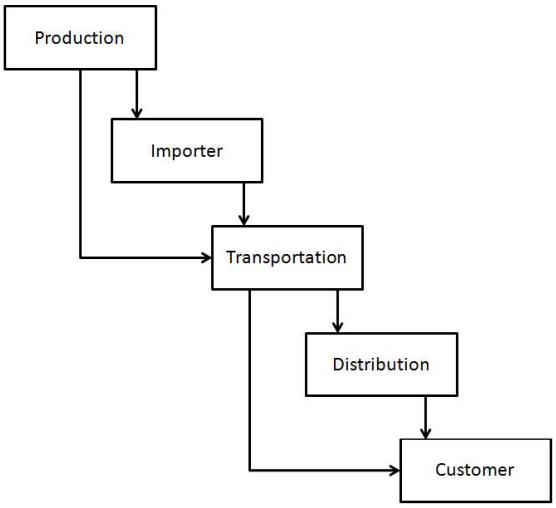


**Figure 2.2:** NG market basic structure

- Production: It consists of companies and technologies that extract and treat NG from the deposits.
- Importer: Intermediates are sometimes necessary to make business between different countries, becoming an important stakeholder in this process.
- Transportation: After the contracts are signed, the transportation companies are responsible for delivering NG to distributors or to customers, directly. There are two kinds of transportation: The Physical Gas lines and the so-called Virtual Gas lines.

  The physical lines are pipelines which link the production and distribution/customer. The figure 2.3 present one example of physical tubulations that operate in Brazil.

  On the other hand, the Virtual Gas lines transport NG without pipelines. But by using trucks and other vehicles, instead, to transport NG in storage

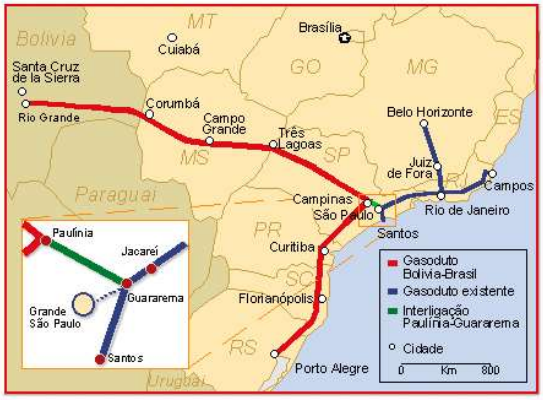


**Figure 2.3:** The "*GasBol*" tubulation between Brazil and Bolivia, adapted from (TBG, 2016)

tanks between production and customers. Figure 2.4 shows an example of small compressed NG storage tanks.

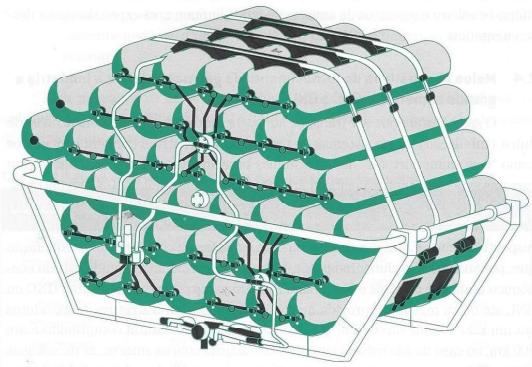

**Figure 2.4:** CNG Storage Tanks, (MONTEIRO; SILVA, 2010)

- Distribution: These companies are responsible for receiving NG from transporters and for delivering it to the customers. It is usual for cities to have distribution companies that send NG to houses and facilities through local pipelines.

- Customer: End-users people or businesses that purchase NG to supply their needs.

This research and other projects related to Natural Gas are been developed in the Research Centre for Gas Innovation (*RCGI*) that investigate all stages of the NG market. In particular, this project is located in the transportation area.

## 2.3 Transportation Technogies

Nowadays, the Transportation companies have two most common technologies to deliver NG without pipelines:

- Compressed Natural Gas (CNG): The simplest way to store NG. It consists of a tank (cylinder or sphere) that receives NG through a compressor. The pressures range from as low as 10 bar up to very high values (200 bar). Figure 2.4 presents a few cylinders that use CNG technology. The biggest advantages are relative simplicity of the compression process, and the possibitity of manufacturing small cylinders to use in vehicles. The two main disavantages are related to the costs: It requires a compressor, which consumes more energy as the nominal pressure increases and the tanks grow heavier with increasing nominal pressure, for structural reliability.

- Liquified Natural GAS (LNG): This technology is more complex than CNG, because it involves cryogenics procedure. The Methane boiling point is close to 112K at atmosphere pressure and LNG involves liquefying NG to increase its specific volume while keeping the pressure lower than CNG technology. The main advantage is the huge storage capacity, but the costs to refrigerate the gas and the thermal insulation demands make the technology viable only for large scale facilities.

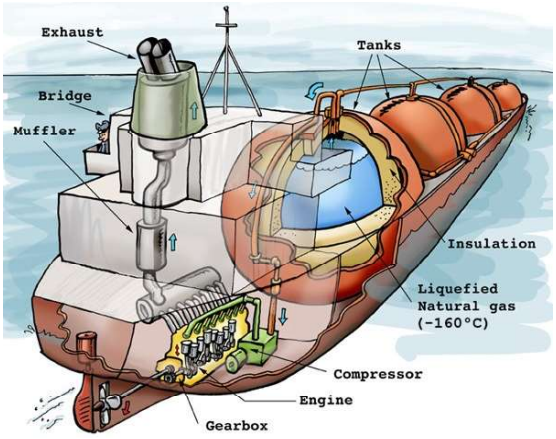


**Figure 2.5:** An example of a LNG carrier, (WIKIPEDIA, 2016)

The LNG technology is particulary relevant for intercontinental transport and commerce of Natural Gas. However the losses of gas due boil-off during transport may be significant for long trips. According the sponsors of the *RCGI*, the losses involving boil-off archieve close to 0.1% per trip day. In other words, a fifty-day trip from middle east to North America causes loss of 5.0% of the total gas transported.

There are other techniques such as Cooled Compressed Natural Gas, but all of them is variations or compositions of CNG and LNG processes.

## 2.4 The ANG technology

In the present scenario, the Adsorbed Natural Gas technology (ANG) has become an attractive alternative for storage systems. To a reasonable extent, the method provides a means of storing gas at substantially higher concentration than can be achieved with CNG at the same pressure. Although it does not attain the density that is typically found with LNG, it is potentially much simpler, since it does not require the energy-demanding of liquefaction process (JUDD; GLADDDING, 1998). The following figure presents a simple compassion between the gas density inside the CNG and ANG tanks for different pressures:

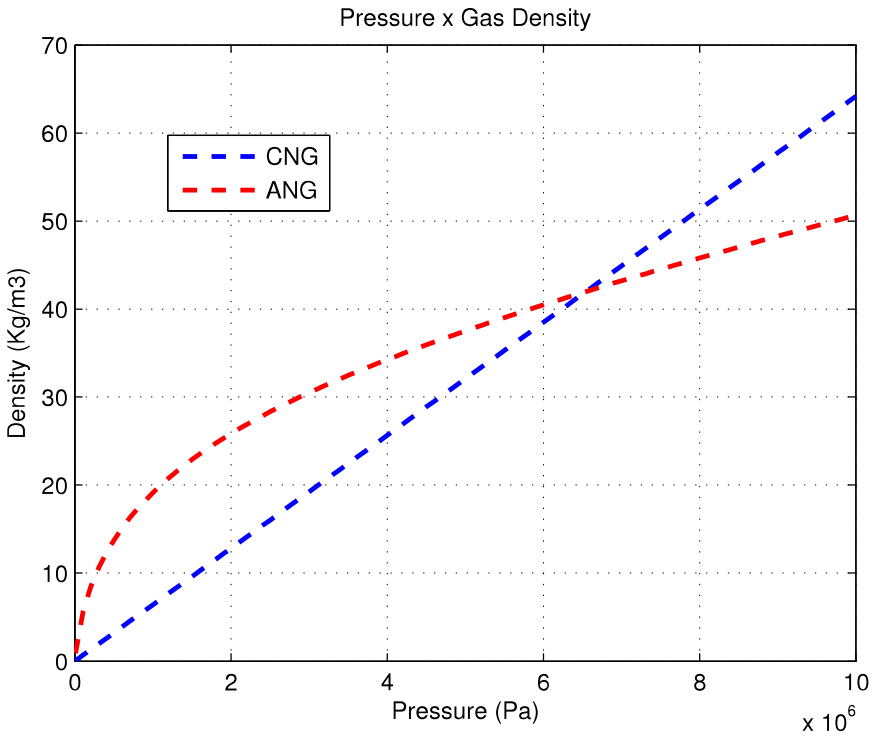


**Figure 2.6:** Density comparasion between CNG and ANG systems at 300K

Observing the fig. 2.6, it is clear that for a certain range of pressures, the ANG systems could store more gas than CNG at the same pressure, considering the isothermal process. In this example, using a standard adsorbent (activated carbon), the differences achieve 44% at $3.5MPa$ and exceed 100% at low pressures, close to 1.5 Mpa. However, above to 6.5 MPa, the density in CNG system overtakes that ANG with the adsorbent used in this example. The values presented in the figure 2.6 change with other adsorbents.

Qualitatively, the table 2.2 presents common pressure, temperature and V/V, defined as volume of gas stored (in STP conditions) divided by physical tank volume, for the types of transportation technologies:

**Table 2.2:** Comparison between transport technologies (HIRATA; COUTO, 2009)

| Storage Methodology | Pressure (bar) | Temperature (℃) | V/V |
|---|---|---|---|
| CNG | 200 | Ambient (-15 ℃- 40 ℃) | 200 |
| LNG | Atmosferic | -163 ℃ | 600 |
| ANG | 35 - 50 | Ambient (-15 ℃- 40 ℃) | 150 - 180 |

The V/V parameter is one of most important metrics to qualify the ANG Storage tanks. To show its importance, the U.S. Department of Energy sets a target of 180 V/V at 35 bar in ambient temperature, as a point where ANG becomes a viable alternative. To achieve this target, some adsorbents have been developed with good adsorption capacity and high packing density for the ANG storage application (RAHMAN, 2011).

However, not only the adsorbent are being improved, but also the configurations of ANG systems need improvements to archieve the whole capacity of this material. It is important to point out that the development of new adsorbent materials are not the scope of this research. All the numerical simulations use available materials and the focus is the optimization of the storage process.

Having made the scope clear to the reader, we turn our attention to the literature survey of ANG systems. However, before we begin a detailed description of the ANG technology, it is useful to introduce the adsorption phenomenon.

## 2.4.1 Adsorption

### 2.4.1.1 Introduction

The Adsorption is defined as the adhesion of molecules in an extremely thin layer (as of gases,solutes or liquids) to the surfaces of solid bodies or liquids with which they are in contact. It can be classified either as physical adsorption or chemical adsorption depending on the occurrence of reactions. In this work, we are only interested in the physical adsorption phenomenom, particularly in a gas-solid interaction.

Physical adsorption is caused mainly by the van der Waals force and electrostatic forces between adsorbate (gas) molecules and the atoms which compose the adsorbent (solid) surface (SUZUKI, 1990). A simple scheme of adsorption process is presented in figure 2.7.

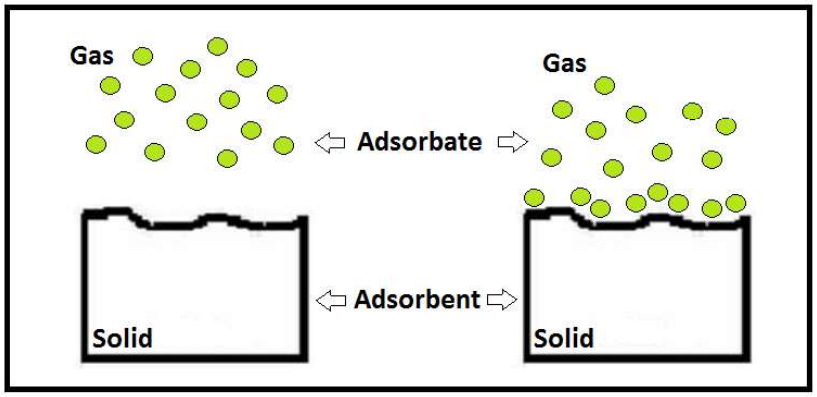


**Figure 2.7:** Representation of the adsorption process of a gas on a solid surface, adapted from (SOLAR C., 2010)

The adsorption is a surface phenomemon and large specific surface area is preferable for providing large adsorption capacity. But the creation of a large internal surface area in a limited volume inevitably gives rise to large numbers of small sized pores between adsorption surfaces. A solid may exhibit different kinds of pores and the figure 2.8 shows some possibilities.

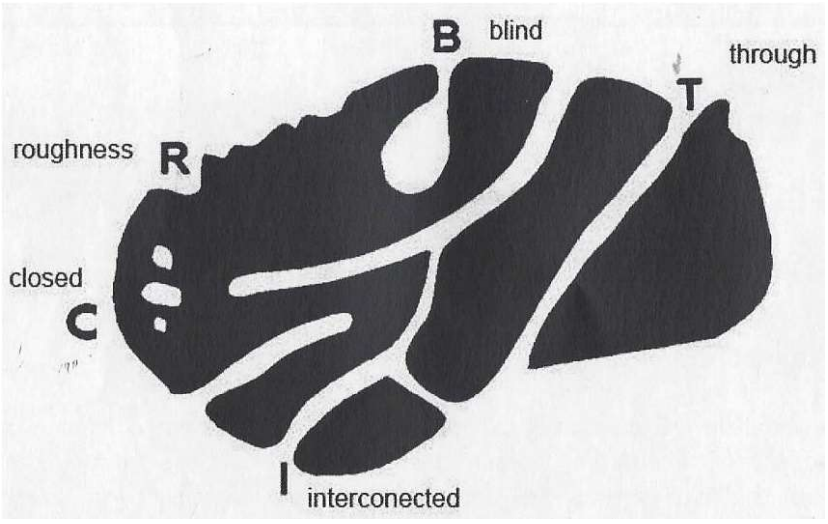


**Figure 2.8:** Types of pores that a solid may exhibit (ROQUEROL F.; J., 1994)

#### 2.4.1.2 Porosity

From the previous considerations, we can define one of most important parameters to modeling adsorption: The Porosity.

Porosity is usually defined as the ratio of the volume of pores and voids to the volume occupied by the solid. However, it should be kept in mind that the recorded value of porosity is not always a simple characteristic property of the material, since it is likely to depend also on the methods used to assess both the pore volume and the volume of the solid. The pore volume is usually regarded

as the volume of open pores, but it may include the volume of closed pores (ROQUEROL F.; J., 1994).

Moreover, the recorded value may depend on the nature of the probe molecule or the experimental conditions. It is not always easy to distinguish between roughness and porosity or between pores and voids. In principle, a convenient and simple convention is to refer to a solid as porous only if the surface irregularities are deeper than they are wide. Furthermore, the area of a rough surface is regarded as an external surface area, whereas the area of the pore walls is the internal surface area. We prefer to use the same consideration presented in Roquerol F. e J. (1994) which regards the porosity as an intrinsic property of the material and we use the term void to refer to the space between particles, which depends on the conditions of packing. In this thesis, the porosity is represented by greek letter $\epsilon$.

#### 2.4.1.3 Heat of Adsorption

The Adsorption phenomemon involves an increment in the gas density in the neighborhood of the contact surface. Since the process is spontaneous, the change in Gibbs free energy is negative. Given that the entropy change is also negative for the system, the enthalpy change also negative (JUDD; GLADDDING, 1998). Thus, the process is exothermic. Therefore, we can define another important parameter: The heat of adsorption, represented by $\Delta H$.

#### 2.4.1.4 Density of Adsorption

The molecules of gas start to gather onto the adsorbent surfaces when they are exposed to it. It takes a long period for the gas on the adsorbent to reach the equilibrium state. It occurs because the adsorbent bed and the gas compose a matrix with low thermal conductivity. As the adsorption (or desorption) is an exothermic (or endothermic) process, the temperature arises (or decreases) and takes a long time to dissipate (or absorb) heat (RAHMAN, 2011).

Then, the amount of gas that acumulates in the solid at the equilibrium condition is known as density of adsorption, that will be represented by the letter "q" in this thesis. This density is a function of pressure and temperature ($q = q(P, T)$). Figure 2.9 represents the density of adsorption as a function of P, with different equilibrium isotherms:

This form of graph is very important to understand all the filling/deflation

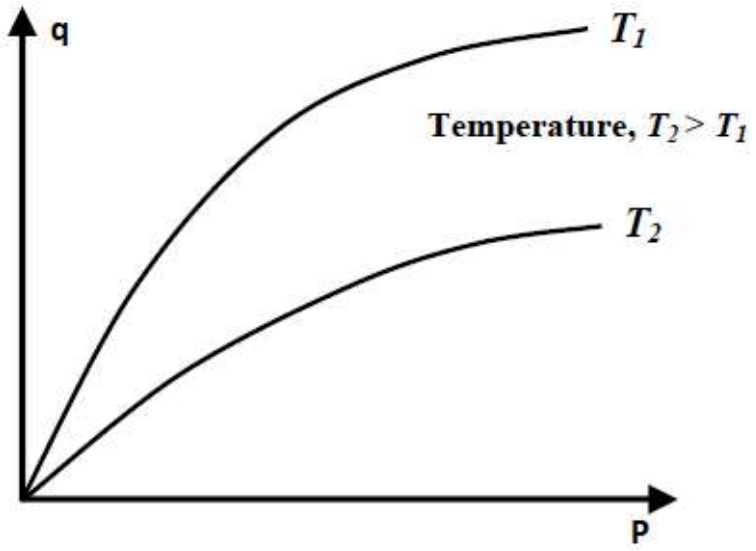


**Figure 2.9:** General representation of adsorption isotherms in P x q graph

process of non isotherm process, because with the measuments of the numerical or experimental tests, the values can be compared with the ideal process (isotherm). Additionally in chapter 3, the equations that relate V/V and $q$ are presented and it is possible to make the same graph using V/V instead of $q$.

### 2.4.2 Adsorbed Natural Gas Storage Systems

The ANG has the potential to substitute the CNG technology for storage systems, at least in certain niches. As it was previously mentioned, the adsorption increases the density of gas close to the adsorbent. Therefore, when a NG storage is filled with a suitable adsorbent material, the energy density will be greater than that of the same vessel without the adsorbent, when filled up to the same pressure.

As an example (JUDD; GLADDDING, 1998), let us consider an ANG tank with nominal pressure of 35 bar. With a good adsorbent, the amount of stored gas is close to that of a half of the amount in a CNG tank under a pressure of 200 bar. So, it is possible to reduce both the compressing costs and the weight of the tank.

#### 2.4.2.1 Technology Challenges

As it is with virtually any developing technology, the ANG imposes challenges and the most important are presented below (JUDD; GLADDDING, 1998):

- Adsorbent development: The most common Adsorbent is Activated Carbon. It has extremely high surface area and pore sizes as low as 2 nanometers. A

typical carbon matrix will be a mixture of small micropores, larger macropores, mesopores from which the gas can scape, and void spaces (JUDD; GLADDDING, 1998). To the first approach, it is the best alternative. Nevertheless, there are several alternatives to increace the storage performance, such as Powdered Activated Carbons ($PAC$), Silica gel, Activated Alumina, natural and synthetic Zeolites and the most recently Carbon Nanotubes.

Again, it is important to point out that we do not intend to develop new adsorbents. Our focus is to optimize device geometries and the management of adsorption heat. The whole work will be done using existing adsorbents, although we shall not be contained to any particular adsorbent material. On the contrary, our approach shall enable one to consider different kinds of available adsorbent materials.

- Deliverability: Not only should we consider the optimization of storage capacity, but there is also the need to study the quantity of gas that will be delivered in the reverse process, the so-called desorption. The storage capacity of an ANG system is always greater than the delivered capacity. The difference is usually around 15% but sometimes it may be as high as 30% (JUDD; GLADDDING, 1998). An adsorbent with large numbers of microporous has very steep initial slopes to their uptakes, and thus it retains a large proportion of the gas on delivery. So, to optimize such storage systems, it is important to consider both the filling and deflation processes.

- Gas Composition: In Section 2.1, we explain that the composition of NG is a mixture of considerable variability. The interest in storage is only for methane, but the other constituents compete for the surface area of the adsorbent. If NG is not pure (100% of $CH_4$), the capacity of storage has a gradual deterioration, because the other gases have different adsorption/desorption conditions.

- Heat Management: As mentioned, the adsorption is an exothermic process and naturally the desorption is endothermic. The density of adsorption is dramatically affected by the temperature and pressure. A good example is presented in Judd e Gladdding (1998), which shows that the filling process of an ANG storage tank can generate enough heat to increase temperatures up to 100°C. A similar analysis can be done on considering the cooling effect of desorption, where the temperatures can drop significantly.

#### 2.4.2.2 Literature Survey

All the technology challenges previously presented are considered by the several studies over the years. The first studies were published in the 80's but only in the 90's, the use of adsorption for storage gained relevance because of its application in the vehicles.

The first relevant works are done by Matranga e Myers (1992), where they performed molecular simulations using Monte Carlo Method to predict the adsorption capacity of Methane in a simple slit-model carbon. The simulations compare the capacity of ANG and CNG with results that show an advantage of the first. For 3.4 MPa in an ANG system, the $V/V$ in the filling process was 209 and the theoretical maximum delivery was 195. However, this model was simple and could only predict the behavior only in isothermal charge and discharge processes.

A two dimensional model was developed by Mota and others which decribes the hydrodynamics, heat transfer and adsorption phenomena (MOTA; SAATDJIAN, 1995). The authors pointed out two important problems in the ANG systems: the first is related to the shape of adsorpion isotherm, which prevents the system from responding linearly to pressure. In other words, the pressure drop required to remove the first 10% of the fuel store is not the same as to remove the last 10%. This problem is related to the description of deliverability in section 2.4.2.1. The second problem is about the heat of adsorption. For methane adsorpion in activated carbons, the values varyring from 10 to $18kJ/mole$. The heat is responsible for increasing the temperature inside the tank during the filling process, thus reducing the storage capacity. In the discharge, the demand of heat reduces the temperature, which compromises the desorption process.

The theoretical model was based on a circular cylinder tank filled by a homogeneous packed-bed of adsorbent particles (MOTA; SAATDJIAN, 1995). An important contribution was the solution to the momentum equation, where they defined a mass flux vector ($\vec{G}$) and expressed the solution as follows:

$$\vec{G} = -\frac{2\rho_g \nabla P}{\alpha + \sqrt{\alpha^2 + 4\beta||\nabla P||}} \tag{2.1}$$

Where the coefficients $\alpha$ and $\beta$ are given by:

$$\alpha = 150\frac{(1-\epsilon_t)^2\mu}{(\epsilon_t^3 d_p^2)} \tag{2.2}$$

$$\beta = 1.75\frac{(1-\epsilon_t)}{(\epsilon_t^3 d_p)} \tag{2.3}$$

and $\epsilon_t$ is the porosity of adsorbent, $\mu$ is the gas viscosity, $d_p$ is the adsorbent particle diameter and $\nabla P$ is the magnitude of the pressure gradient.

This result had been used in the mathematical model of the Primal Problem, and it is presented in chapter 3.

As already mentioned, the article by Judd et al describes the challenges and presents experimental and numerical results. The work by Menon e Komarneni (1998) focuses on experimental tests using different adsorbents such as Zeolites, Coal, Silica Gel and Novel Adsobents and their data has been very useful to set up the numerical simulations in this work.

With the growth of computational power, detailed numerical models were developed. A study of impact of natural gas composition on cycling effect of the ANG storage systems was published by Mota (MOTA, 1999). The simulations performed by the author showed a dramatic reduction in the deliverable capacity on extended cyclic operation, due to heavier hydrocarbons which are present in small amounts in natural gas. The same behavior was found in that (PUPIER; GOETZ; FISCAL, 2005). Figure 2.10 extracted from the reference shows the results.

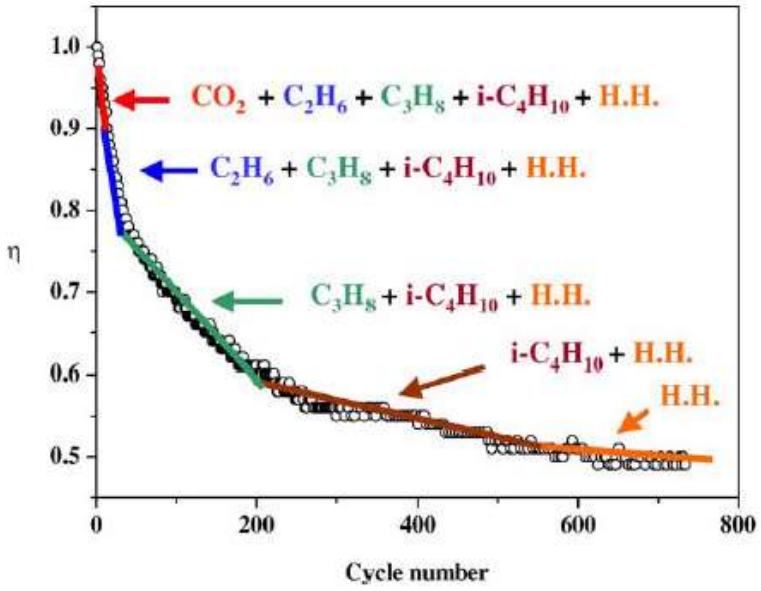


**Figure 2.10:** Experimental profile of the efficiency as a function of the cycle number (H.H. is for heavy hydrocarbons) reproduced from (PUPIER; GOETZ; FISCAL, 2005)

The efficiency of ANG systems, which was defined as the ratio between the volume of gas delivered in the *nth* cycle and the volume delivered in the first cycle, reduces by 50% after 700 cycles. This is the result of the adsorption of other gases in the mixture with methane. Another important result is the behavior of the efficiency curve. The straight lines were drawn to indicate the progressive saturation of the adsorbent. The first line indicates the saturation of the carbon dioxide and the other gases are presented in the sequence (PUPIER; GOETZ; FISCAL, 2005). The main conclusion of the work was that, despite the reduction of the efficiency, the number of cycles corresponding to aproximately to 250,000 km for a vehicle with a fuel tank allowing 400 km range or to 125,000 km for 200 km range. This corresponds to the average life of a commercial car.

The work of Yang e Zheng (2005) focused on the discharge process. They performed numerical and experimental tests with the following conclusions: The central region of the adsorbent bed suffers from the severest temperature fluctuation during discharging the ANG; Application of the supplemental heat should be emphasized in this region for limiting the temperature fluctuation; Drastic changes of the temperature occur in a short period of the initial discharge states, in which the majority of the ANG will be discharged; The time of the occurrence of the lowest temperature is almost in correspondence with the moment of finishing the discharge of the ANG. The authors tested a solution which consisted in a introduction of hot water into the central region of ANG. The result was satisfactory, with the maximum drop of the temperature cut down from $37K$ to $3.2K$ and quicken the discharge process for about 60%.

In the last decade, many works were done using CFD. We can point some references, such as Basumatary e Dutta (2005) which studied the variation of thermal conductivity of adsorbent bed; J.C. e Marcondes (2009) studied a filling process with gas recirculation passed throught a heat exchanger; Nouh e Lau (2010) focused on the influence of carbon dioxide concentration in the ANG system and Himeno e Komatsu (2005a) and Himeno e Komatsu (2005b) whose works provide important parameters for different adsorbents that be used in our numerical simulations.

To finish this literature survey, we point two authors that significantly contribute to ANG development. The work of Rahman (2011), which produces a US patent number (PCT/SG2011/000217), achieved important objetives. They are described below with a brief analysis of how we use the results:

- They have measured the adsorption uptake capacity of methane/adsorbent

using different types of activated carbon, such as powdered, fibrous and granular types; These data are an important input to use in our CFD simulations.

- They have measured the adsorption Kinectics of methane in the activated carbon. This information is required to determine the diffusion rate of gas molecules in adsorbent bed; These data are an important input to use in our CFD simulations.

- They have measured the adsorption isotherms for Methane/Maxsorb III (Adsorbent) at cryogenic temperature ranges are maintained using purpose-built cryostat. These data are important to study the ANG storage system, when low temperature natural gas is considered as the stored gas. This information is useful to our analysis of storage of "boil off gas" in LNG carriers.

- They have perfomed a theoretical analysis of the thermodynamic quantities for adsorption of methane onto activated carbons; Provided informations to validate our theoretical model.

- They have provided a detailed theoretical modeling of the ANG storage system with internal thermal control of the activated carbon bed based on finned type heat exchanger; This is a case to apply the optimization.

- They have conducted experiments of an ANG storage prototype mainly for the charge and discharge processes; This information is used to validate our CFD model

And finally, the work of Sahoo e John (2011) provided a detailed case of CFD validation using experimental tests. The *COMSOL MULTIPHYSICS* was used and produced satisfatory results. In chapters 3 and 4, the reference is thoroughly described.

#### 2.4.2.3 Conclusions about literature survey

The survey of the main researches of Adsorbed Natural Storage Systems provides an important starting point to apply the optimization based on Adjoint Method. Additionally, we are able to develop a numerical modeling of the flow physics which is required to achieve suitable results with the method. The mathematical model and the validation tests are described in the next chapters.

As the technology challenges are determined, we are also able to choose engineering applications where the method could lead to improvements. It is important to remember that the U.S. Department of Energy set a target of 180 V/V at 35 bar at ambient temperature as a point where ANG becomes a viable alternative. The literature shows different aprroaches in the attempts to get around of this value. One of the objetives of this work is to change some parameters (geometric or otherwise) so that the application could perform better the operation of filling. The next chapters presented that the Adjoint Method is a suitable tool for the taste.

# 3 Primal Problem - Mathematical Model

## 3.1 Introduction

In this chapter, we will describe the governing equations for a ANG system. These equations will be divided into two groups: Flow in porous media (adsorbent bed) and adsorption modeling.

### 3.1.1 ANG parameters

Before discussing the Mathematical model, it is useful to introduce the main parameters which describe an ANG system:

- Tank Dimensions and Geometry: To discretize the domain of the numerical simulations, it is necessary to know the tank dimensions. The main examples are the total length and the radius, when we consider circular cylinder tanks.
- Environmental conditions: As the heat generation is a critical parameter in adsorption performance, it is necessary to know the environmental conditions to model the heat exchange between tank walls and their surroundings. Here, the natural (or forced) convection coefficients, represented by letter ($h$), are necessary along with the ambient temperature, represented by $T_\infty$.
- Gas properties: In this report, we consider pure NG. So, the following thermodynamic properties of the methane are required: the specific heat at constant pressure ($C_{pg}$), molar mass ($M_g$), thermal conductivity ($\lambda_g$), viscosity ($\mu_g$) and obviously, pressure and temperature.
- Adsorbent properties: Following those of the gas, some properties of the adsorbent are needed: specific heat ($C_{ps}$) and thermal conductivity ($\lambda_s$).

- Bed properties: Just as with, the adsorbent material, we need properties of the bed, itself. However, in ANG systems, we fill the tank with adsorbent, thus forming an adsorbent bed. Figure 3.1 shows the basic structure. Two parameters are important for its mathematical modeling: Bed Density ($\rho_b$) and the permeability, defined by letter $K$.

- Porosity: As it was previously mentioned, the porosity is one of most important parameters of ANG systems. In this work, we consider $\epsilon$ as a input and its distribution is kept constant through the optimization process.

### 3.1.2 Flow in Porous Media

This section describes the single-phase flow through porous media. By a porous medium we mean a material consisting of a solid matrix with an interconnected void, as previously mentioned.

An important question is: "How do we treat a flow through a porous structure?". In their book, Nield e Bejan (2006) have a suitable explanation: "It is largely a question of the distance between the problem solver and the actual flow structure".

In other words, when the observer sees only one or two particle channels, or one or two open or closed pores, it is possible to use conventional fluid mechanics and convective heat transfer to describe what happens at every point of the fluid and solid filled spaces.

On the other hand, when the distance is large so that there are many particle channels and pore cavities in the field of vision, the complications of the flow paths rule out the conventional approach. In this limit, volume-averaging methods (WHITAKER, 1996) and global measurements such as permeability and conductivity (KAVIANY, 1995) are useful in describing the flow. In this work, we use this approach with simplifications presented in the next sections.

Here we shall account for the fact that the final form of governing equations is entirely similar to the well-known Navier-Stokes equations as they are presented in the literature. However, in the equations for porous media, the physical quantities represent volume averaged values, as opposed to local variables.

We will start with the generic form of the Navier–Stokes equations (eqs. 3.1 to 3.3):

$$\frac{\partial \rho}{\partial t} + \nabla.(\rho.\vec{v}) = 0 \tag{3.1}$$

$$\frac{\partial (\rho v)}{\partial t} + \nabla.(\rho.\vec{v}.\vec{v}) = -\nabla p + \mu.\nabla^2 v + F \tag{3.2}$$

$$\frac{\partial (\rho E)}{\partial t} + \nabla(\vec{v}(\rho E + p)) = \nabla(\lambda \nabla T) + Q \tag{3.3}$$

Where $\rho$ represents the density of the fluid, $\vec{v}$ is the velocity vector, $p$, is the pressure, $F$ is the momentum source term, $E = (h - p/\rho) + v^2/2$ is the sum of internal energy and the kinetic energy, written in terms of the enthalphy $h$, $T$ is the temperature, $\lambda_{eff}$ is the thermal conductivity and $Q$ is the energy source term.

Before proceeding with the derivation, we presented the main assumptions of the model:

- (i) Pure NG: 100% of Methane ($CH_4$);
- (ii) Methane is considered an ideal gas.
- (iii) Adsorbent bed: All thermo-physical properties (density ($\rho_b$), specific heat ($Cp_s$), thermal conductivity ($\lambda_s$), etc) are constant in the range of temperatures and pressures that are considered here;
- (iv) Thermal Equilibrium: The adsorbed gas phase and solids are locally in thermal equilibrium;
- (v) The adsorbed bed is considered isotropic, moreover, we consider all particles as spheres with homogeneus pores distribution;
- (vi) Intraparticle and film resistances to mass and heat transfer are neglected;
- (vii) Natural convection inside the adsorbent bed is neglected;
- (viii) The Heat of Adsorption $\Delta H$ is constant;
- (ix) The thermal effect of the ANG cylinder wall is neglected;

- (x) The kinectic energy is neglected

To facilitate the undestanding of equations, figure (3.1) presents the basic structure of the ANG tank, showing the different regions that the NG could be stored:

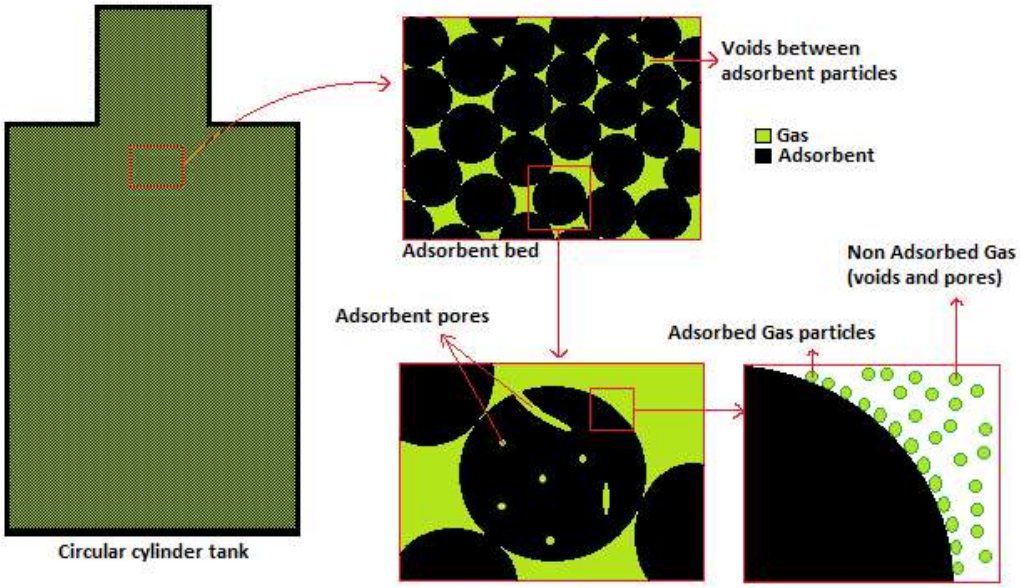


**Figure 3.1:** Simple Scheme of ANG Tank

#### 3.1.2.1 Continuity Equation

The equation of continuity has the two terms presented as follows:

$$\underbrace{\frac{\partial \rho}{\partial t}}_{\text{Time-dependent Term}} + \underbrace{\nabla.(\rho \vec{v})}_{\text{Convective Term}} = 0 \tag{3.4}$$

Each of them will be treated separately and the modified equation will be presented at the end of the deduction.

#### 3.1.2.2 Time-dependent Term

The first term of eq. (3.4) represents the time variation of mass in the control volume. Therefore, we can represent in eq.(3.5) the density $\rho$ in terms of the total mass $M_t$ and the control volume $V_t$:

$$\rho = \frac{M_t}{V_t} \tag{3.5}$$

In fig. (3.1), we can observe that gas particle could be located in three different places: Pores, Voids or Adsorbed. We use this division to expand $M_t$ in four terms, presented in the eq.(3.6):

$$\rho = \frac{M_{gv} + M_{gp} + M_{ga} + M_s}{V_t} = \underbrace{\frac{M_{gv}}{V_t}}_{\text{a}} + \underbrace{\frac{M_{gp}}{V_t}}_{\text{b}} + \underbrace{\frac{M_{ga}}{V_t}}_{\text{c}}\underbrace{\frac{M_s}{V_t}}_{\text{d}} \tag{3.6}$$

Where $M_{gv}$ represents the mass of gas in the particle voids, $M_{gp}$ is the mass of gas in the particle pores, $M_{ga}$ is the mass of adsorbed gas and $M_s$ is the mass of solid (adsorbent). Again, we treat the terms separately. In the term "a", we multiply and divide by $V_v$ which represents the total volume of voids in the porous media:

$$\frac{M_{gv}}{V_t} = \frac{M_{gv}}{V_t}.\frac{V_v}{V_v} = \underbrace{\frac{M_{gv}}{V_v}}_{\text{I}} \cdot \underbrace{\frac{V_v}{V_t}}_{\text{II}} \tag{3.7}$$

The term $I$ in eq.(3.7) represents the free gas density, which will be denoted by $\rho_g$. The term $II$ is a volume ratio, or in the other words, a value of porosity. In this case, we call porosity of the bed, represented by $\epsilon_b$. The modified term becomes the eq.(3.8):

$$\frac{M_{gv}}{V_t} = \rho_g.\epsilon_b \tag{3.8}$$

The term "b" in eq. (3.6) will be multiplied and divided by two parameters: First, by $V_p$, which represents the total volume of occupied by pores and second, by $V_s$ which represents the volume occupied by the solid particle (adsorbent):

$$\frac{M_{gp}}{V_t} = \frac{M_{gp}}{V_t}.\frac{V_p}{V_p}.\frac{V_s}{V_s} = \underbrace{\frac{M_{gp}}{V_p}}_{\text{III}} \cdot \underbrace{\frac{V_p}{V_s}}_{\text{IV}} \cdot \underbrace{\frac{V_s}{V_t}}_{\text{V}} \tag{3.9}$$

The term $III$ in eq.(3.9) also represents the free gas density, because the adsorbed gas is considered in "c" term of eq.(3.6). Therefore, we represent by $\rho_g$ too. The term $IV$ is other value of porosity, called particle porosity, represented by $\epsilon_p$. Finally, in the term $V$, it is important to see that the volume occupied by the adsorbent is the total volume less the volume occupied by the voids, in the other words, $V_s = V_t - V_v$. So, using this relation in term $V$, we get $(1 - \epsilon_b)$. The

modified term "b" then becomes the eq.(3.10):

$$\frac{M_{gp}}{V_t} = \rho_g.\epsilon_p.(1-\epsilon_b) \tag{3.10}$$

Term "c" will be multiplied and divided by three parameters: First, by $V_s$, second, by $V_s - V_p$, which represents the volume of solid without the pores and third, by $M_s$, which represents the total mass of adsorbent:

$$\frac{M_{ga}}{V_t} = \frac{M_{ga}}{V_t}.\frac{V_s}{V_s}.\left(\frac{V_s - V_p}{V_s - V_p}\right).\frac{M_s}{M_s} = \underbrace{\frac{M_s}{V_s - V_p}}_{\text{VI}} \cdot \underbrace{\frac{M_{ga}}{M_s}}_{\text{VII}} \cdot \underbrace{\frac{V_s}{V_t}}_{\text{VIII}} \cdot \underbrace{\frac{V_s - V_p}{V_s}}_{\text{IX}} \tag{3.11}$$

The term $VI$ in eq. (3.11) is the density of solid (adsorbent), represented by $\rho_s$. Term $VII$ is the ratio between the adsorbed gas mass and adsorbent mass which definition is the density of adsorption, represented by letter "$q$".

Term $VIII$ is also $(1-\epsilon_b)$, based on the term $V$ from eq. (3.9) and the result in eq. (3.10). Using the same analogy, the term $IX$ will be represented by $(1-\epsilon_p)$. The modified "c" term is given by the eq.(3.12):

$$\frac{M_{ga}}{V_t} = \rho_s.q.(1-\epsilon_b).(1-\epsilon_p) \tag{3.12}$$

Term "d" is a constant, so it remains as it, when we apply the operator $\frac{\partial}{\partial t}$, it becomes zero.

With all terms modified, we can substitute them in eq. (3.6) and form eq. (3.13):

$$\rho = \rho_g.\epsilon_b + \rho_g.\epsilon_p.(1-\epsilon_b) + \rho_s.q.(1-\epsilon_b).(1-\epsilon_p) + \frac{M_s}{V_t} \tag{3.13}$$

Then, on expanding the terms and collecting like terms, we get eq. (3.14):

$$\begin{aligned} \rho &= \rho_g.(\epsilon_b + (1-\epsilon_b).\epsilon_p) + \rho_s.q.(1-\epsilon_b-\epsilon_p+\epsilon_b\epsilon_p) + \frac{M_s}{V_t} = \\ \rho &= \rho_g.(\epsilon_b + (1-\epsilon_b).\epsilon_p) + \rho_s.q.(1-(\epsilon_b + (1-\epsilon_b).\epsilon_p)) + \frac{M_s}{V_t} \end{aligned} \tag{3.14}$$

By defining total porosity $\epsilon_t = \epsilon_b + (1 - \epsilon_b).\epsilon_p$ and by substituting it into eq. (3.14), it yields the eq. (3.15):

$$\rho = \rho_g.\epsilon_t + \rho_s.q.(1 - \epsilon_t) + \frac{M_s}{V_t} \tag{3.15}$$

And finally, by using the definition of bed density when the fluid is a gas: $(\rho_b = (1 - \epsilon_t).\rho_s)$ (SAHOO; JOHN, 2011) and remembering that $\frac{\partial}{\partial t}(\frac{M_s}{V_t}) = 0$, we find the modified Time-dependent term in the eq.(3.16):

$$\frac{\partial \rho}{\partial t} = \frac{\partial(\epsilon_t \rho_g + \rho_b.q)}{\partial t} \tag{3.16}$$

#### 3.1.2.3 Convective Term

The convective term represents the mass flux in the control volume. On assuming the adsorbent bed is fixed, we represent only the free gas flux, so the modified term is presented in eq. (3.17):

$$\nabla.(\rho\vec{v}) = \nabla.(\rho_g\vec{v_g}) \tag{3.17}$$

Naturally, the adsorbed gas does not flow, so this velocity is also zero. Hence, on having accounted for all contributions, the modified continuity equation is presented in eq.(3.18):

$$\frac{\partial(\epsilon_t.\rho_g + \rho_b.q)}{\partial t} + \nabla.(\rho_g.\vec{v_g}) = 0 \tag{3.18}$$

This result is according with all references in the literature survey (KAVIANY, 1995; SAHOO; JOHN, 2010; SAHOO; JOHN, 2011; XIAO; PENG, 2013; XIAO; TONG, 2012; NOUH; LAU, 2010; MOTA; SAATDJIAN, 1995).

#### 3.1.2.4 Momentum Equation

The literature shows different approaches to the momentum equation in porous media. The first studies started with Darcy in 1856 (KAVIANY, 1995). His experiment used nearly uniform-size particles in a tube, and the objetive was to

measure the head loss in it. The macroscopic flow was steady, one-dimensional, and driven by gravity. He found eq. (3.19) that relates the pressure drop to velocity ($u_d$), viscosity ($\mu$) and permeability ($K$):

$$\frac{dp}{dx} = -\frac{\mu}{K} u_d \tag{3.19}$$

At low gas pressures and for small pore size, the mean free path of the gas molecules may be of the order of the pore size and, therefore, velocity slip occurs (Knudsen effect), resulting in higher permeabilites. The references shows that the measured gas and liquid permeabilities can be noticeably different (KAVIANY, 1995), but the Darcy model is consistent with both.

The eq.(3.20) presented the Darcy model in a 3D flow:

$$\nabla p = -\frac{\mu}{K} \vec{u_d} \tag{3.20}$$

The equation of Darcy can substitute the equation of momentum under specific conditions and is one of the assumptions used in this thesis. In the book by Kaviany (KAVIANY, 1995), he shows four distinct flow regimes, where that simplification holds, based on Reynolds number, eq.(3.21), referred to pores diameter ($\bar{d}$):

$$Re_d = \frac{\rho . \bar{u_p} . \bar{d}}{\mu} \tag{3.21}$$

Where $u_p = u_d/\epsilon$ is the average velocity in the pores, calculated in terms of the average flow velocity and total porosity. The flow regimes are described below:

- $Re_d < 1$, Darcy or creeping flow regime: The viscous forces dominate over the inertia forces and only the local (pore-level) geometry influences the flow. It is the best regime to apply the Darcy model.
- $1 - 10 < Re_d < 150$, inertial-flow regime: Steady nonlinear laminar flow begins between 1 and 10 (inertial force affected). As $Re_d$ increases, the cores become larger and the boundary-layer thickness decreases. This an indication of the dominance of the inertia forces over the viscous forces.

In this scenario, the Darcy model must be modified by using the "Ergun inertial term", presented in eq. (3.22):

$$\nabla p = -\frac{\mu}{K} u_d - \frac{C_E}{K^{1/2}} . \rho . |u_d| . u_d \tag{3.22}$$

Where $C_E$ is Ergun constant, defined in terms of the porous media.

- $150 < Re_d < 300$, unsteady laminar-flow regime: Oscillations with frequencies of the order of 1Hz and amplitudes of the order of one-tenth of the particle diameter will be observed. The laminar wake instability may be responsible for the transition from laminar steady flows to unsteady flows. This regime is not in the scope of this work.

- $Re_d > 300$, unsteady and chaotic flow regime: The observed highly unsteady chaotic flow does not appear to be laminar, and turbulent type mixing (turbulent dispersion) of dye appears in the pores. As with the previous regime, this is beyond the scope of this work.

This work focuses on the so-called Darcy regime. But, so far, future studies with the inertial flow regime can not be discarded.

#### 3.1.2.5 Energy Equation

The Energy equation (3.23) is presented below in terms of total energy:

$$\underbrace{\frac{\partial(\rho E)}{\partial t}}_{\text{Time-dependent Term}} + \underbrace{\nabla \cdot (\vec{v}(\rho E + p))}_{\text{Convective Term}} = \underbrace{\nabla(\lambda \nabla T)}_{\text{Diffusive Term}} + \underbrace{Q}_{\text{Source Term}} \tag{3.23}$$

Where $E = u_i + v^2/2$, $u_i$ is the specific internal energy and $v^2/2$ is the specific kinetic energy.

There are two equivalent forms that are presented in the literature. One of them is based on total energy as the eq. (3.23) above (XIAO; PENG, 2013; XIAO; TONG, 2012; NOUH; LAU, 2010), whereas the other is based on specific heat and temperature (SAHOO; JOHN, 2010; SAHOO; JOHN, 2011; MOTA; SAATDJIAN, 1995). We choose the second strategy for future convenience during the deduction of the Adjoint Equations.

#### 3.1.2.6 Time-dependent Term

The first step, as with the the continuity equation, is the split of the term $\rho E$ into four parts: Gas in the voids, Gas in the pores, Adsorbed gas and Adsorbent, becoming the eq. (3.24):

$$\rho E = \underbrace{(\rho E)_v}_{\text{a}} + \underbrace{(\rho E)_p}_{\text{b}} + \underbrace{(\rho E)_a}_{\text{c}} + \underbrace{(\rho E)_s}_{\text{d}} \tag{3.24}$$

Here again, by assuming that the gas is ideal and the kinetic energy is neglected, we can write the total energy in terms of temperature as defined in the eq. (3.25):

$$E = u_i = h - \frac{p}{\rho} = Cp.T - \frac{p}{\rho} \tag{3.25}$$

The term "a" can be modified using the eq.(3.25) and forming the eq.(3.26):

$$(\rho E)_v = \rho_v \Big( C_{pg}.T - \frac{p_v}{\rho_v} \Big) = \rho_v.C_{pg}.T - p_v \tag{3.26}$$

Where $\rho_v$ is the density of free gas in the voids in terms of the total volume and it is expanded in eq. (3.27), $C_{pg}$ is the gas specific heat and $p_v$ is the partial pressure of gas in the voids.

$$\rho_v.C_{pg}.T - p_v = \frac{M_{gv}}{V_t}.C_{pg}.T - p_v \tag{3.27}$$

As seen in eq. (3.8), the term $\frac{M_{gv}}{V_t}$ can be cast in the form:

$$\frac{M_{gv}}{V_t}.Cpg.T - p_v = \rho_g.\epsilon_b.C_{pg}.T - p_v \tag{3.28}$$

The term "b" is modified using the same eq. (3.25) and forming the eq. (3.29):

$$(\rho E)_p = \rho_p\Big(C_{pg}.T - \frac{p_p}{\rho_p}\Big) = \rho_p.C_{pg}.T - p_p \tag{3.29}$$

Where $\rho_p$ is the density of free gas in the pores in terms of the total volume and it is expanded in eq. (3.30) where $p_p$ is the partial pressure of gas in the pores:

$$\rho_p.C_{pg}.T - p_p = \frac{M_{gp}}{V_t}.C_{pg}.T - p_p \tag{3.30}$$

As seen in eq. (3.10), the term $\frac{M_{gp}}{V_t}$ can be rewritten and the modified term is presented in the eq. (3.31):

$$\frac{M_{gp}}{V_t}.C_{pg}.T - p_p = \rho_g.\epsilon_p.(1-\epsilon_b).C_{pg}.T - p_p \tag{3.31}$$

The term "c" is modified as terms "a" and "b", forming the eq. (3.32):

$$(\rho E)_a = \rho_a\Big(C_{pg}.T - \frac{p_a}{\rho_a}\Big) = \rho_a.C_{pg}.T - p_a \tag{3.32}$$

Where $\rho_a$ is the density of adsorbed gas in terms of the total volume and it is expanded in eq. (3.33), where $p_a$ is the partial pressure of adsorbed gas.

$$\rho_a.C_{pg}.T - p_a = \frac{M_{ga}}{V_t}.C_{pg}.T - p_a \tag{3.33}$$

As seen in eq. (3.12), the term $\frac{M_{ga}}{V_t}$ can be rewritten and the modified term is presented in the eq. (3.34):

$$\frac{M_{ga}}{V_t}.C_{pg}.T - p_a = \rho_s.q.(1-\epsilon_p).(1-\epsilon_b).C_{pg}.T - p_a \tag{3.34}$$

The term "d" is expanded as follows in the eq. (3.35):

$$(\rho E)_s = \tilde{\rho}_s.C_{ps}.T \tag{3.35}$$

Where $\tilde{\rho}_s$ is the density of adsorbent in terms of the total volume and it is expanded in eq. (3.36):

$$\tilde{\rho}_s.C_{ps}.T = \frac{M_s}{V_t}.C_{ps}.T \tag{3.36}$$

This term will be modified by using the same strategy that was applied to the continuity equation. We multiply and divide it by two terms: $V_s$ and $V_s - V_p$:

$$\frac{M_s}{V_t} = \frac{M_s}{V_t}.\frac{V_s}{V_s}.\left(\frac{V_s - V_p}{V_s - V_p}\right) = \underbrace{\frac{M_s}{V_s - V_p}}_{\text{X}} \cdot \underbrace{\frac{V_s}{V_t}}_{\text{XI}} \cdot \underbrace{\frac{V_s - V_p}{V_p}}_{\text{XII}} \tag{3.37}$$

Term X in eq. (3.37) represents the density of solid, $\rho_s$. The terms XI and XII are known, based on eqs. (3.10) and (3.12). The term "d" is rewritten as follows in the eq. (3.38):

$$(\rho E)_s = \rho_s.(1 - \epsilon_b).(1 - \epsilon_p).C_{ps}.T \tag{3.38}$$

Therefore, substituting eqs.(3.28), (3.31), (3.34) and (3.38) into eq.(3.24), we get the eq.(3.39):

$$\begin{aligned}(\rho E)_v + (\rho E)_p + (\rho E)_a + (\rho E)_s = \rho_g.\epsilon_b.C_{pg}.T - p_v + \\ +\rho_g.\epsilon_p.(1 - \epsilon_b).C_{pg}.T - p_p + \rho_s.q.(1 - \epsilon_p).(1 - \epsilon_b).C_{pg}.T - p_a + \\ +\rho_s.(1 - \epsilon_b).(1 - \epsilon_p).C_{ps}.T\end{aligned} \tag{3.39}$$

By collecting the first two terms and on by recalling that: $\epsilon_t = \epsilon_b + \epsilon_p.(1 - \epsilon_b)$, $(1 - \epsilon_t) = (1 - \epsilon_b).(1 - \epsilon_p)$ and $\rho_b = \rho_s.(1 - \epsilon_t)$, we can simplify the eq.(3.39), presented in the eq.(3.40):

$$\begin{aligned}(\rho E) = \rho_g.\epsilon_t.C_{pg}.T + (1 - \epsilon_t).\rho_s.q.C_{pg}.T + (1 - \epsilon_t).\rho_s.C_{ps}.T = \\ = \rho_g.\epsilon_t.C_{pg}.T + \rho_b.q.C_{pg}.T + \rho_b.C_{ps}.T - p_v - p_p - p_a\end{aligned} \tag{3.40}$$

By collecting the terms and recalling that total pressure is the sum of the partial pressures: $p = p_v + p_p + p_a$, we find the modified energy time-dependent

term, presented in the eq. (3.41):

$$\frac{\partial(\rho E)}{\partial t} = \frac{(\epsilon_t.\rho_g + \rho_b.q).C_{pg}.T + \rho_b.C_{ps}.T - p}{\partial t} \tag{3.41}$$

#### 3.1.2.7 Convective Term

The convective term will be modified using the same assumptions that were made regarding eq. (3.17). On assuming the adsorbent bed is fixed, we have only the free gas flux, so the modified term is presented in eq.(3.42):

$$\nabla \cdot (\vec{v}(\rho E + p)) = \nabla \cdot (\vec{v_g}(\rho E_g + p)) \tag{3.42}$$

By using the definition of total Energy, eq. (3.25), we obtain the modified convective term in the eq. (3.43):

$$\nabla(\vec{v}(\rho E_g + p)) = \nabla\Big(\vec{v_g}\Big(\rho_g\Big(C_{pg}.T - \frac{p}{\rho_g}\Big) + p\Big)\Big) = \nabla(\vec{v_g}.\rho_g.C_{pg}.T) \tag{3.43}$$

#### 3.1.2.8 Diffusive Term

The only assumption regarding the diffusive term is the definition of conductivity. Here it is important to consider the contributions of gas and adsorbent. The modeling consists of a weighted average between gas ($\lambda_g$) and adsorbent ($\lambda_s$) conductivities. Then, by making use of the total porosity as a weight, we get the eq. (3.44):

$$\lambda_{eff} = \epsilon_t.\lambda_g + (1 - \epsilon_t).\lambda_s \tag{3.44}$$

#### 3.1.2.9 Source Term

The source term considers the processes of adsorption/desorption. In the previous chapter, we have defined the heat of adsorption that describes the phenomena. The source term model is based on the references Sahoo e John (2010), Mota e Saatdjian (1995), Nouh e Lau (2010), Xiao e Peng (2013):

$$Q = \frac{\Delta H}{M_g}.\frac{\partial(\rho_b.q)}{\partial t} \tag{3.45}$$

Where $M_g$ is molar mass of the gas and the other parameters are known from previous sections.

On combining the above terms, we obtain the eq. (3.46) which consists in the modified energy equation:

$$\frac{\partial[(\epsilon_t.\rho_g + \rho_b.q).C_{pg}.T + \rho_b.C_{ps}.T]}{\partial t} - \frac{\partial p}{\partial t} + \nabla(\vec{v_g}.\rho_g.C_{pg}.T) = \\ = \lambda_{eff}.\nabla^2 T + \frac{\Delta H}{M_g}.\frac{\partial(\rho_b.q)}{\partial t} \tag{3.46}$$

### 3.1.3 Adsorption Modeling

The adsorption equations that are used in in this work include models of isotherms and heat of Adsorption. The Dubinin-Astakhov (D−A) model, which is widely accepted in the literature, is used to obtain the adsorbed amount at different temperatures and pressures (SAHOO; JOHN, 2010; SAHOO; JOHN, 2011; MOTA; SAATDJIAN, 1995; NOUH; LAU, 2010; XIAO; PENG, 2013; XIAO; TONG, 2012). There are two kinds of description: Molar based or Mass based. From the previous equations, it is clear that we use the second description.

First, we present the eq. (3.47) that is based to estimate "$q$":

$$q = \rho_{ads}.W_0.exp\Big[-\Big(\frac{A}{\beta.E_0}\Big)^n\Big] \tag{3.47}$$

Where $\rho_{ads}$ is the adsorbed gas density, $W_0$ is the microporous volume per unit mass of adsorbent, $\beta$ is the affinity coefficient related to the adsorbate-adsorbent interaction. $E_0$ is the characteristic energy of adsorption, and $n$ is the DA exponent which is related to the pore size dispersion (SAHOO; JOHN, 2010). All of these values depend on the adsorbent, ambient temperature and the gas.

The variable $A$ is the so-called as Polany adsorption potential and it is defined in eq. (3.48), where the gas saturation vapor pressure ($P_s$) is calculated by Dubinin form, which is presented in eq.(3.49). Where $P_{cr}$ and $T_{cr}$ are the critical pressure and temperature of the gas, respectively (SAHOO; JOHN, 2010).

In addition, the adsorbed gas density is expressed in the eq.(3.50) (SAHOO; JOHN, 2010):

$$A = R.T.ln\left(\frac{P_s}{p}\right) \tag{3.48}$$

$$P_s = P_{cr}.\left(\frac{T}{T_{cr}}\right)^2 \tag{3.49}$$

$$\rho_{ads} = \frac{\bar{\rho_{ads}}}{exp[\alpha_e(T - T_b)]} \tag{3.50}$$

Where $\bar{\rho_{ads}}$ is the density of liquid phase of the adsorbed fluid in the saturation region ($T_b$) and $\alpha_e$ is the mean value of the thermal expansion of liquified gas, a parameter is also function of gas.

The last aspect to be considered in the adsorption model is how to evaluate the time derivative $\partial q/\partial t$, which appears in Continuity and Energy equations. In his paper, Xiao describes briefly the model called *Linear Driving Force* (LDF) (XIAO; TONG, 2012):

$$\frac{\partial q}{\partial t} = k.(q^* - q) \tag{3.51}$$

Where $q^*$ is the adsorbed gas in equilibrium with saturated gas phase, which is calculated using the eq.(3.47) and $k$ is a mass transfer coefficient at an aggregated level. In numerical simulations, the value of $q$ is calculated explicitly using the previous time step and $k$ is estimated based on the experimental results presented in the literature (SAHOO; JOHN, 2010; SAHOO; JOHN, 2011).

# 4 Primal Problem - Numerical Results

## 4.1 Introduction

The CFD implementation started on the basis of the equations described in chapter 3. The *FREEFEM++* platform was chosen to run the numerical simulations.

This platform is a high level integrated development environment (IDE) for numerically solving partial differential equations (PDE) in 2 and 3 dimensions. It is an ideal tool for studying the finite element method, but it is also very useful for research, to quickly test new ideas or multi-physics and complex applications (HECHT, 2012).

The main advantages of *FREEFEM++* are described below (FREEFEM, 2011):

- Problem description (real or complex valued) by their variational formulations, with access to the internal vectors and matrices,if needed . This is very important for our implementation not only of the governing equations, but also of the Adjoint Method.
- It allows one to program multi-variables, multi-equations, bi and three dimensional steady or time dependent, linear or nonlinear coupled systems.
- It has an automatic mesh generator, based on the Delaunay-Voronoi algorithm. The inner point density is proportional to the density of points on the boundaries. As the NG tanks have simple geometries, we circumvent the need for comercial mesh generator software packages.
- It is a high level user friendly typed input language with an algebra of analytic and finite element functions.
- It has a large variety of linear direct and iterative solvers (LU, Cholesky, Crout, CG, GMRES, UMFPACK, MUMPS, SuperLU, ...) and eigenvalue

and eigenvector solvers (ARPARK).

- It also has a parallel version using mpi. The optimization loop has a number of iterations to archieve the optimal solution. With parallel version is possible to save time during the Flow and Adjoint processing.

## 4.2 Mathematical considerations

We start by recalling the whole set of governing equations, eqs.(4.1) to (4.4) that have been derived in chapter 3.

$$\frac{\partial(\epsilon_t.\rho_g + \rho_b.q)}{\partial t} + \nabla \cdot (\rho_g \vec{v_g}) = 0 \tag{4.1}$$

$$\nabla p = -\frac{\mu}{K}\vec{v_g} \tag{4.2}$$

$$\frac{\partial[(\epsilon_t.\rho_g + \rho_b.q).C_{pg}.T + \rho_b.C_{ps}.T]}{\partial t} - \epsilon_t \frac{\partial p}{\partial t} + \nabla \cdot (\vec{v_g}\rho_g C_{pg} T) = \\ = \lambda_{eff}.\nabla^2 T + \frac{\Delta H}{M_g}\frac{\partial(\rho_b.q)}{\partial t} \tag{4.3}$$

$$q = \rho_{ads}.W_0.exp\Big[-\Big(\frac{A}{\beta.E_0}\Big)^n\Big] \tag{4.4}$$

On substituting the ideal gas equation ($p = \rho.R.T$) to eq. (4.1), it becomes the eq. (4.5):

$$\frac{\partial(\epsilon_t.\frac{p}{RT} + \rho_b.q)}{\partial t} + \nabla \cdot (\rho_g \vec{v_g}) = 0 \tag{4.5}$$

Where R, is the Methane Gas Constant. The term $\rho_g\vec{v_g}$ is defined as specific mass flux vector, which is represented by letter $\vec{G}$. This assumption is used to solve for $\vec{G}$ rather than velocity, because it is most common to input the value of mass flow rate during the filling and deflation processes. Then, it is a good practice to consider $\vec{G}$ as variable (MOTA; SAATDJIAN, 1995). By expanding the time dependent term, the continuity equation becomes:

$$\frac{\epsilon_t}{R}\left(\frac{1}{T}.\frac{\partial p}{\partial t} - \frac{p}{T^2}.\frac{\partial T}{\partial t}\right) + \rho_b.\frac{\partial q}{\partial t} + \nabla.\vec{G} = 0 \tag{4.6}$$

As to the consideration of mass flux vector ($\vec{G}$), it is also necessary to change Momentum and Energy equations. The former, eq. (4.2) is multiplied through by $\rho_g$, and becomes:

$$\rho_g.\nabla p = -\frac{\mu}{K}.\vec{G} \tag{4.7}$$

The Energy equation (4.3) is changed in the time dependent-term, where we define $C_{eff} = (\epsilon_t.\rho_g + \rho_b.q).C_{pg} + \rho_b.C_{ps}$ as the thermal capacity of an average volume (WHITAKER, 1996) and on substituting $\vec{G} = \rho_g.\vec{v_g}$ in the convective-term, them yields:

$$C_{eff}\frac{\partial T}{\partial t} - \epsilon_t\frac{\partial p}{\partial t} + C_{pg}\nabla\cdot(\vec{G}T) = \lambda_{eff}\nabla^2 T + \rho_b\frac{\Delta H}{M_g}\frac{\partial q}{\partial t} \tag{4.8}$$

Eq. (4.4) does not change. It is important to mention that that equation is solved separately from the other equations in the main set. The terms with $q$ are treated as source terms. Moreover, the quantity $q$, itself, is evaluated by eq.(4.4) on the basis of values of a previous time step (XIAO; PENG, 2013; XIAO; TONG, 2012; MOTA; SAATDJIAN, 1995; SAHOO; JOHN, 2010; SAHOO; JOHN, 2011).

## 4.3 Dimensionless Equations

The adimensionalization of flow governing equations is important to better equalize the orders of magnitude of the different physical quantities (density, pressure, temperature, velocity, etc) and indentify the sensitivity in different flow conditions.

With a suitable flow caracterization, it is possible to compare different scales and relate laboratory tests with future prototypes. Additionally, the dimensionless equations avoids bad conditioning of matrices that are used in numerical flow solutions and this gains more importance when we apply the Adjoint Method, because we do not know, *a priori*, the magnitude of the adjoint variables.

We start defining the nondimensional variables which are represented with

symbol $'*'$:

- Non-dimensional Time:

$$t^* = t\frac{v_\infty}{l_{ref}} \Rightarrow \frac{\partial()}{\partial t} = \frac{v_\infty}{l_{ref}}\frac{\partial()}{\partial t^*} \tag{4.9}$$

  Where $v_\infty$ is the reference velocity and $l_{ref}$ is the reference lenght.

- dimensionless lenght:

$$l^* = \frac{l}{l_{ref}} \Rightarrow \frac{\partial()}{\partial l} = \frac{1}{l_{ref}}\frac{\partial()}{\partial l^*} \tag{4.10}$$

- Non-dimensional density,pressure and temperature:

$$\rho^* = \frac{\rho}{\rho_\infty} \tag{4.11}$$

$$p^* = \frac{p}{p_\infty} \tag{4.12}$$

$$T^* = \frac{T}{T_\infty} \tag{4.13}$$

  Where $\rho_\infty$, $p_\infty$ and $T_\infty$ are the density, pressure and temperature in reference state respectively. These properties must be choose according with perfect gas law:

$$p_\infty = \rho_\infty.R.T_\infty \tag{4.14}$$

  Which implies in the non-dimensional perfect gas law:

$$p^* = \rho^*.T^* \tag{4.15}$$

- Non-dimensional mass flux:

$$\vec{G^*} = \frac{\vec{G}}{\rho_\infty.v_\infty} \tag{4.16}$$

- Non-dimensional Specific Heat and Heat capacity

$$C^*_{px} = \frac{C_{px}}{C_{pg}} \tag{4.17}$$

$$C^*_{eff} = \frac{C_{eff}}{\rho_\infty.C_{pg}} \tag{4.18}$$

Where $C_{pg}$ is the specific heat of the natural gas.

- Non-dimensional Heat of Adsorption

$$\Delta H^* = \frac{\Delta H}{\rho_\infty . C_{pg} . T_\infty . l_{ref}^3} \tag{4.19}$$

- Non-dimensional Molar Mass

$$M_g^* = \frac{M_g}{\rho_\infty . l_{ref}^3} \tag{4.20}$$

The density of adsorption, $q$, is already in non-dimensional form.

### 4.3.1 Mass

On using eq. (4.6) and substituting the corresponding non-dimensional variables, it yields;

$$\begin{aligned} \epsilon_t \frac{\rho_\infty T_\infty}{p_\infty}\Big(\frac{1}{T^* T_\infty}\Big(\frac{v_\infty}{l_{ref}}\Big)\frac{\partial p^* p_\infty}{\partial t^*} - \frac{p^* p_\infty}{T^{*2} T_\infty^2}\Big(\frac{v_\infty}{l_{ref}}\Big)\frac{\partial T^* T_\infty}{\partial t^*}\Big) \;&+\; \rho_b^* \rho_\infty \Big(\frac{v_\infty}{l_{ref}}\Big)\frac{\partial q}{\partial t^*} + \\ +\Big(\frac{1}{l_{ref}}\Big)\nabla.(\vec{G^*}\rho_\infty v_\infty) \;&=\; 0 \end{aligned} \tag{4.21}$$

It is possible to simplify $\rho_\infty$,$p_\infty$, $T_\infty$, $v_\infty$ and $l_{ref}$. The non dimensional mass equation becomes the eq. (4.22):

$$\epsilon_t\Big(\frac{1}{T^*}\frac{\partial p^*}{\partial t^*} - \frac{p^*}{T^{*2}}\frac{\partial T^*}{\partial t^*}\Big) + \rho_b^*\frac{\partial q}{\partial t^*} + \nabla.\vec{G^*} = 0 \tag{4.22}$$

### 4.3.2 Momentum

By using eq. (4.7) and substituting the corresponding non-dimensional variables, it yields;

$$\frac{\mu}{K}.\vec{G^*}\rho_\infty v_\infty + \frac{\rho_g^* \rho_\infty}{l_{ref}}\nabla(p^* p_\infty) = 0 \tag{4.23}$$

In the eq. (4.23), it is possible to collect $\rho_\infty$ and defining the pressure number as follows in the eq. (4.24):

$$N_P = \frac{Kp_\infty}{\mu l_{ref} v_\infty} \tag{4.24}$$

Then, the non-dimensional momentum equation becomes the eq. (4.25):

$$\vec{G^*} + N_P \rho_g^* \nabla^* p* = 0 \tag{4.25}$$

### 4.3.3 Energy

On using eq. (4.8), substituting the corresponding non-dimensional variables and using the state gas equation: $p_\infty = \rho_\infty R T_\infty$ it yields the eq. (4.26):

$$\begin{aligned}(C^*_{eff}\rho_\infty C_{pg})\Big(\frac{v_\infty}{l_{ref}}\Big)\frac{\partial T^* T_\infty}{\partial t^*} &- \epsilon_t\Big(\frac{v_\infty}{l_{ref}}\Big)\frac{\partial p^* \rho_\infty R T_\infty}{\partial t^*} + C^*_{pg} C_{pg}\Big(\frac{1}{l_{ref}}\Big)\nabla^*(\vec{G^*}\rho_\infty v_\infty T^* T_\infty) \\ &- \lambda_{eff}\Big(\frac{1}{l^2_{ref}}\Big)\nabla^{*2}(T^* T_\infty) \\ &- (\rho^*_b \rho_\infty)\frac{\Delta H^* \rho_\infty C_{pg} T_\infty l^3_{ref}}{M^*_g \rho_\infty l^3_{ref}}\Big(\frac{v_\infty}{l_{ref}}\Big)\frac{\partial q}{\partial t^*} = 0\end{aligned} \tag{4.26}$$

It is possible to simplify $T_\infty$ and $l_{ref}$. It becomes the eq. (4.27):

$$\begin{aligned}(C^*_{eff}\rho_\infty C_{pg} v_\infty)\frac{\partial T^*}{\partial t^*} - \epsilon_t v_\infty \rho_\infty R\frac{\partial p^*}{\partial t^*} + C^*_{pg} C_{pg}\rho_\infty v_\infty \nabla^*(\vec{G^*}T^*) \\ -\lambda_{eff}\Big(\frac{1}{l_{ref}}\Big)\nabla^{*2}(T^*) - (\rho^*_b\rho_\infty)\frac{\Delta H^* C_{pg}}{M^*_g} v_\infty \frac{\partial q}{\partial t^*} = 0\end{aligned} \tag{4.27}$$

On defining the Pecklet number:

$$Pe = \frac{\rho_\infty C_{pg} v_\infty l_{ref}}{\lambda_{eff}} \tag{4.28}$$

And by assuming that $C^*_{pg} = 1$, according to the non-dimensional variables, $\gamma = \frac{C_{pg}}{C_{vg}}$ and $R = C_{pg} - C_{vg}$, the non-dimensional energy equation becomes the eq. (4.29):

$$C^*_{eff}\frac{\partial T^*}{\partial t^*} - \epsilon_t\Big(\frac{\gamma-1}{\gamma}\Big)\frac{\partial p^*}{\partial t^*} + \nabla^*(\vec{G}^*T^*) - \frac{1}{Pe}\nabla^{*2}T^* - \rho^*_b\frac{\Delta H^*}{M^*_g}\frac{\partial q}{\partial t^*} = 0 \quad (4.29)$$

### 4.3.4 Adsorption

For adsorption model, no changes are necessary because the density of adsorption $q$ is already dimensionless.

## 4.4 Boundary Conditions

To describe the boundary conditions, fig.(4.1) illustrates the axi-symmetric model that is used in the simulations.

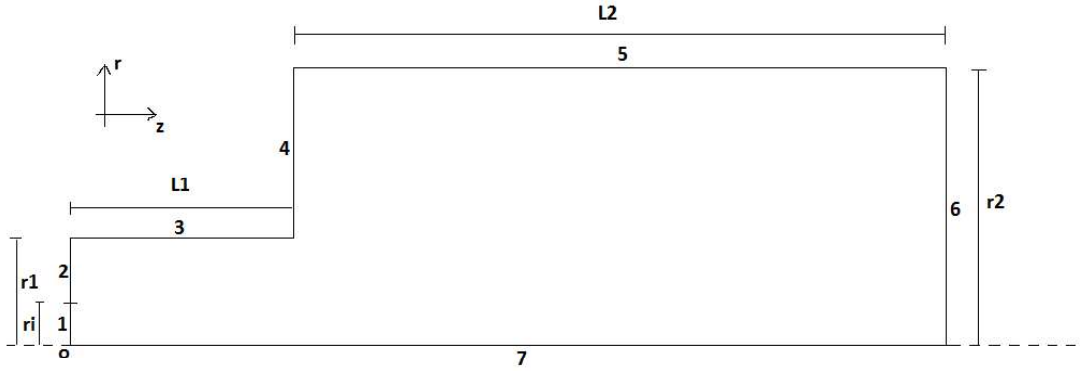


**Figure 4.1:** Schematic of a ANG Storage System - The point "o" represents the origin of coordinate system

Fig. 4.1 indicates the boundaries (numbered from 1 to 7) and the basic tank dimensions. We have already considered the non-dimensional equations.

To the inlet, boundary 1, eq.(4.30) presents the boundary conditions applied:

$$\begin{aligned} \vec{G^*_z} &= 2.G^*_m.\Big(1-\frac{r^2}{r_i^2}\Big) \\ \vec{G^*_r} &= 0 \\ T^* &= T^*_{inlet} \end{aligned} \quad (4.30)$$

It represents a parabolic profile for the specific mass flow rate, where $G^*_m$ is the non-dimensional average mass flux, defined as an input to the algorithm.

The boundaries 2 to 6 are considered as solid tank walls. There, the no slip boundary condition is imposed, along with an external convective heat flux

boundary condition, presented in eq. (4.31):

$$\begin{aligned} \vec{G_r^*} &= 0 \\ \vec{G_z^*} &= 0 \\ -n.\nabla^* T^* &= Nu(T^* - T_{ext}^*) \end{aligned} \tag{4.31}$$

Where $T_{ext}$ is the ambient air temperature in the surroundings and $Nu$ is the Nusselt number defined in the eq. (4.32)):

$$Nu = \frac{hl_{ref}}{\lambda_{eff}} \tag{4.32}$$

A symmetry boundary condition must impose the zero normal derivative conditions. The position of boundary 7 implies in a normal vector $\vec{n} = (0, 1)$. Then, the inner product $\vec{G} \cdot \vec{n} = (G_z^*, G_r^*).(0, 1)$ reduces to $\vec{G} \cdot \vec{n} = \vec{G_r^*}$. Eq. (4.33) describes the symmetry condition:

$$\vec{G_r^*} = 0 \tag{4.33}$$

There is no heat transfer in this boundary, then the temperature gradient is zero, attending the zero normal derivative condition.

## 4.5 Numerical Discretization

### 4.5.1 Weak Formulation and Spatial Discretizations

**From this section, we suppress the symbol $*$ of the equations and the reader should consider all terms adimensionalized.**

Eqs. (4.22) to (4.29) and the respective boundary conditions (4.30) to (4.33) must be implemented into the FREEFEM++ platform, in the weak form.

By defining a inner product $< f, g >= \int_\Omega f.gdV$ and the generic weight functions for Mass, Momentum, Energy and Adsorption equations (pw,vr,vz,tw and qw), one can apply the volume integration to the equations, forming the eqs. (4.34):

$$\begin{aligned}
\Big\langle \epsilon_t\Big(\frac{1}{T}.\frac{\partial p}{\partial t}+\frac{p}{T^2}.\frac{\partial T}{\partial t}\Big), pw\Big\rangle + \Big\langle \rho_b.\frac{\partial q}{\partial t}, pw\Big\rangle \\
+\Big\langle \frac{\partial Gr}{\partial r}+\frac{\partial Gz}{\partial z}+\frac{Gr}{r}, pw\Big\rangle = 0 \\
\Big\langle \vec{Gr}, vr\Big\rangle + \Big\langle N_p\rho_g.\frac{\partial p}{\partial r}, vr\Big\rangle = 0 \\
\Big\langle \vec{Gz}, vz\Big\rangle + \Big\langle N_p\rho_g.\frac{\partial p}{\partial z}, vz\Big\rangle = 0 \\
\Big\langle C_{eff}.\frac{\partial T}{\partial t}, tw\Big\rangle - \Big\langle \epsilon_t(\frac{\gamma-1}{\gamma})\frac{\partial p}{\partial t}, tw\Big\rangle + \Big\langle \nabla(\vec{G}.T), tw\Big\rangle \\
-\Big\langle \frac{1}{Pe}\nabla^2 T, tw\Big\rangle - \Big\langle \rho_b.\frac{\Delta H}{M_g}.\frac{\partial q}{\partial t}, tw\Big\rangle = 0
\end{aligned} \tag{4.34}$$

For the Adsorption model we have the eq. (4.35):

$$\Big\langle q-\rho_{ads}.W_0.exp\Big[-\Big(\frac{A}{\beta.E_0}\Big)^n\Big], qw\Big\rangle = 0 \tag{4.35}$$

The FREEFEM++ has hard coded algorithms to evaluate the partial derivatives of first order. Therefore, the operators $\frac{\partial}{\partial r}$ and $\frac{\partial}{\partial z}$ do not require any special discretization.

The energy diffusive term was treated by using integration by parts, presented in eq. (4.36):

$$-\int_\Omega \frac{1}{Pe}.\nabla^2 T.twdV = -\frac{1}{Pe}(\nabla T.\vec{n}.tw)_{\partial\Omega} + \frac{1}{Pe}\int_\Omega \nabla T.\nabla twdV \tag{4.36}$$

Where the first term represents a Neumman boundary condition, as applied to the boundary $\partial\Omega$, which is evaluated in eq. (4.31). The second term has only partial derivatives with respect to $r$ and $z$.

Moreover, the equations of mass, momentum and energy have non-linear terms. We have used explicit forms to implement this equations into FREEFEM++. The time-dependent term in the mass equation, the pressure gradient in the Momentum equation and the convective term in energy Equation become, respectively the eqs.(4.37) to (4.40):

$$\epsilon_t\Big(\frac{1}{T}.\frac{\partial p}{\partial t}+\frac{p}{T^2}.\frac{\partial T}{\partial t}\Big) = \epsilon_t\Big(\frac{1}{T_{aux}}.\frac{\partial p}{\partial t}+\frac{p_{aux}}{T_{aux}^2}.\frac{\partial T}{\partial t}\Big) \tag{4.37}$$

$$N_p \rho_g . \frac{\partial p}{\partial r} = N_p \rho_{aux} . \frac{\partial p}{\partial r} \tag{4.38}$$

$$N_p \rho_g . \frac{\partial p}{\partial z} = N_p \rho_{aux} . \frac{\partial p}{\partial z} \tag{4.39}$$

$$\nabla(\vec{G}.T) = \left( Gr_{aux} . \frac{\partial T}{\partial r} + Gz_{aux} . \frac{\partial T}{\partial z} \right) \tag{4.40}$$

Where variables with subscript "$aux$" are the auxiliary variables, which are estimated by linear extrapolation from previous steps, presented as a generic variable in the eq.(4.41):

$$\eta_{aux} = 2.\eta_{m-1} - \eta_{m-2} \tag{4.41}$$

On using temperature as example: $T_{aux} = 2.T_{m-1} - T_{m-2}$.

### 4.5.2 Time Discretization

The time-dependent terms are discretized by using backward differentiation multistep method (GUNZBURGER, 1989). Given a variable $u$ and a sequence of $k$ time steps $u^0, u^1, ..., u^{k-1}$, a second order discretization at $m$-step is presented as follows:

$$\left( \frac{\partial u}{\partial t} \right)_m = \frac{3.u^m - 4.u^{m-1} + u^{m-2}}{2.dt} + \mathscr{O}(dt^2) \tag{4.42}$$

Where $dt$ is the time step. The variables $u^{m-1}$ and $u^{m-2}$ are the values of $u$ in the previous two time steps before the current one. Again, it is important to mention that the terms with $\frac{\partial q}{\partial t}$ are considered as source terms and will be evaluated using the considerations made in the end of chapter 3.

Finally, on applying the above considerations to the original equations, we have obtained the following set of equations (4.43), which we have implemented into the FREEFEM++ platform:

$$\int_{\Omega} \epsilon_t \Big( \frac{1}{T_{aux}} . \frac{3.p - 4.p_{m-1} + p_{m-2}}{2.dt} + \frac{p_{aux}}{T_{aux}^2} . \frac{3.T - 4.T_{m-1} + T_{m-2}}{2.dt} \Big) .pwdV +$$

$$+ \int_{\Omega} \rho_b . k . (q - q_{m-1}) .pwdV +$$

$$+ \int_{\Omega} \Big( \frac{\partial Gr}{\partial r} + \frac{\partial Gz}{\partial z} + \frac{Gr}{r} \Big) .pwdV = 0$$

$$\int_{\Omega} \Big( \vec{Gr} + N_p \rho_{aux} . \frac{\partial p}{\partial r} \Big) .vrdV = 0$$

$$\int_{\Omega} \Big( \vec{Gz} + N_p \rho_{aux} . \frac{\partial p}{\partial z} \Big) .vzdV = 0$$

$$\int_{\Omega} \Big( C_{eff} . \frac{3.T - 4.T_{m-1} + T_{m-2}}{2.dt} - \epsilon_t \Big( \frac{\gamma - 1}{\gamma} \Big) \frac{3.p - 4.p_{m-1} + p_{m-2}}{2.dt} +$$

$$+ \Big( Gr_{aux} . \frac{\partial T}{\partial r} + Gz_{aux} . \frac{\partial T}{\partial z} \Big) \Big) .tw +$$

$$+ \frac{1}{Pe} . \nabla T . \nabla tw - \Big( \rho_b . \frac{\Delta H}{M_g} . k . (q^* - q_{m-1}) \Big) .twdV = 0 \quad (4.43)$$

## 4.6 Numerical Simulations

After the equations were implemented into FREFEEM++, we have carry out validation tests, to check if the model could reproduce the results that are presented in the literature. We choose to compare our results to those that are presented by Sahoo e John (2011) because not only do the authors show numerical simulations, but they also discuss experimental results.

### 4.6.1 Mesh Geometry

With reference to fig. 4.1 , the actual values of the tank dimensions are presented in table 4.1 below:

**Table 4.1:** Tank Dimensions (SAHOO; JOHN, 2011)

| Parameter | Value (mm) |
|---|---|
| Inlet Radius ($r_i$) | 3.175 |
| Inlet Head Radius ($r_1$) | 13.000 |
| Tank Radius ($r_2$) | 53.300 |
| Inlet Head Lenght ($L_1$) | 30.000 |
| Tank Lenght ($L_2$) | 202.000 |

The FREEFEM++ mesh generator is a suitable tool and it was used to generate a 1851 triangle elements mesh, with specific refinements at the inlet region. Fig. 4.2 depicts the mesh geometry:

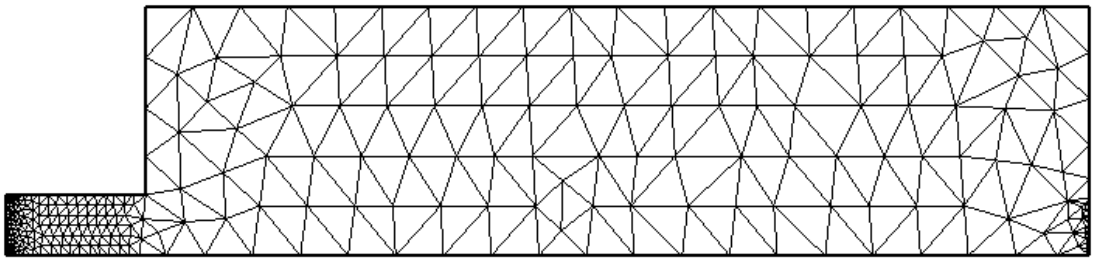

**Figure 4.2:** Mesh generated by FREEFEM++

### 4.6.2 Boundary and Initial Conditions

Table 4.2 presents all the values that we have used in the simulation setup:

**Table 4.2:** Data used in Simulation (SAHOO; JOHN, 2011)

| Parameter | Value | Parameter | Value |
|---|---|---|---|
| $K$ | $3.7 \cdot 10^{-10}\ m^2$ | $T_\infty$ | $300K$ |
| $C_{pg}$ | $2450\ J/kg.K$ | $C_{ps}$ | $650\ J/kg \cdot K$ |
| $\mu_g$ | $1.25 \cdot 10^{-5}\ Pa \cdots$ | $\lambda_g$ | $0.0343\ W/m \cdot K$ |
| $\epsilon_t$ | 0.65 | $\epsilon_b$ | 0.30 |
| $\lambda_s$ | $0.54\ W/m \cdot K$ | $\rho_b$ | $500\ kg/m^3$ |
| $\Delta H$ | $12000\ J/mol$ | $h$ | $5W/K$ (natural) |
| $M_g$ | $0.016\ kg/mol$ | | $700W/K$ (forced) |
| *STP conditions | | | |

Tests were performed with two values of volumetric flow rate: 10 $L/min$ and 30 $L/min$, which values of $G_m$ are 3.708 and 11.123 $kg/m^2s$ respectively.

As for the adsorption model, the table (4.3) presents the setup parameters:

**Table 4.3:** Data used in Simulation (SAHOO; JOHN, 2011)

| Parameter | Value | Parameter | Value |
|---|---|---|---|
| $\alpha$ | $2.5e-3\ K^{-1}$ | $Beta$ | 0.35 |
| $E_0$ | $25.04e+3\ J/mol$ | $W_0$ | $3.3e-4\ m^3/kg$ |
| $P_{cr}$ | $45.96e+5\ Pa$ | $T_{cr}$ | $191\ K$ |
| $\rho_{ads}^{-}$ | $422.62\ kg/m^3$ | $T_b$ | $111.2\ K$ |
| $n$ | 1.8 | $k$ | $3.2\ s^{-1}$ |

Finally, the initial conditions are as follows in table 4.4:

**Table 4.4:** Initial Conditions (SAHOO; JOHN, 2011)

| Parameter | Value | Parameter | Value | Parameter | Value |
|---|---|---|---|---|---|
| $P_i$ | $20000\ Pa$ | $T_i$ | $303K$ | $q$ | $q(P_i, T_i)$ |

### 4.6.3 Results

The numerical simulations performed by Sahoo e John (2011) used the COMSOL MULTIPHYSICS 3.5a software, which is also based on the finite element method. First, we calibrate the precision of the numerical model, by studying the sensitivity of mesh refinement. This is followed by the validation tests, in which we compare our results to those that are presented in the literature (SAHOO; JOHN, 2011).

Afterwards, we ran exploratory simulations, with the objective of identifying which parameters affect the ANG system performance significantly. Finally, we

study the influence of the tank size in the results, thus comparing the validation results with the same geometry, but scaled in 2 and 5 times of the original size.

#### 4.6.3.1 Mesh Sensitivity

On using the fig. 4.1 as reference, fig. 4.3 shows the sections and their correspondent refinements with parameters representing the quantity of points in each section. Boundary 7 was divided into three parts for convenience. The table below presents the values that describe the mesh geometry.

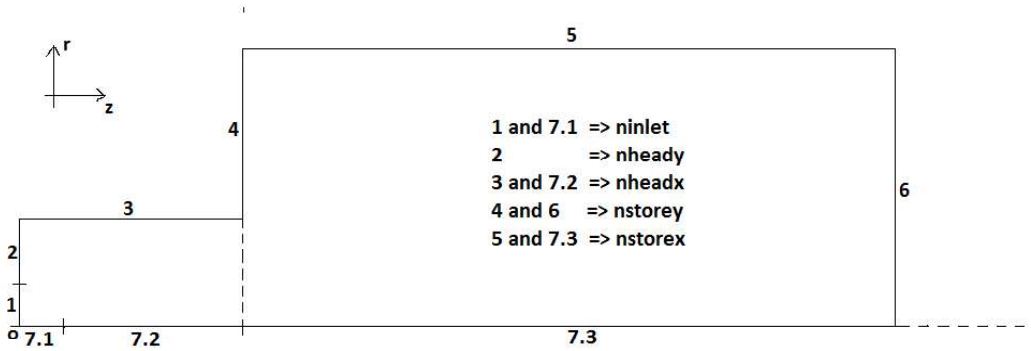


**Figure 4.3:** Schematic of a ANG Storage System for mesh geometry

**Table 4.5:** Mesh Refinement

| Test | ninlet | nheady | nheadx | nstorey | nstorex | Number of Elements | Simulation time (hh:mm) |
|---|---|---|---|---|---|---|---|
| 1 | 3 | 10 | 10 | 2 | 10 | 266 | 04:00 |
| 2 | 5 | 10 | 10 | 5 | 20 | 490 | 06:20 |
| 3 | 10 | 10 | 5 | 5 | 25 | 494 | 06:30 |
| 4 | 10 | 15 | 15 | 5 | 20 | 676 | 09:50 |
| 5 | 10 | 15 | 15 | 5 | 20 | 614 | 09:15 |
| 6 | 10 | 15 | 15 | 10 | 30 | 886 | 12:15 |

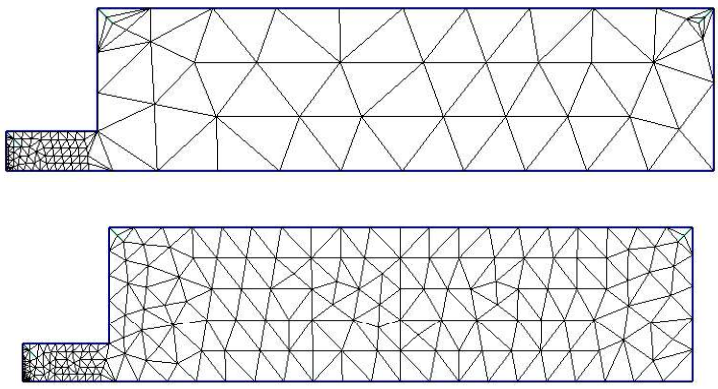

**Figure 4.4:** Mesh Geometry of tests 1 and 2

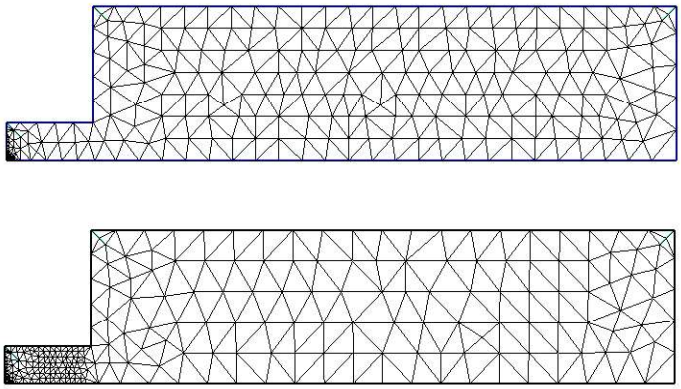

**Figure 4.5:** Mesh Geometry of tests 3 and 4

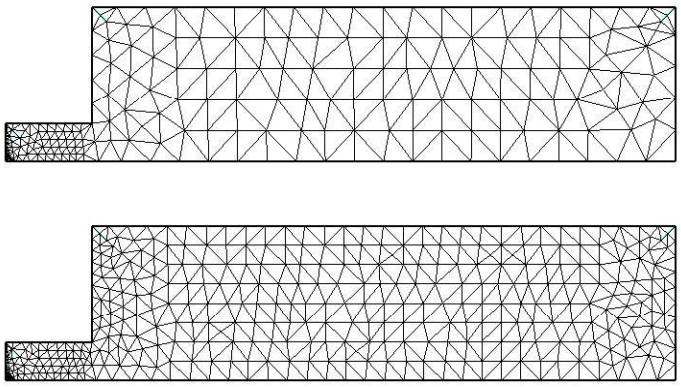

**Figure 4.6:** Mesh Geometry of tests 5 and 6

Table 4.6 shows the comparison between results in some time steps, where $\bar{T}$ represents the volume average temperature inside the tank, $p$ is the pressure, $\dot{m}$ is the mass flow rate and $V/V$ is the ratio between the volume of gas under STP conditions and the volume of the tank.

**Table 4.6:** Evolution of Temperature for different mesh refinements

| Test | $\dot{m}$ $(g/s)$ | $\bar{T}$ (60s-K) | $\bar{T}$ (120s-K) | $\bar{T}$ (180s-K) | $\bar{T}$ (210s-K) | Filling Time (s) | $\bar{T}$ (end-K) |
|---|---|---|---|---|---|---|---|
| 1 | 0.353107 | 315.878 | 327.060 | 333.520 | 335.433 | 233 | 336.145 |
| 2 | 0.353107 | 316.026 | 327.219 | 333.671 | 335.639 | 232 | 336.629 |
| 3 | 0.353107 | 316.018 | 327.206 | 333.653 | 335.607 | 232 | 336.619 |
| 4 | 0.353107 | 316.023 | 327.214 | 333.664 | 335.631 | 232 | 336.620 |
| 5 | 0.353107 | 316.024 | 327.218 | 333.671 | 335.640 | 232 | 336.630 |
| 6 | 0.353107 | 316.051 | 327.235 | 333.683 | 335.652 | 232 | 336.643 |

The results show an error below 0.2% for the average temperatures with respect to the tests analysed two by two. The mass flow at the inlet has an error below $10^{-6}$ and the filling time changes $1s$ only in the test 1, which uses a coarse mesh. Table (4.7) shows the evolution of the pressure:

The same behavior was found for pressure. The errors still remain below 0.2%

**Table 4.7:** Evolution of Pressure for different mesh refinements

| Test | P (60s-MPa) | P (120s-MPa) | P (180s-MPa) | P (210s-MPa) |
|---|---|---|---|---|
| 1 | 0.221203 | 0.875110 | 2.05144 | 2.81235 |
| 2 | 0.222009 | 0.877498 | 2.05512 | 2.84511 |
| 3 | 0.221970 | 0.877315 | 2.05468 | 2.84395 |
| 4 | 0.221995 | 0.877420 | 2.05493 | 2.84486 |
| 5 | 0.221997 | 0.877482 | 2.05512 | 2.84512 |
| 6 | 0.221153 | 0.877742 | 2.05539 | 2.84544 |

and it is consistent with the filling time, which value is the time instant when the pressure inside the tank archieves 3.5 MPa.

**Table 4.8:** Evolution of V/V for different mesh refinements

| Test | $V/V$ (60s) | $V/V$ (120s) | $V/V$ (180s) | $V/V$ (210s) | $V/V$ (end) |
|---|---|---|---|---|---|
| 1 | 15.4523 | 31.7348 | 48.0027 | 55.8575 | 62.3413 |
| 2 | 15.4524 | 31.7350 | 48.0032 | 55.1289 | 61.8129 |
| 3 | 15.4524 | 31.7350 | 48.0032 | 55.1289 | 61.8129 |
| 4 | 15.4524 | 31.7350 | 48.0032 | 55.1289 | 61.8129 |
| 5 | 15.4524 | 31.7350 | 48.0032 | 55.1289 | 61.8129 |
| 6 | 15.4524 | 31.7350 | 48.0032 | 55.1289 | 61.8129 |

For $V/V$, the differences are below $10^{-4}$, except in the coarse mesh (Test 1).

With these results, we choose test 2 as a reference to validations tests, because it has a good precision (necessary to the Adjoint Method) and the processing time is suitable, considering the simulations were done in an ordinary computer.

#### 4.6.3.2 Validation Tests

Figs. 4.7 to 4.8 present the evolution of maximum temperature and the average pressure during the filling process. External natural convection was considered in these simulations.

At $10L/min$, our values of pressure during the filling time are between the numerical and experimental results reported by Sahoo e John (2011). On considering $3.5MPa$ as the target pressure, our simulation achieved this value in 618 seconds, that is, $22s$ before that of the reference. Our values of maximum temperature were over those from Sahoo e John (2011). However, the maximum difference between numerical simulations was $4K$, which represents 1.15%.

Results using $30L/min$ were error better than those for $10L/min$. The pressure achieved 3.5 MPa in $215s$, which is very close to COMSOL simulation

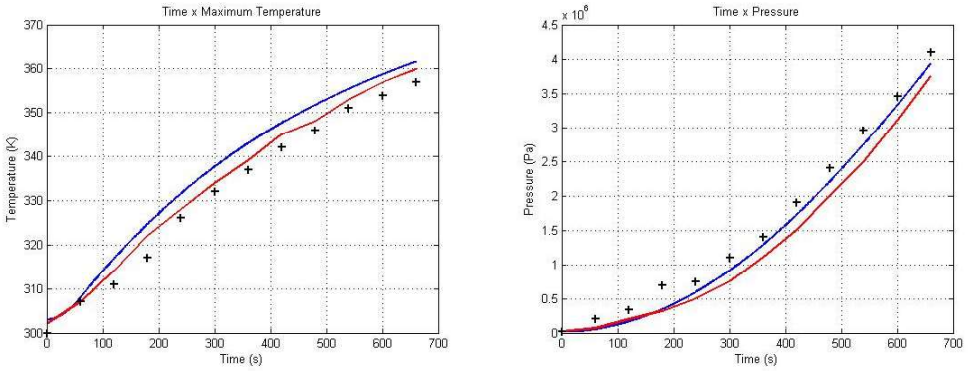


**Figure 4.7:** Results from 10 L/min - Blue: Simulations using FREEFEM++; Red: Numerical Simulations performed by Sahoo e John (2011) using COMSOL; Black points: Experimental Tests performed by Sahoo e John (2011)

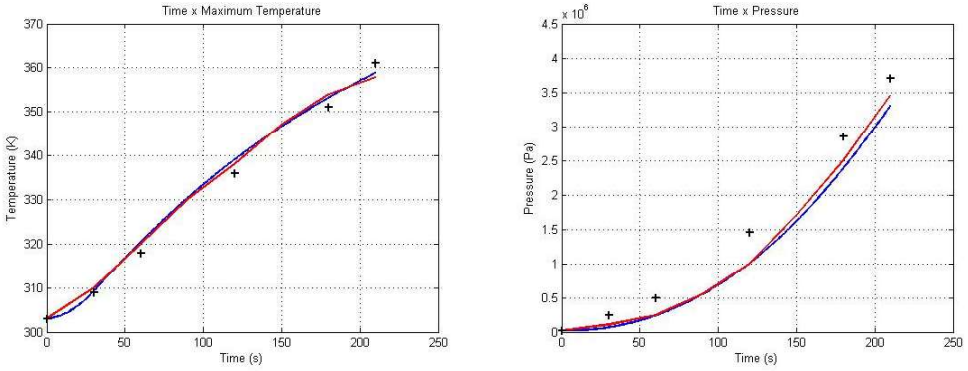


**Figure 4.8:** Results from 30 L/min - Blue: Simulations using FREEFEM++; Red: Numerical Simulations performed by Sahoo e John (2011) using COMSOL; Black points: Experimental Tests performed by Sahoo e John (2011)

($3.5MPa$ in $212s$). The differences between the maximum temperatures were less than $1K$, and the maximum temperature in $212s$ was $359.1K$

The figs. 4.9 and 4.10 illustrate the temperature evolution found in our simulations, for both values of volumetric flow rate.

Fig. 4.11 shows that the sensitivity of $q$ to the filling volumetric flow rate. As the pressure increases, a small volumetric flow can store more adsorbed gas and the difference between higher values also grows up. The reason for that could be seen in figs. 4.9 and 4.10 where at the end of the filling process ($600s$ and $300s$ respectively), the values of pressure are the same, but the temperature distributions are totally different. At $30L/min$, almost the whole volume was at temperatures that are close to $360K$. On the other hand, the higher values of temperature in the simulation with $10L/min$ are located in a small region near to the center of the tank. The major part is in green scale, which represents temperatures close to $340K$.

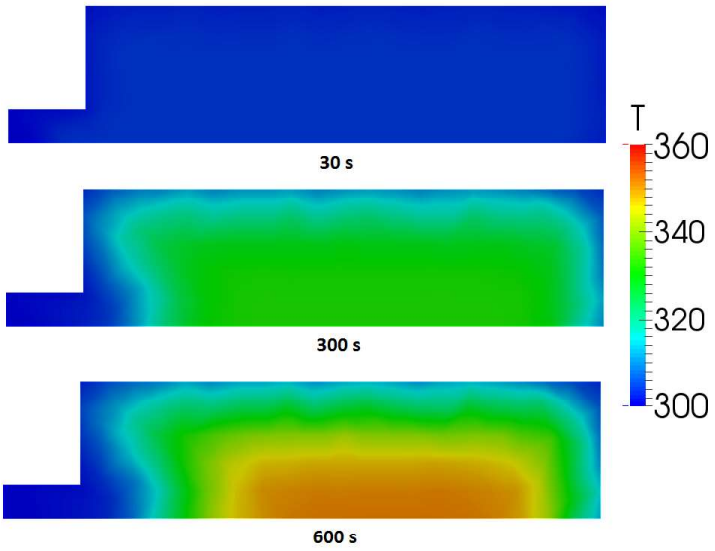


**Figure 4.9:** Temperature distribution for volumetric flow = 10 LPM

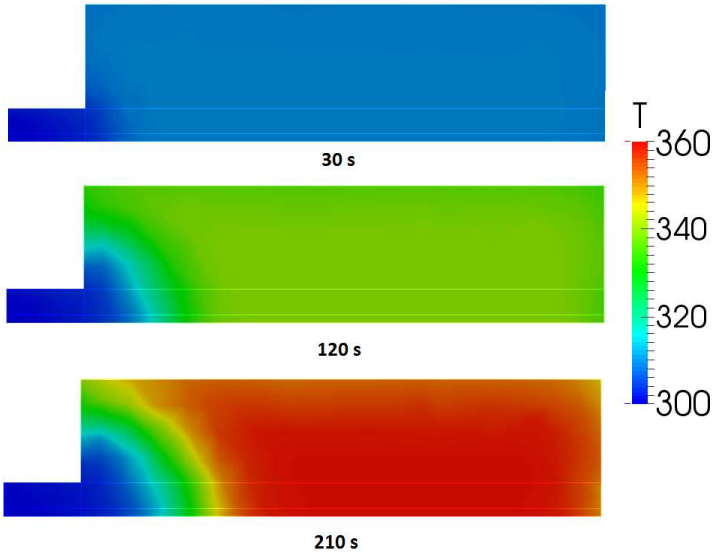


**Figure 4.10:** Temperature distribution for volumetric flow = 30 LPM

This difference is also related to heat transfer through the tank walls. Both tests have the same ambient temperature, but the amount of energy produced in the system is greater at $30L/min$, and it seems that there is not enough time to dissipate this amount of heat. The result is a rapid increase in temperature. To put the difference in numbers, the density of adsorption is 3.1% greater at $10L/min$ in compassion with $30L/min$.

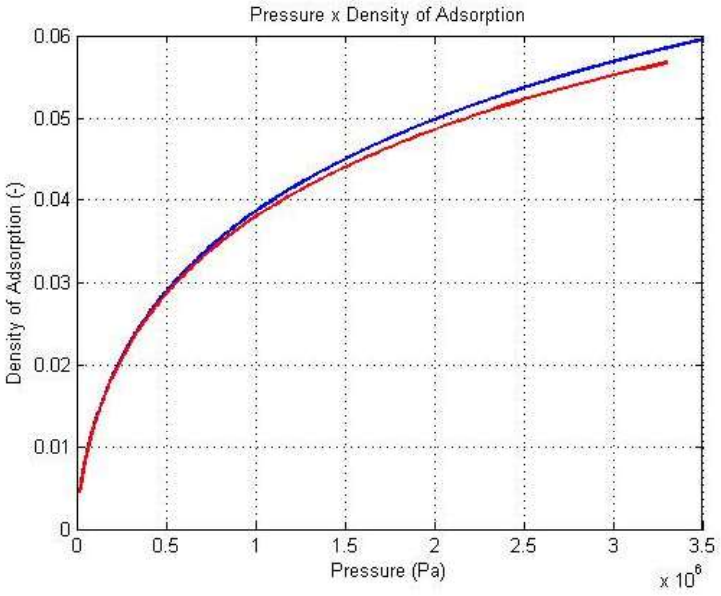


**Figure 4.11:** Average density of adsorption at different values of pressure. Blue: 10L/min; Red: 30L/min

## 4.7 Exploratory Simulations

### 4.7.1 Comparison with isothermal process

On considering the validation tests, one can evaluate the values of density of adsorption for different pressures, but without any temperature variations (isothermic process). In this scenario, one can use the eqs. (3.47) − (3.50) at ambient temperature ($300K$) to evalute the density of adsorption in an isothermic process. Fig. 4.12 shows the results.

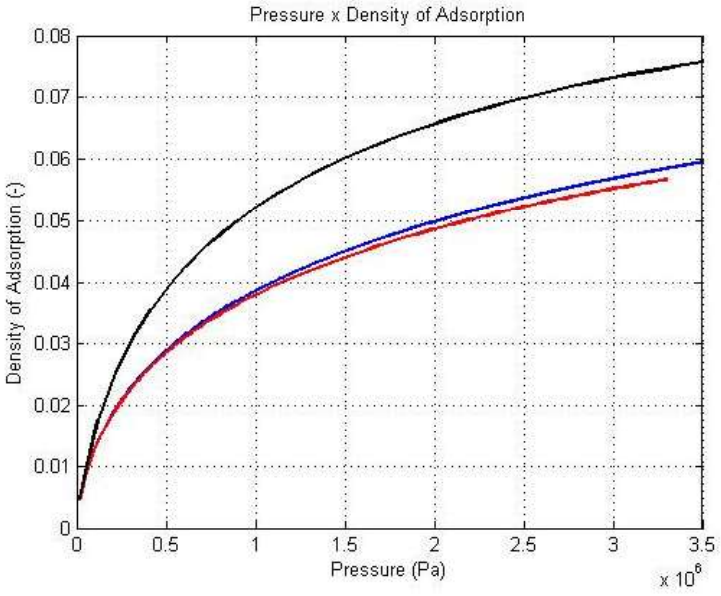


**Figure 4.12:** Average density of adsorption at different values of pressure. Blue: 10L/min; Red: 30L/min; Black: Isothermal - 300K

The amount of gas adsorbed in an isothermal process is 28.7% greater than that of the simulation with $10L/min$, and this difference is very relevant. There are two possibilities to achieve an isothermal process:

- By Filling the tank with lower volumetric flow rate, but the consequence is a large time span of the process and probably this is not a suitable economic alternative;
- Management of the heat produced during the filling process. This is better than first alternative because there is a possibility of keeping the same filling time while achieving a larger amount of stored gas. In the chapter 2, we discuss important considerations about this theme.

### 4.7.2 Forced Convection

As the heat management is a means of increasing the tank capacity, it is important to consider a forced convection outside of it, so as to increase the heat dissipation. To that end, the flow rate of $30L/min$ was considered for two distinct values for the external convection coefficient, 5.0 $W/K$ and 700.0 $W/K$. The results of maximum temperature and pressure are presented in the figs. 4.13 and 4.14:

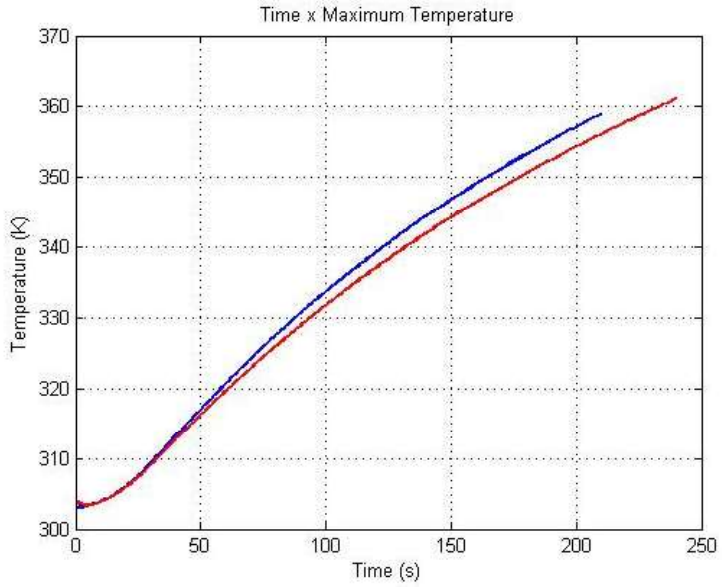


**Figure 4.13:** Maximum Temperature from $30LPM$ - Blue: $h = 5\ W/m^2K$; Red: $h = 700\ W/m^2K$

The difference between filling times, when the pressure achieve $3.5MPa$, was $20s$, which represents an increase of 9.4%. The maximum temperature was not

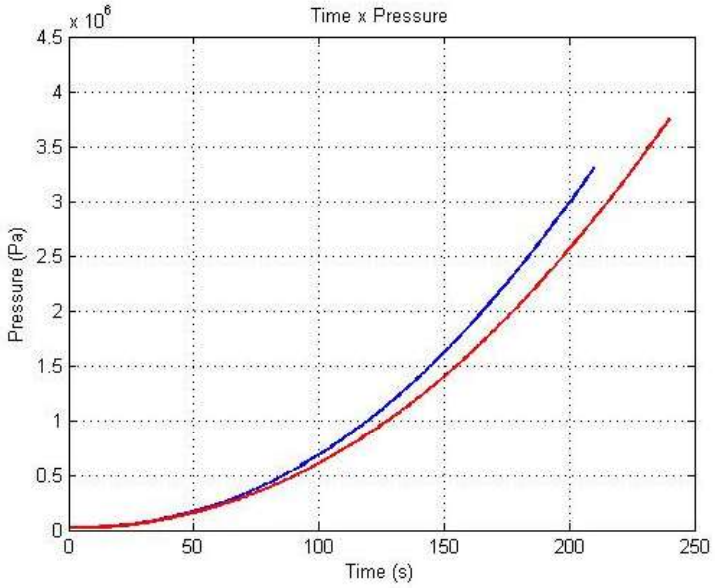


**Figure 4.14:** Pressure from $30LPM$ - Blue: $h = 5\ W/m^2K$; Red: $h = 700\ W/m^2K$

changed from $359K$. The figs. 4.15 and 4.16 represent the average temperature inside the tank and the density of adsorption with compassion between the isothermal process:

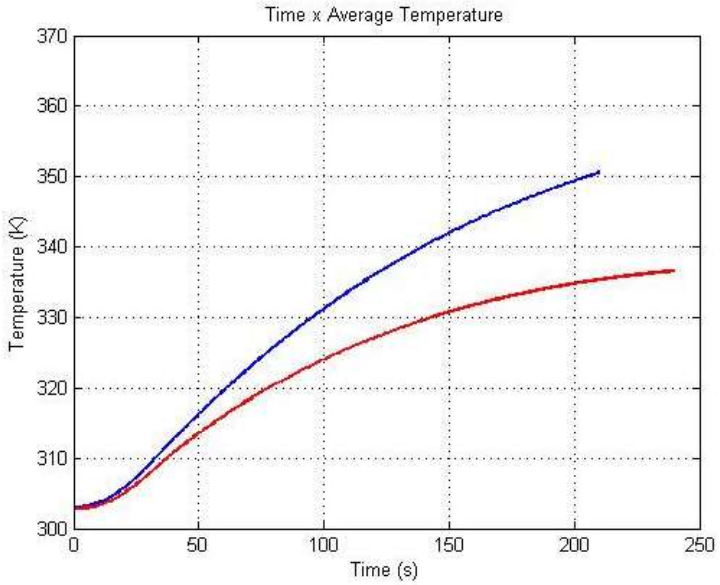


**Figure 4.15:** Average Temperature from $30LPM$ - Blue: $h = 5\ W/m^2K$; Red: $h = 700\ W/m^2K$; Black: Isothermal - $300K$

There is an important increase of storage capacity. The average temperature decreases from $350.6K$ to $336.6K$, which represents a reduction of 3.99%. The average density of adsorption increases from 0.05624 to 0.06277, which represents 11.6%. However, the isothermal process stores 19.8% more adsorbed gas in comparison between a tank with $h = 700\ W/m^2K$. The results are in agreement with

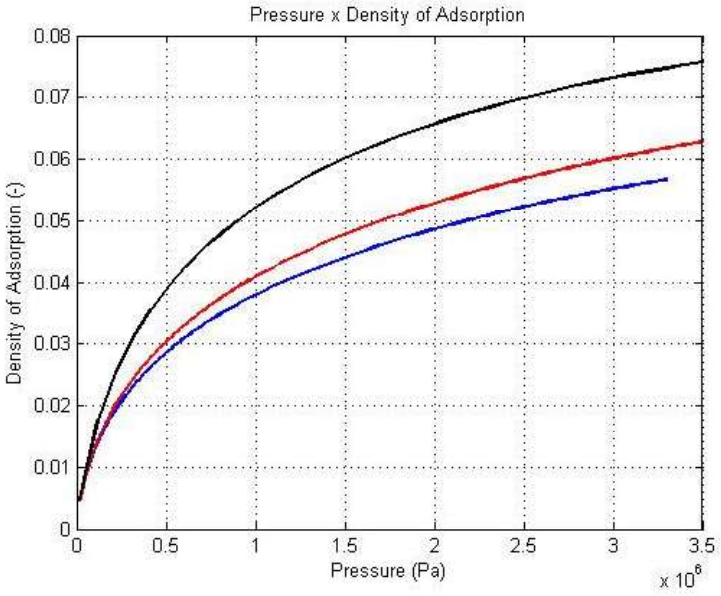


**Figure 4.16:** Density of Adsorption from $30LPM$ - Blue: $h = 5\ W/m^2K$; Red: $h = 700\ W/m^2K$; Black: Isothermal - $300K$

Sahoo e John (2011) that found the same behavior in their simulations.

It is important to observe that the differences between the temperature distributions of the tests. Fig. 4.17 shows the reduction of temperature close to the tank walls in the test with forced convection. By considering a cylinder geometry, this region has more volume that the region close to the symmetry axis. Then, the quantity of gas stored increase significantly.

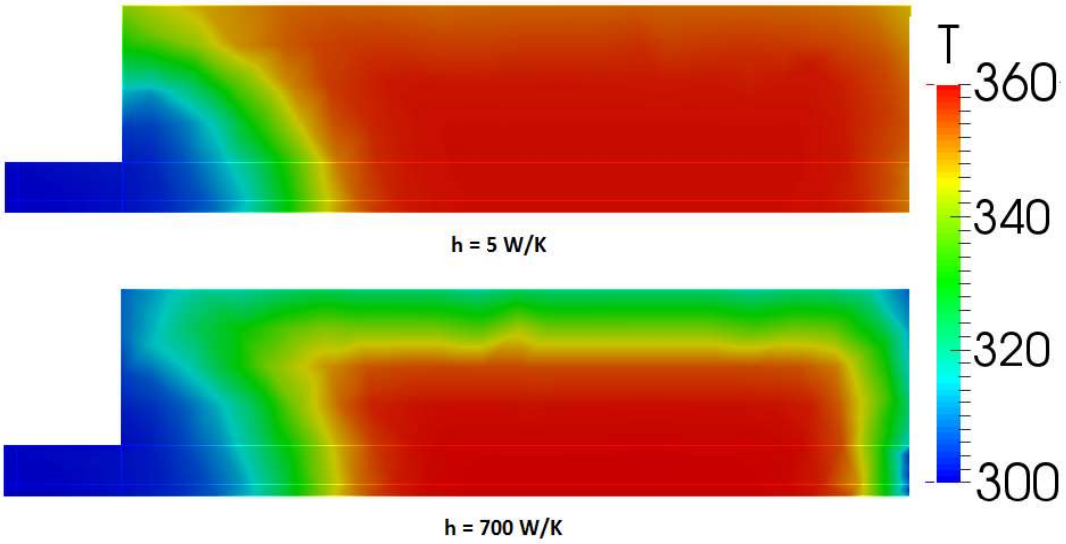


**Figure 4.17:** Temperature distribution for volumetric flow = 30 L/min

### 4.7.3 Aspect Ratio analysis

The tank geometry is also important to thermal management. According to the literature, the tank aspect ratio contributes to a greater heat transfer and a consequent reduction of the temperature inside the tank. For these simulations, we consider $30L/min$ as volumetric flow rate and two values of Aspect Ratio: 1.9 which is the value used in validation tests and 7.8. The aspect ratio is defined as the ratio between length and diameter:

$$LD = \frac{L_2}{2r_2} \tag{4.44}$$

Where $L_2$ and $r_2$ are defined in figure 4.1.

The results of pressure and maximum temperature are presented in the figs. 4.18 and 4.19. We also consider a forced external convection in this analysis:

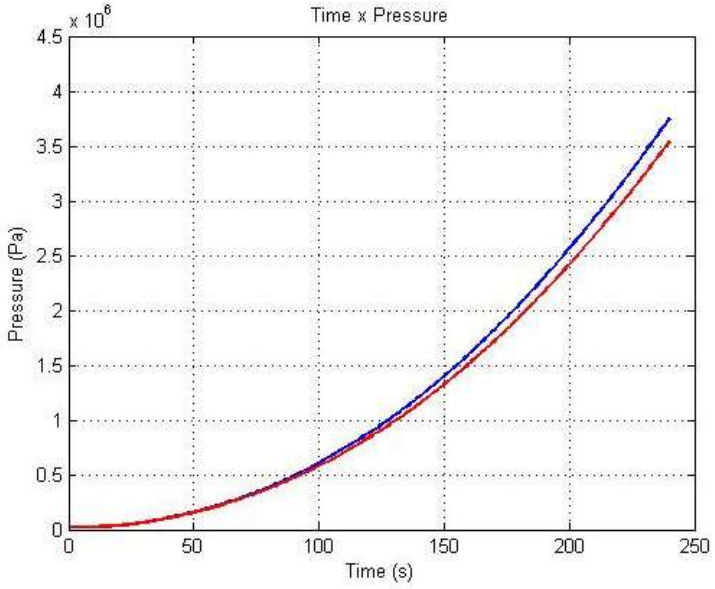


**Figure 4.18:** Inside Pressure from $30LPM$ - Blue: $LD = 1.9$; Red: $LD = 7.8$

The difference between filling time for the test with aspect ratio 7.8 and 1.9 was $7s$ which represents an increase of 3.0%. With the reduction of pressure, the filling process spend more time to archive $3.5MPa$.

The maximum temperature reduces only from $359K$ to $358.1K$. However, as we seen in the previous test, the temperature distribution is more important in the quantity of gas inside the tank that the value of maximum temperature itself. It is more important the regions close to the tank walls has less values of temperature than the central region, with is located the maximum temperature.

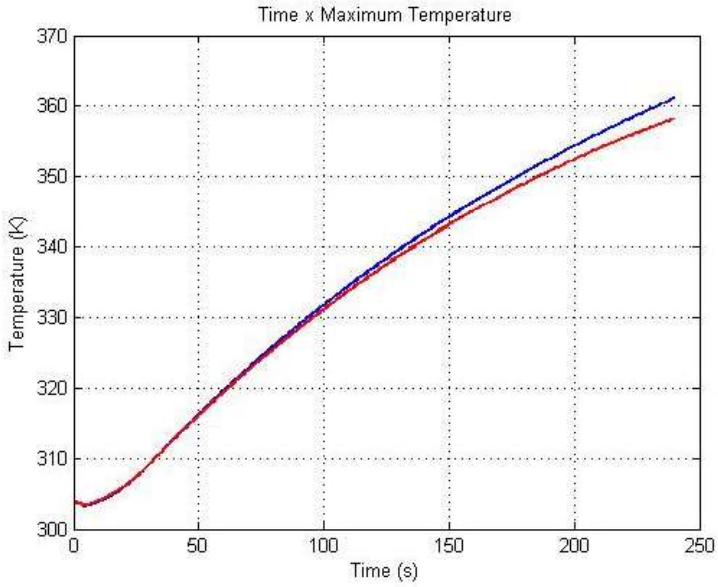


**Figure 4.19:** Maximum temperature from $30LPM$ - Blue: $LD = 1.9$; Red: $LD = 7.8$

The figs.(4.20) and (4.21) represent the average temperature inside the tank and the density of adsorption in a compassion between the isothermal process:

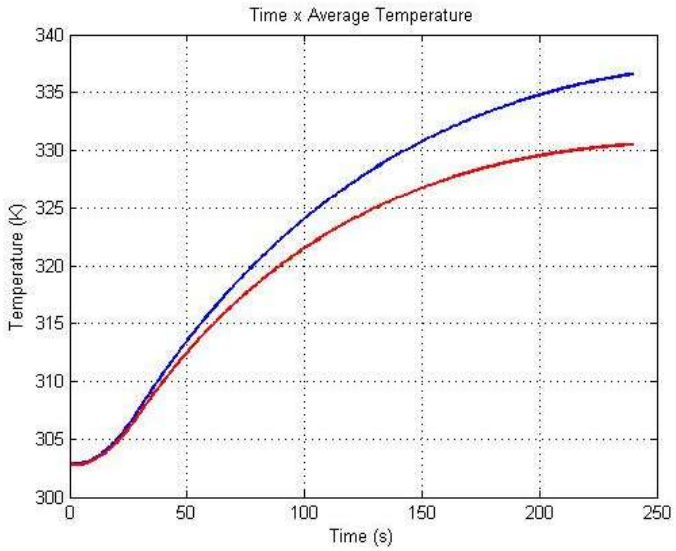


**Figure 4.20:** Average Temperature from $30LPM$ - Blue: $LD = 1.9$; Red: $LD = 7.8$; Black: Isothermal - $300K$

In this test, we can see the increase in storage capacity. The average temperature reduces from $336.3K$ ($LD = 1.9$) to $330.5K$ ($LD = 7.8$), which represents a reduction of 1.72%. Consequently, the average density of adsorption increases, from 0.06277 for $LD = 1.9$ to 0.06470 for $LD = 7.8$, which represents 3.0% rise. The isothermal process stores 16.25% more adsorbed gas in comparison with a tank with $LD = 7.8$ with external forced convection. The results are in agreement with Sahoo e John (2011) who found the same behavior in their simulations.

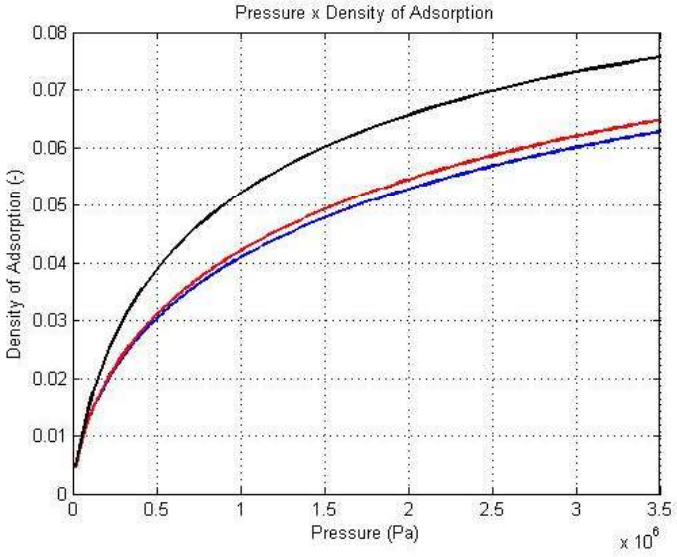


**Figure 4.21:** Density of adsorption from $30LPM$ - Blue: $LD = 1.9$; Red: $LD = 7.8$; Black: Isothermal - $300K$

Fig.(4.22) present the temperature distribution for both cases. The test with larger aspect ratio concentrates the higher values of temperature ($> 340K$) close to the symmetry axis, below of the 50.0% of the tank radius, more precisely. The test with aspect ratio 1.9 has temperatures above $340K$ close to the tank walls, where is concentrated the major of the tank volume. The consequence is the reduction of the quantity of the gas stored.

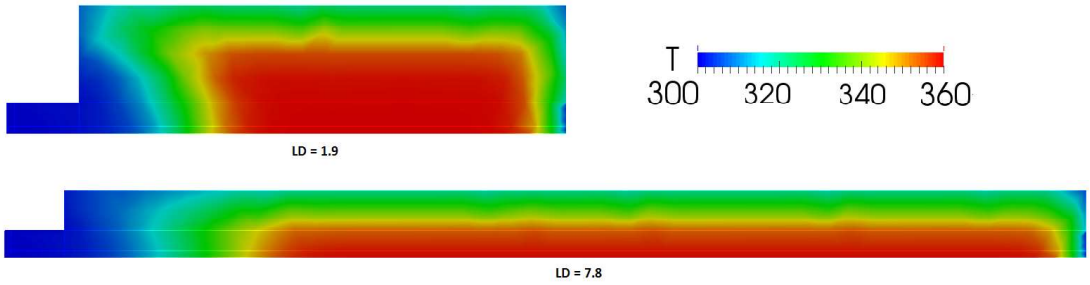


**Figure 4.22:** Temperature distribution for volumetric flow= 30 L/min

### 4.7.4 Tubular Heat Exchangers

One of possible solutions to increase the quantity of gas inside the tank is the heat management during the filling process. Because of the limitation of axisymmetric model, we considered only tubular heat exchangers positioned in radial direction.

The tank geometry is the same of the validation tests (SAHOO; JOHN, 2011), and the analysis is divided in three parts: Quantity and position of tubes using the same tube diameter, conservation of heat exchanger surface, changing diameter

and number of tubes and the previous simulations varying a heat exchanger fluid temperature.

#### 4.7.4.1 Quantify and Position of tubes

These tests using a 5 mm diameter tubes and varying their quantity and position. The temperature of the fluid inside the tubes was kept at 300 K in all tests and the coefficient of heat transfer was $7000 W/m^2K$. With this values, we can define a wall boundary condition for the heat exchanger analogous to eqs. 4.31 and 4.32. Natural convection conditions are imposed on the tank walls, because the objetive here is identify the performance of the heat exchangers.

The Fig. 4.23 explains the nomenclature:

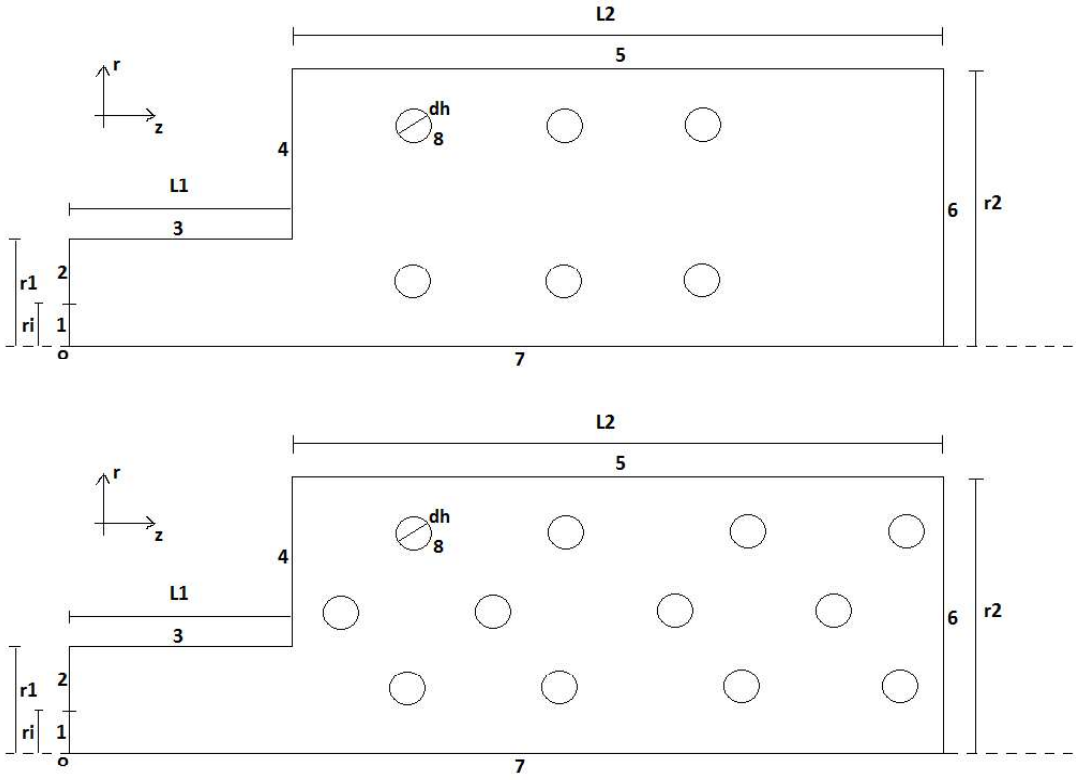


**Figure 4.23:** Ilustration of tubular heat exchanger geometry. Up: Two lines and three colums in aligned configuration; Down: Three lines and four colums in tandem configuration

Table 4.9 presents the values for the tests that were performed. "Config." means tubes configuration either aligned (L) or tandem (T), $R_i$ represents the radial position of the lines referred to the center of the tank, in $mm$, and $Z_i$ is the axial position of the tubes in the same line which is expressed in percents of $L_2$.

To make it clear, fig. 4.24 presents the geometry of the tests 4,5,7 and 8. The

**Table 4.9:** Heat Exchanger Tests - Same Diameter

| Test | Config. | Matrix | $R_1$ | $R_2$ | $R_3$ | $Z_1$ | $Z_2$ | $Z_3$ | $Z_4$ | obs. |
|---|---|---|---|---|---|---|---|---|---|---|
| 1 | L | 1x1 | 10 | $N/A$ | $N/A$ | 50.0 | $N/A$ | $N/A$ | $N/A$ | |
| 2 | L | 1x2 | 10 | $N/A$ | $N/A$ | 33.3 | 66.7 | $N/A$ | $N/A$ | |
| 3 | L | 1x3 | 10 | $N/A$ | $N/A$ | 25.0 | 50.0 | 75.0 | $N/A$ | |
| 4 | L | 2x3 | 10 | 26 | $N/A$ | 25.0 | 50.0 | 75.0 | $N/A$ | |
| 5 | L | 3x3 | 10 | 26 | 42 | 25.0 | 50.0 | 75.0 | $N/A$ | |
| 6 | L | 3x4 | 10 | 26 | 42 | 20.0 | 40.0 | 60.0 | 80.0 | |
| 7 | T | 3x4 | 10 | 26 | 42 | 15.0<br>25.0 | 35.0<br>45.0 | 55.0<br>65.0 | 75.0<br>55.0 | Lin. 1,3<br>Line 2 |
| 8 | T | 3x4 | 10 | 26 | 42 | 25.0<br>15.0 | 45.0<br>35.0 | 65.0<br>55.0 | 85.0<br>75.0 | Lin. 1,3<br>Line 2 |

results were post-processed in MATLAB and presented as follows. It is important to point out that as the number of tubes grows, the internal volume that is available to store gas reduces, and the $V/V$ parameter must be used carefully. To make a precise compassion, the reference volume will be a geometric volume of the cylinder, which is 1.82 L in these tests.

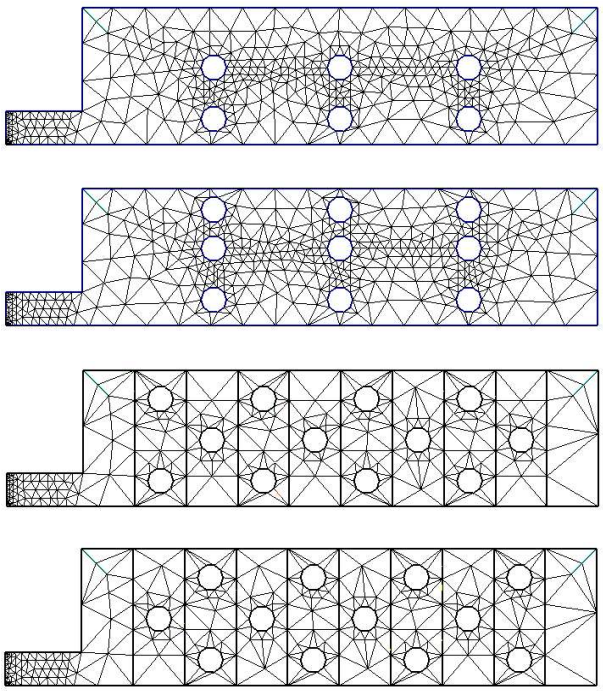

**Figure 4.24:** Mesh geometries of tests 4,5, 7 and 8 respectively

The reference result is the filling process in a tank without heat exchanger, presented in the validation tests. As we insert new tubes, the average temperature reduces and the filling time grows up. However, that does not mean an increase in $V/V$. The figs. 4.25 and 4.26 present the results for the tests 1,2 and 3.

For the test 1, the temperature reduces to 350.8 K but $V/V$ kept at 57.49, the same value of the reference simulation (57.50). In the tests 2 and 3, the

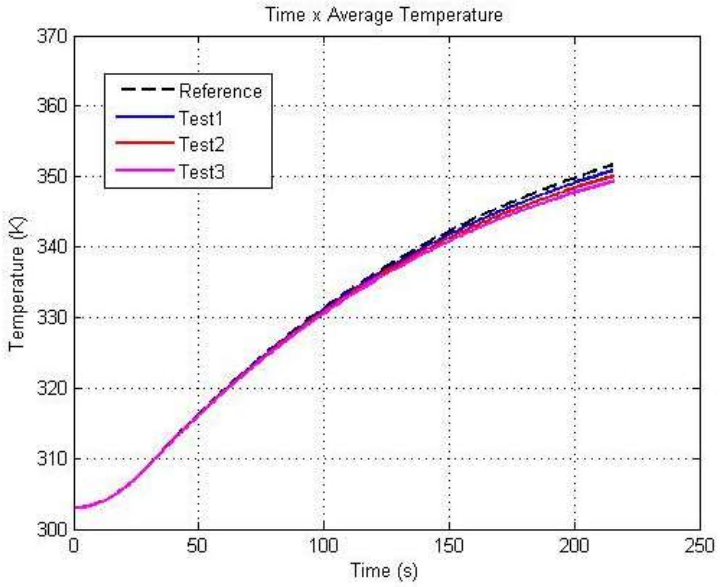


**Figure 4.25:** Results from Tests 1 to 3: Evolution of volumetric average temperature

results were marginally better with a increase in $V/V$ to 57.75 for both tests. The average temperature is reduced to 350.1 and 349.4 K. The reason for low difference between these tests was the reduction of available volume to store gas (0.50% in test 2 and 0.76% in the test 3) by the addition of tubes, which affects the gain due to reduction of average temperature.

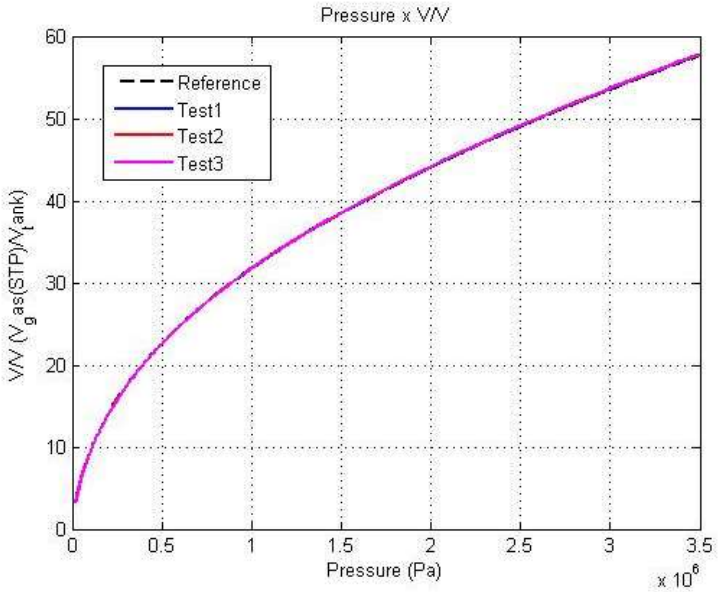


**Figure 4.26:** Results from Tests 1 to 3: Evolution of $V/V$ at the same pressure.

On the other hand, the density of adsorption increases as tubes are added. For test 1, the average value of $q$ increases by 0.38% and for tests 2 and 3, the growth in the adsorption densities are 1.02 and 1.37% respectively. The fig.(4.27) presents the influence in temperature distribution close to the tubes. Each tube

creates a region where the temperature reduces and the density of adsorption increases as consequence.

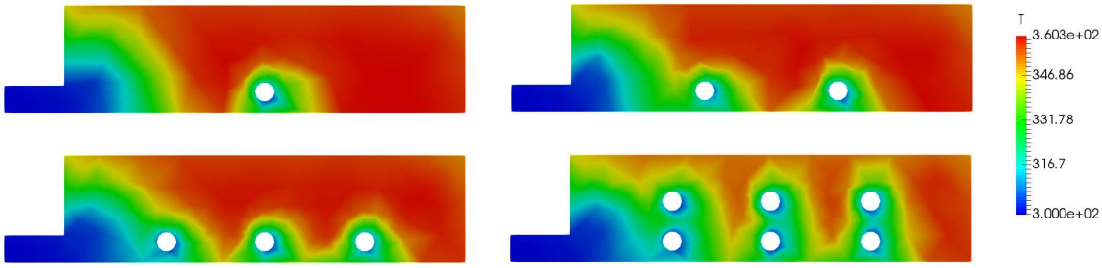


**Figure 4.27:** Temperature distribution for volumetric flow= 30 L/min (Tests 1,2,3 and 4)

For tests 4 and 5, presented in the figs.(4.28) and (4.29), the increase in $V/V$ was over 1.0%. This low result could be explained, again, by a trade-off between the reduction of available volume (3.05 and 6.47%) to store gas and the gain of density of adsorption, in terms of reduction of the temperature (342.4 K to test 4 and 334.8 K to test 5).

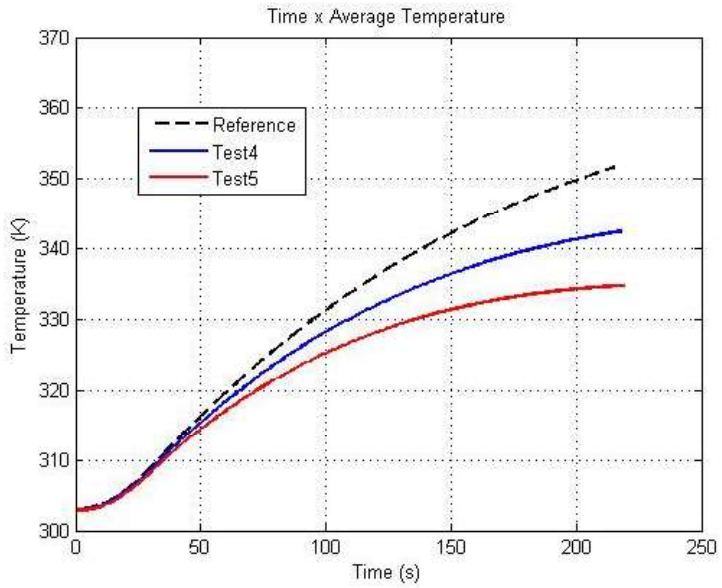


**Figure 4.28:** Results from Tests 4 and 5: Evolution of volumetric average temperature.

On the other hand, on following the previous behavior, as the number of tubes increases, the density of adsorption grows also. For test 4, the density grows by 5.33% and for the test 5, the growth was 10.09%.

The results concerning density of adsorption are another indication of the need to search the best position and the choise of a suitable diameter for the heat exchanger tubes.

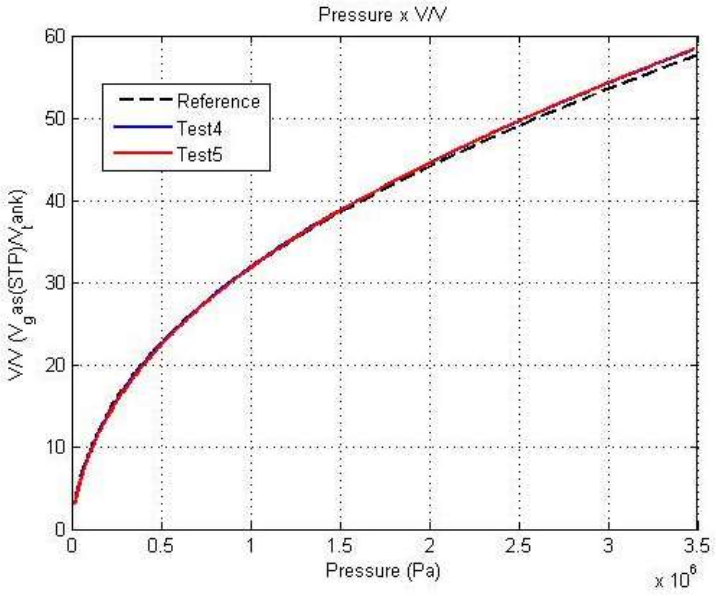


**Figure 4.29:** Results from Tests 4 and 5: Evolution of $V/V$ at the same pressure.

In the figs. 4.30 and 4.31 where are presented the results of the tests 6,7 and 8, we found an important consideration about the position of tubes. The three cases had the same available volume and the increase in $V/V$ in the tests 7 and 8, compared to test 6 were considerable. The value in test 6 was 58.6 with an average temperature of $330.2K$ and for the tests 7 and 8, the values were 59.1 and $328.5K$. Then, the position of the tubes is extremely important and an optimization process, as the one we intend to do, could be very appropriate to find the best configurations.

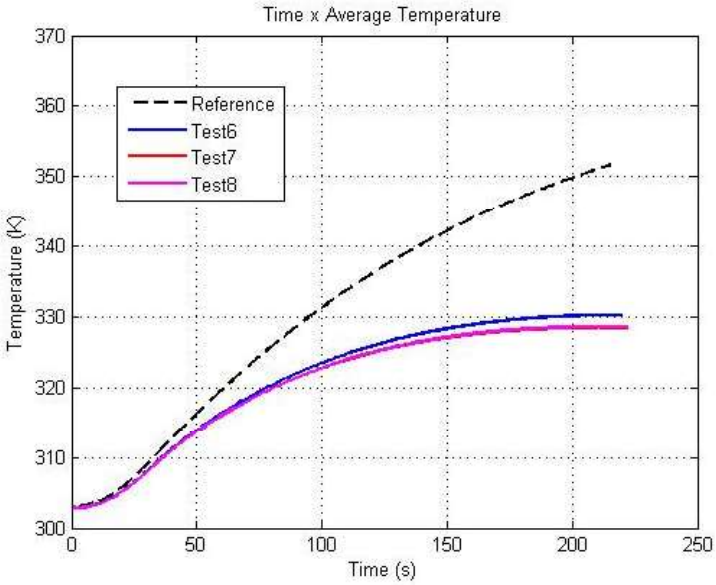


**Figure 4.30:** Results from Tests 6 to 8: Evolution of volumetric average temperature.

As was mentioned in tests 1,2 and 3, the density of adsorption increases in these configurations. For test 6, at the pressure of 3.5 MPa, the growth was 12.7% and for tests 7 an 8, at the same pressure, the values increased by 13.86 and 13.83%, respectively.

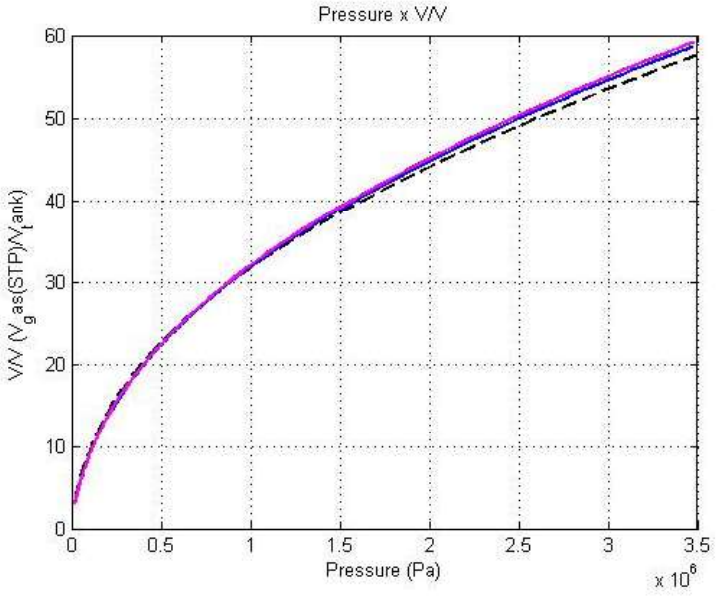


**Figure 4.31:** Results from Tests 6 to 8: Evolution of $V/V$ at the same pressure.

Again, with this growth in the adsorpion eficacy, a geometric optimization could be advantageous to make the best of the improvement and the Adjoint Method appears as an important tool to accomplish this task. Observing the fig.(4.32), the test 8 was able to eliminate almost of the regions with temperatures above $340K$ which consequence is the relevant growing of the quantity of gas stored, measured by the parameter $V/V$.

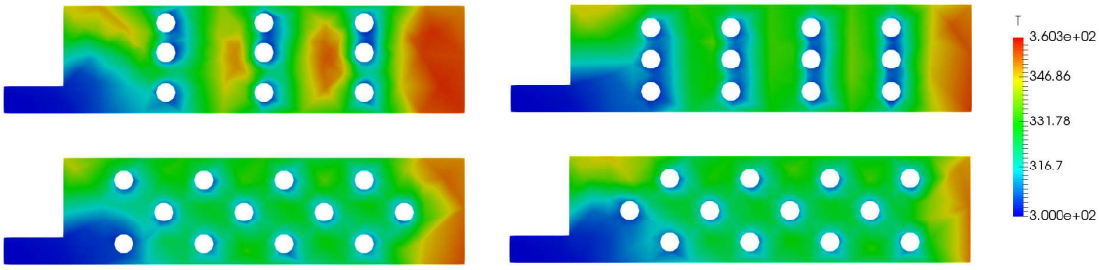


**Figure 4.32:** Temperature distribution for volumetric flow= 30 L/min (Tests 5,6,7 and 8)

### 4.7.4.2 Conservation of the Heat Exchanger Surface Area

Using the value of the heat exchanger tubes surface area that is presented in tests 6,7 and 8, we setup two more tests, by varying the quantity of the tubes

and their diameters. The values of tubes diameters for tests 9 and 10 were 3.94 and 2.35 mm respectively and the mesh geometry is presented in the fig. 4.33. The tables 4.10 and 4.11 present the other parameters:

**Table 4.10:** Heat Exchanger Test 9 parameters

| Test | Config. | Matrix | $R_1$ | $R_2$ | $R_3$ | $R_4$ | $Z_1$ | $Z_2$ | $Z_3$ | $Z_4$ | $Z_5$ |
|---|---|---|---|---|---|---|---|---|---|---|---|
| 9 | T | 4x5 | 10 | 20 | 30 | 40 | 15 | 35 | 55 | 75 | 95 |
| | | | | | | | 5 | 25 | 45 | 65 | 85 |

**Table 4.11:** Heat Exchanger Test 10 parameters

| Test | Config. | Matrix | $R_1$ | $R_2$ | $R_3$ | $R_4$ | $R_5$ | $R_6$ | $Z_1$ | $Z_2$ | $Z_3$ | $Z_4$ | $Z_5$ |
|---|---|---|---|---|---|---|---|---|---|---|---|---|---|
| 10 | T | 6x5 | 8 | 16 | 24 | 32 | 40 | 48 | 15 | 35 | 55 | 75 | 95 |
| | | | | | | | | | 5 | 25 | 45 | 65 | 85 |

The fig.(4.33) presents the mesh geometry of these tests.

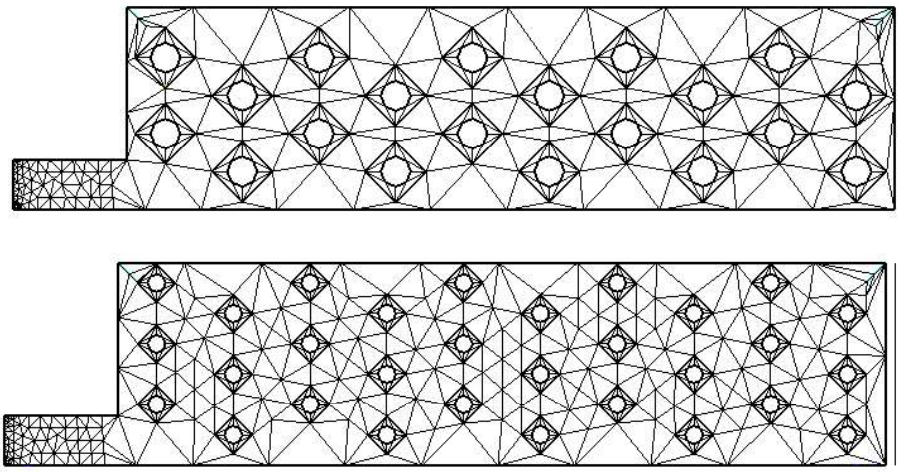

**Figure 4.33:** Mesh geometries of tests 9 and 10 respectively

The results proved that diameter and position of the tubes are relevant in the optimal configuration. The internal volume of test 9 is 1.68 L , more than tests 6,7 and 8 (1.67 L), but the $V/V$ achieves 61.1 instead of 59.1, which represents an increase of 6.2% related to a tank without heat exchanger. The average temperature reduced from 328.5 K in the tests 7 and 8 to 322.9$K$ in the test 9. The figs. 4.34 and 4.35 presents the results for volumetric average temperature and $V/V$.

Test 10 assigns an internal volume of 1.73 L, between the values of tests 5 (1.70) and 4 (1.76L). However, the value of $V/V$ reached 64.4, which represents a increase of 12.0% compared to the baseline case, namely the tank without heat exchanger tubes. The average temperature has reduced to 318.5 K, the lowest of all the tests. As a consequence, the best increases in density of adsorption were

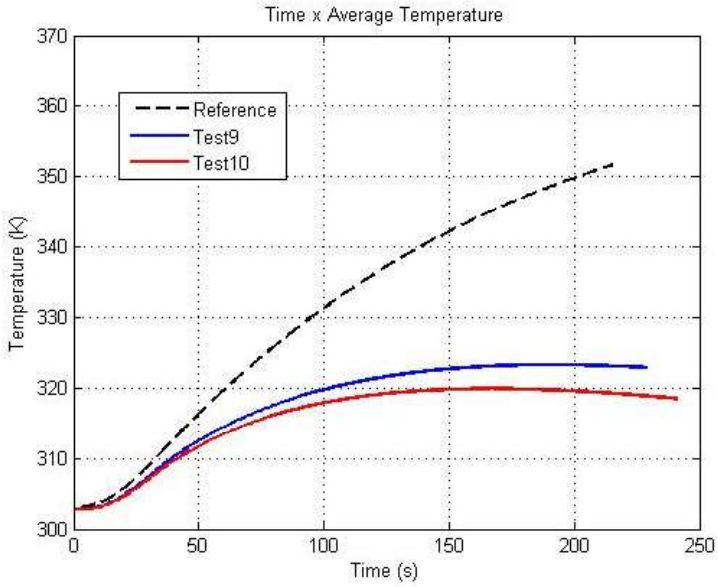


**Figure 4.34:** Results from Tests 9 and 10: Evolution of volumetric average temperature.

found in these two tests. For test 9, the growth was 17.45% and for test 10, the result achieved 20.2% growth.

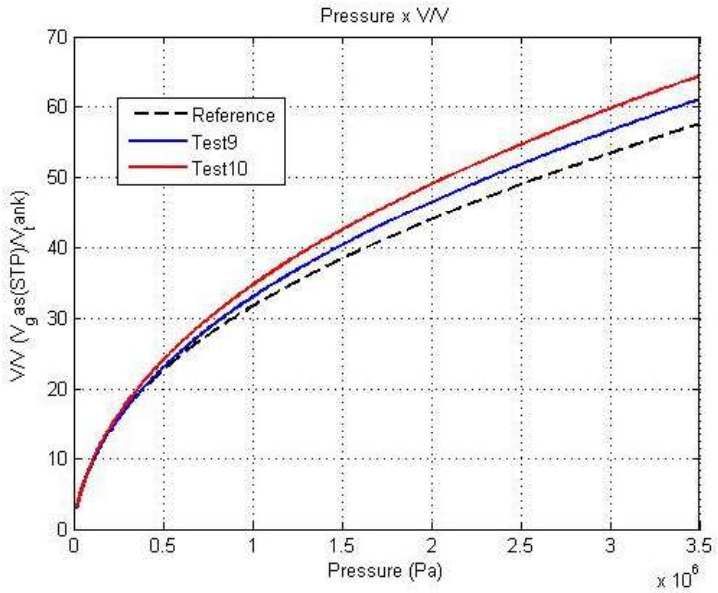


**Figure 4.35:** Results from Tests 9 and 10: Evolution of $V/V$

The results showed the importance of a good choice of the number, diameter and position of the tubes in the heat exchanger. There is a trade-off between the increase in tank capacity (measured by $V/V$) and the available volume inside the tank (which is reduced by the use of the device).

#### 4.7.4.3 Changing the Fluid Temperature

Four tests were performed, on the basis of tests numbers 6,7,9 an 10 of the previous sections. The temperature of the fluid was reduced to 288 K, keeping the heat transfer coefficient at 7000 $W/m^2K$. The figs.(4.36) and (4.37) present the results using the same heat exchanger geometry of the Test 6.

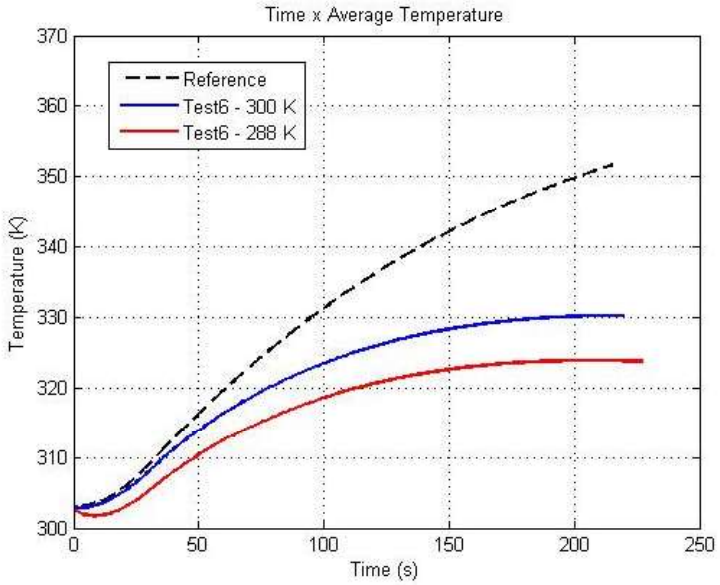


**Figure 4.36:** Results for the test 6 with fluid at $288K$ and $300K$: Evolution of volumetric average temperature.

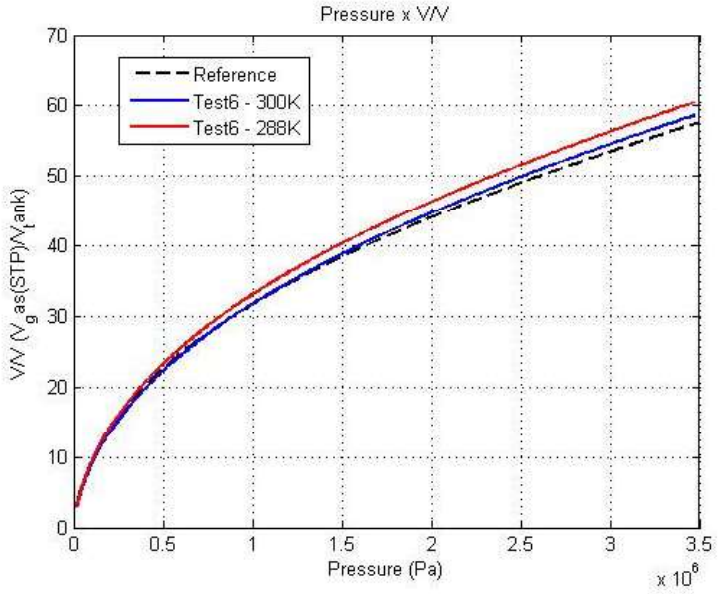


**Figure 4.37:** Results for the test 6 with fluid at $288K$ and $300K$: Evolution of $V/V$

The average temperature inside the tank reduces from 330.6 to 323.8 K and the density of adsorption increased by 3.6% consequently. The $V/V$ has grown

up from 58.59 up to 60.21 which represents a increase of 2.7%.

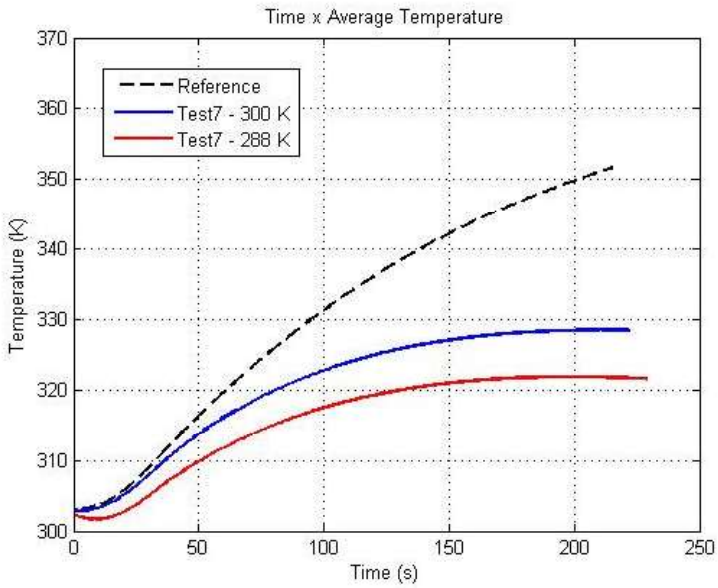


**Figure 4.38:** Results for the test 7 with fluid at $288K$ and $300K$:Evolution of volumetric average temperature.

In test 7, the average temperature inside the tank, presented in the fig. 4.38 reduces from 328.4 to 321.6 K and the density of adsorption increases 3.7% consequently. The $V/V$ grows from 58.9 up to 61.0 as seen in the fig. 4.39.

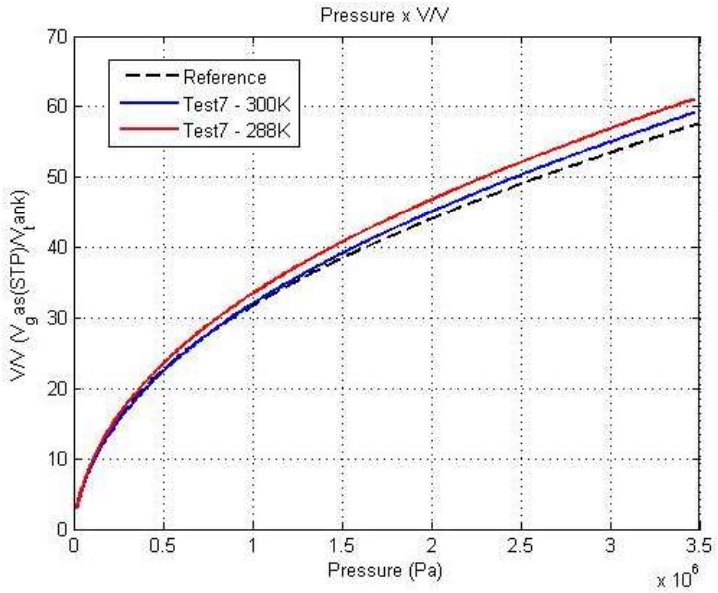


**Figure 4.39:** Results for the test 7 with fluid at $288K$ and $300K$: Evolution of $V/V$

In test 9, the average temperature inside the tank reduces from $322.9K$ to $314.0K$ as presented in the fig. 4.40. The lines of temperature evolution of tests with $288K$ (red) and 300K (blue) are parallel, showing that inlet temperature is not change the behavior of the curve, causing only a vertical displacement.

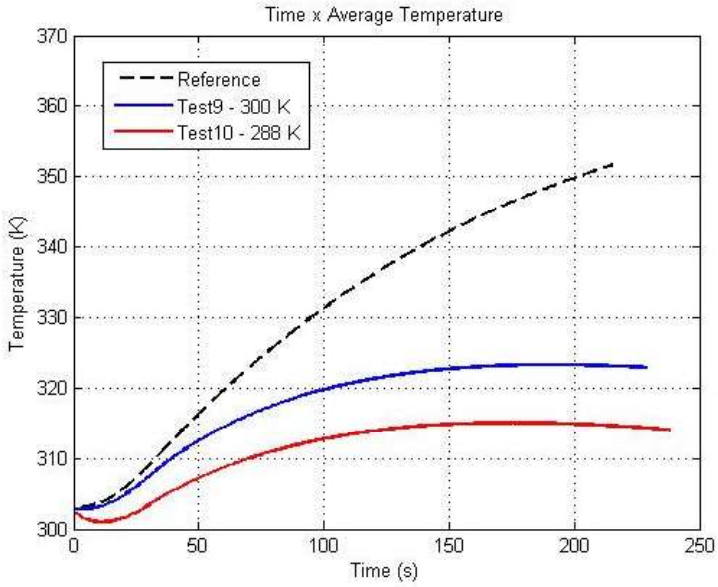


**Figure 4.40:** Results for the test 9. Evolution of volumetric average temperature.

The density of adsorption increases 4.6% due the temperature reduction. For $V/V$, presented in the fig. 4.41, the growing is from 61.0 up to 63.5 which means 4.0% additional gas stored.

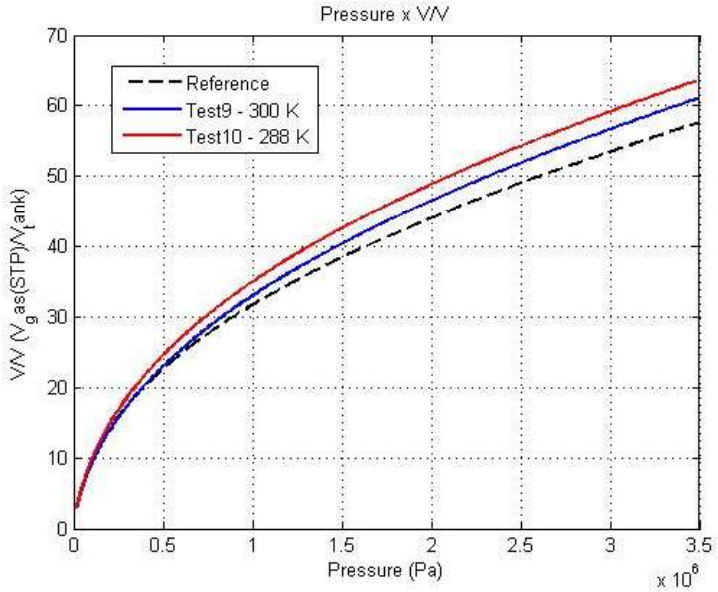


**Figure 4.41:** Results for the test 9. Evolution of $V/V$

And finally in test 10, the average temperature inside the tank reduces from $318.5K$ to 308.6K, as presented in the fig. 4.42, keeping the same parallel behavior of the test 9, with a vertical displacement only.

The density of adsorption increased 5.7%, caused by temperature reduction. The $V/V$ grows up from 64.4 up to 67.4, an increase of 4.7%. The result is

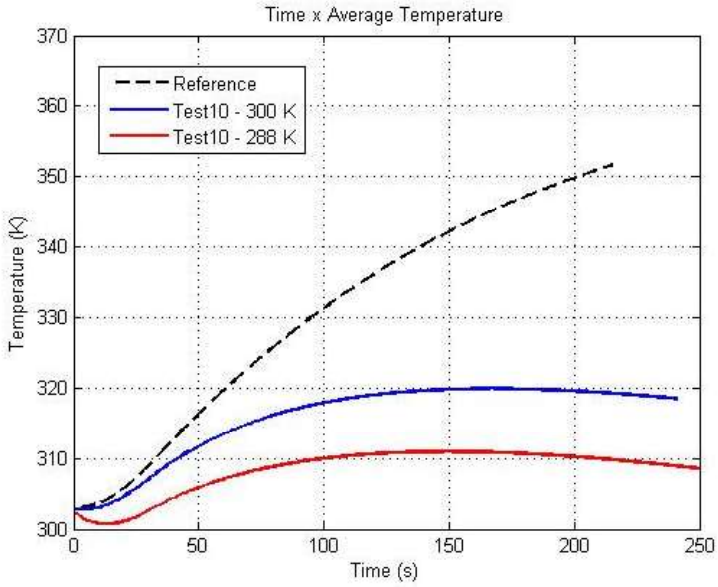


**Figure 4.42:** Results for the test 10. Evolution of volumetric average temperature.

presented in the fig. 4.43.

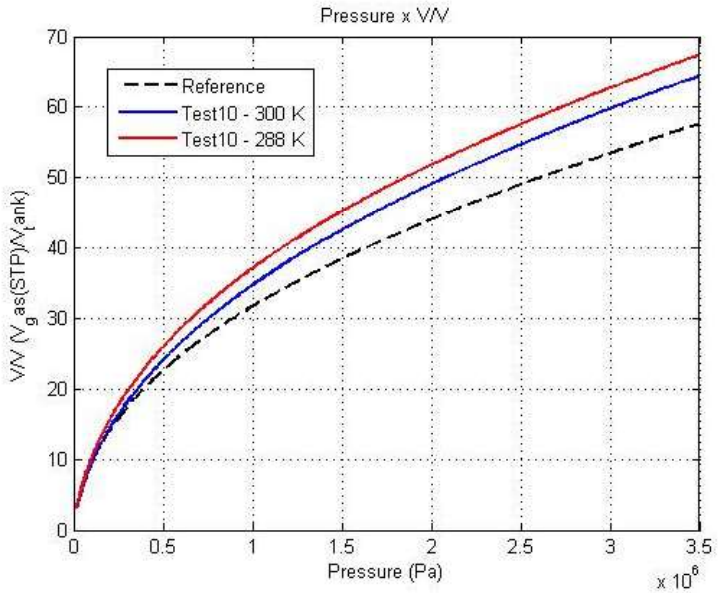


**Figure 4.43:** Results for test 10. Evolution of $V/V$

Since this test was the best in terms of $V/V$, fig. 4.44 shows the behavior of density of adsorption during the filling process.

The fig. 4.44 summarizes the objective of all the tests previously presented. It indicates that a possibility of optimizing the filling process, by using a heat exchanger. With a good configuration, by changing the parameters that specify the device operation conditions, it is possible to close the ideal (isotherm) process. This opens uo a window of opportunities for optimization.

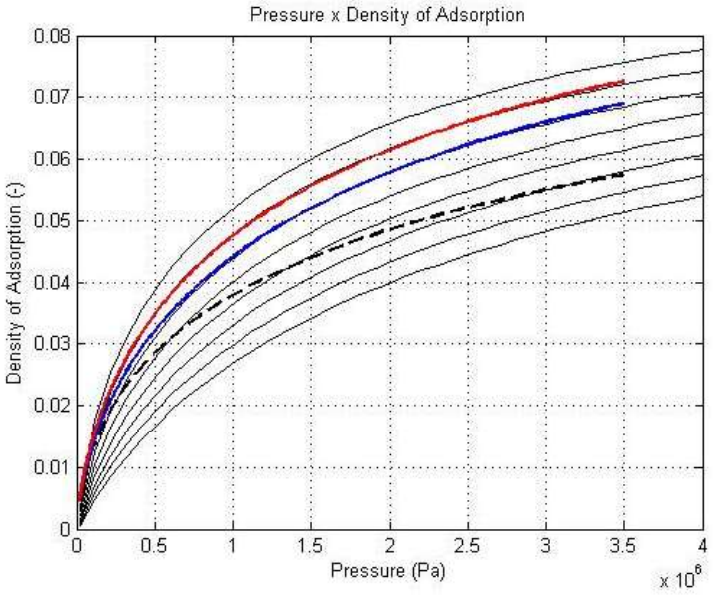


**Figure 4.44:** Density of adsorption in terms of pressure during the filling process. Blue: Test 10 with fluid at 300 K. Red: Test 10 with fluid at 288 K. Black (dash): Reference Test. Black Continuous: Isotherms

### 4.7.5 Scale Analysis

The previous numerical simulations have focused on a geometry which results were known in the literature (SAHOO; JOHN, 2011). This was important to validate the modeling and to explore some parameters sensitivities. Now, we are able to expand this analysis for other configurations.

However, there is an important question to be addressed, as to whether the ANG tecnology could be competitive for large reservoir applications.

Naturally, gas companies are still interested in small scale systems, such as in vehicular applications for instance, which where the technology was born. On the other hand, if they have a possibility to improve the capacity of transport vessels or stationary tanks for instance, it is clear that technology will have attention in large scale applications.

To increase tank dimensions, we make use of a scale factor, called $f$, to specify the new configurations. We consider two values: $f = 2$ and $f = 5$. The tanks are geometrically similar, but their sizes are scaled by $f$. Then, for $f = 2$, all the dimensions were multiplied by 2 which implies in a growing of the surface area by $2^2 = 4$ and an increase of the volume by $2^3 = 8$. Using the same consideration, in a configurations factor 5, the dimensions were multiplied by 5, the surface area by 25 and the volume by 125.

Moreover, for a suitable compassion between the different tank dimensions,

we need to keep the same flow conditions. In the other words, it is necessary to keep the same Reynolds number ($Re_d$, eq. 3.21) that was defined in terms of average flow velocity.

In a first analysis, as the volume grows by $f^3$, to keep the same gas density (adsorbed and in the voids between the adsorbent particles), we need to increase the filling flow by $f^3$ also. However, the surface areas (including the inlet surface) increase by $f^2$. So if we change the filling flow by this factor, instead, then the average velocity would increase by $f$, affecting the value of $Re_d$.

To solve this problem, we enhance the filling flow only by $f^2$ and "sacrifice" the filling time, which grows by $f$. Then, it was expected that the tanks with factor 2 would take the double of the filling time of the 1.82 L tank (used as tank with $f = 1$) and those tanks with the factor 5 would have their filling times close to the time with $f = 1$ multiplying by 5.

To validate the last paragraph expectation, we did three simulations, each one using a scale factor ($f$ = 1,2 and 5). To remove the influence of the heat transfer, we consider the tank walls to be insulated (adiabatic) and use a configuration without heat exchangers. The expectation was the values of filling times grows exactly by $f$. The results are presented in the table 4.12.

**Table 4.12:** Results for Adiabatic ANG tests

| Factor | Internal Volume (L) | Average Temperature (at 3.5MPa) | (V/V) (at 3.5MPa) | Filling Time (s) | Ratio between filling times |
|---|---|---|---|---|---|
| 1 | 1.82 | 354.3 K | 56.7 | 212 s | 212 : 212 = 1 |
| 2 | 14.56 | 354.3 K | 56.7 | 424 s | 424 : 212 = 2 |
| 5 | 227.5 | 354.3 K | 56.7 | 1060 s | 1060 : 212 = 5 |

The results prove our conjectures, since the results at $3.5MPa$ were very close and the ratio between the filling times are equal to the value of $f$. Then, we use this approach to analyze the configurations with heat exchangers and the tank walls submitted by natural convection.

The tests were performed with different heat exchangers tubes diameters but the position and the quantity are the same (14 tubes cross the section in a Tandem position). The external geometry is kept as a circular cylinder, thus using the same geometry dimensions that were explored in the validation tests (SAHOO; JOHN, 2011). The fig. 4.45 presents the geometries studied.

Also, we varying the values of the tubes heat transfer coefficient (presented in the Nusselt Number) to study its sensitivity. However, we kept the natural

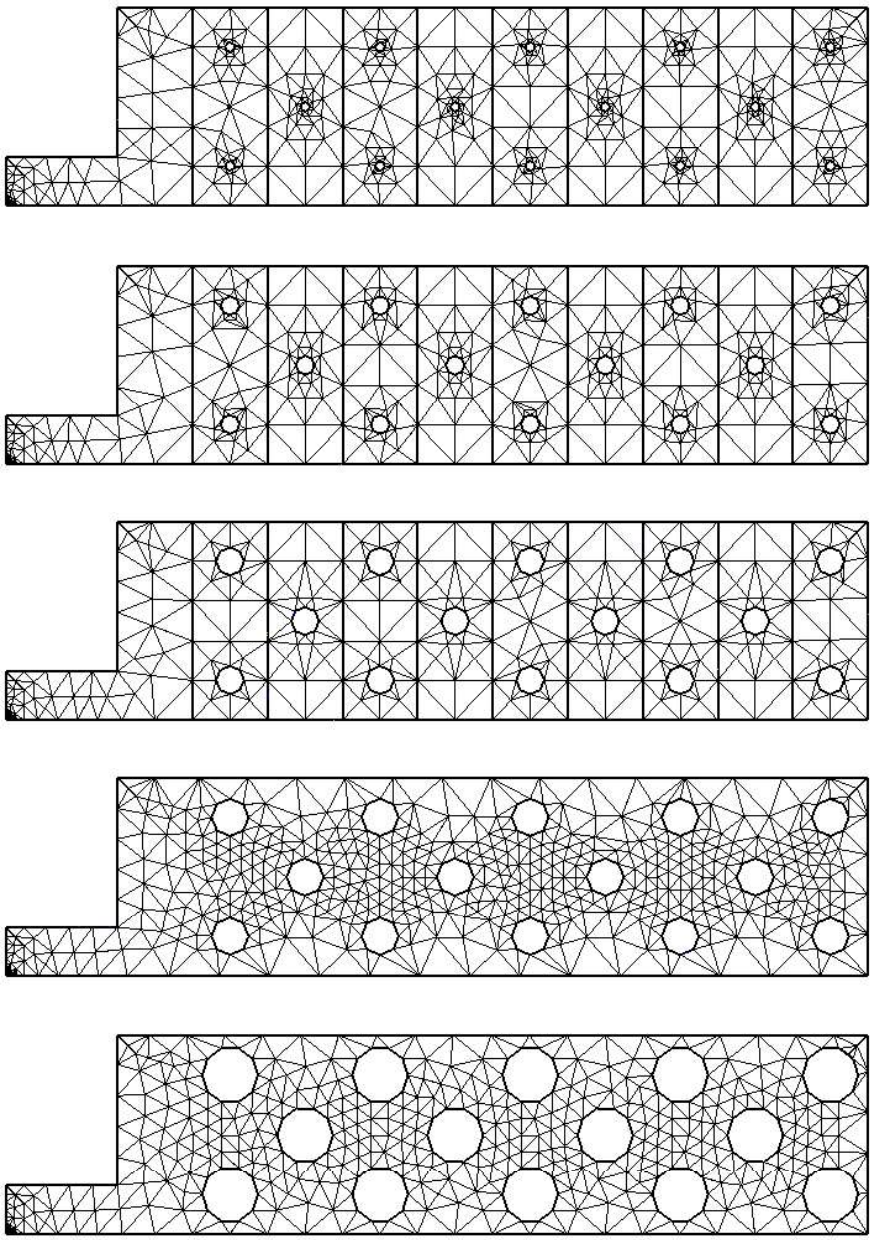

**Figure 4.45:** Mesh geometries for different tubes diameters. In this order: $d/D = 2.35, 4.69, 7.04, 9.38$ and $14.07\%$

convection in the tank walls ($h = 5\ W/m^2.K$). Then, for each value of $f$, we run 21 simulations, 5 different tube diameters times 4 values of heat transfer coefficients (500,1000,2000 and 5000 $W/m^2K$) plus 1 reference simulation without heat exchanges.

The results for $f = 1$ are in agreement with those from the validation and exploratory tests. In addition, figs. 4.46 and 4.47 show the influence of the heat transfer coefficient in the final result. For average temperature, the maximum difference between a result using $h = 500\ W/m^2.K$ and a test with $h = 5000\ W/m^2.K$ was $2.1K$.

This difference produces a small variation in the value of $V/V$ which in the

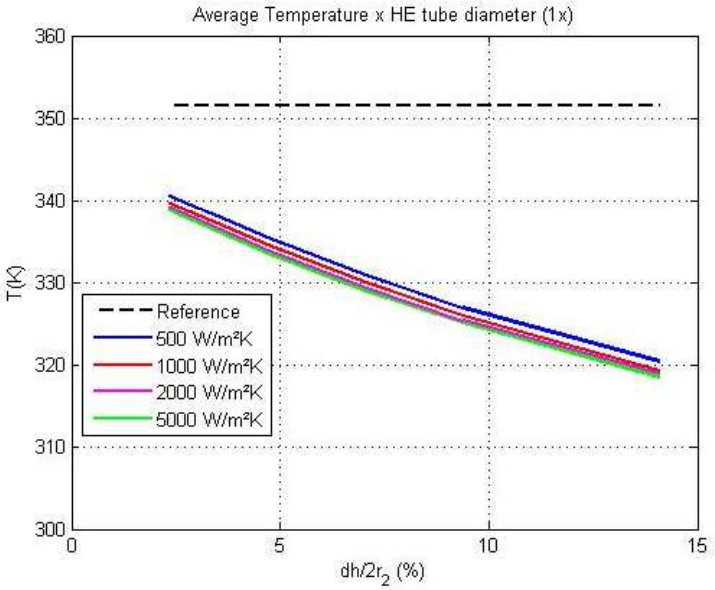


**Figure 4.46:** Results from scale factor $f = 1$. Average Temperature at 3.5 MPa versus of tubes diameter.

best result, at $d/D = 4.69\%$, for $h = 500\ W/m^2.K$, the $V/V$ was 60.4, less than 1% lower in compassion between the result with $h = 5000\ W/m^2.K$ (61.0).

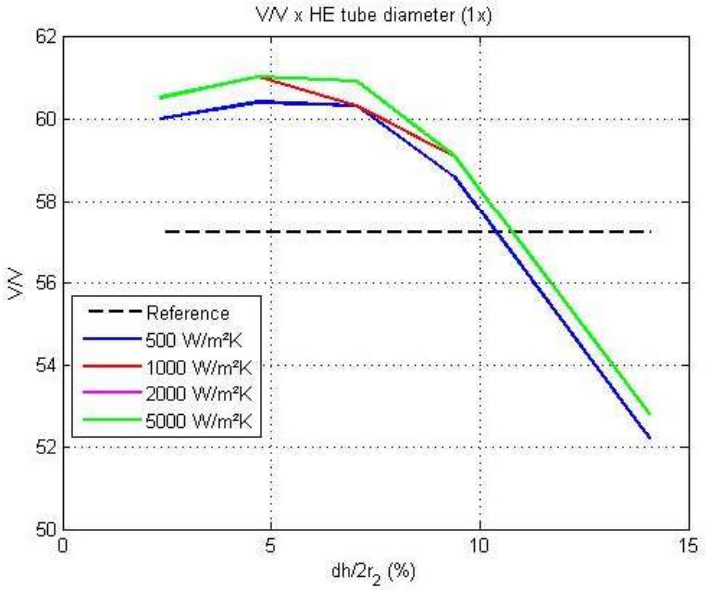


**Figure 4.47:** Results from scale factor $f = 1$. V/V at 3.5 MPa versus of tubes diameter.

The preliminary conclusions are the possibility of making a suitable configurations, by using low values of heat transfer coefficient. If a good distribution of the heat exchanger tubes, we can achieve values of $V/V$ above 60.0, and that reduces the operational costs related to a management of the conditions for a heat tranfer with $h = 5000\ W/m^2.K$. On other words, the sensitivity of the $h$ related to $V/V$ are lower than the changing of tubes layout.

Additionally, on using the value of $V/V$ achieved by a tank without heat exchanger as refference, as the tubes diameter increase, there is a point above which results gets worse than the reference, when the use of heat exchangers cease to be advantageous.

As we have seen in the tests with insulated tank walls (adiabatic), there is no difference between the average temperature and $V/V$. However, when we consider heat transfer through the tank walls and heat exchangers, we can see the influence of the tank size.

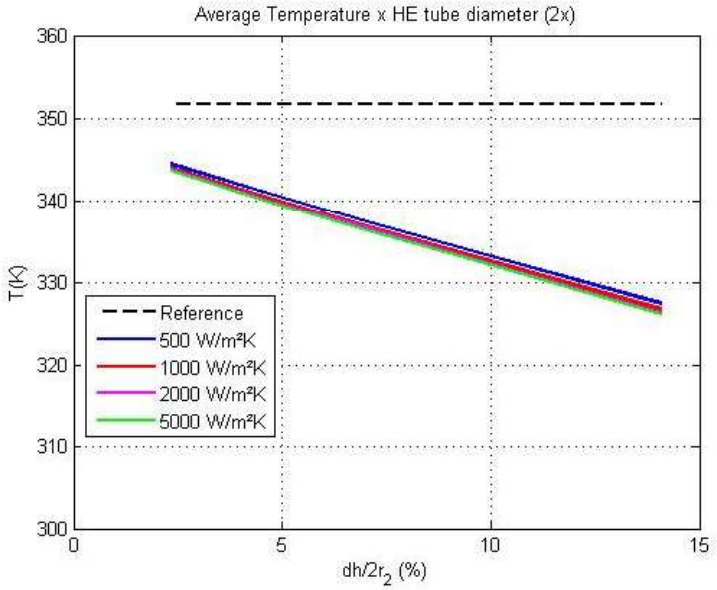


**Figure 4.48:** Results from scale factor $f = 2$. Average Temperature at 3.5 MPa versus of tubes diameter.

In the figs. 4.48 and 4.49, the results for $f = 2$ are presented. For the average temperature, the values in a tank were between 1 and 2.5% higher than that a tank with a $f = 1$, and this difference affects the results for $V/V$. The maximum value achieved was 59.8 for $h = 5000W/m^2.K$. In addition, the value of $V/V$ for $h = 500\ W/m^2.K$ was 58.8, which is 2.65% smaller than a tank with $f = 1$.

This result proves that we do not have the same ANG performance only by changing the scale. Moreover, in $V/V$ results we do not find a maximum point as we found in the test with $f = 1$ ($d/D = 4.69\%$). We suspect that the maximum point is located below the smallest diameter we simulated ($d/D = 2.35\%$).

This is an important result, because the the optimal point in certain configuration is changed if we test the same geometry with a scale factor. We also found this behavior for $f = 5$ and the results are presented in the figs (4.50) and (4.51).

In the biggest tank that we have tested, the results show the scale effects in

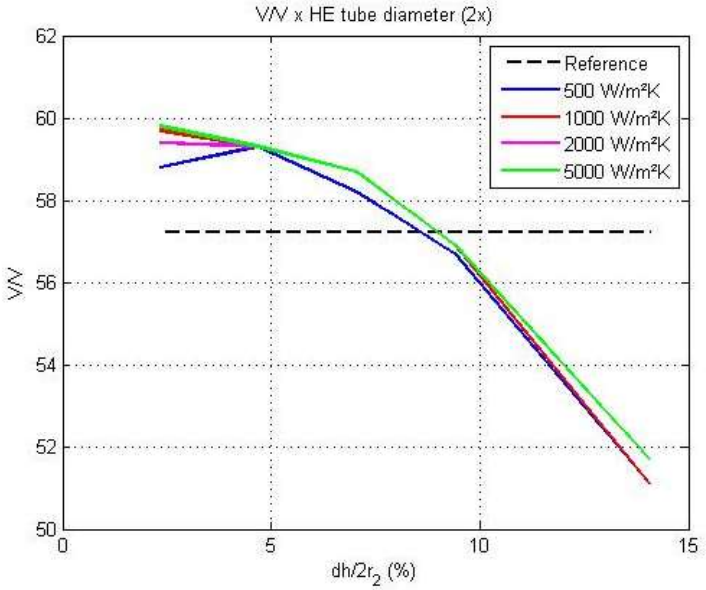


**Figure 4.49:** Results from scale factor $f = 2$. V/V at 3.5 MPa versus of tubes diameter.

ANG performance. For average temperature, the values were between 2.0 and 5.0% higher than a tank with $f = 1$.

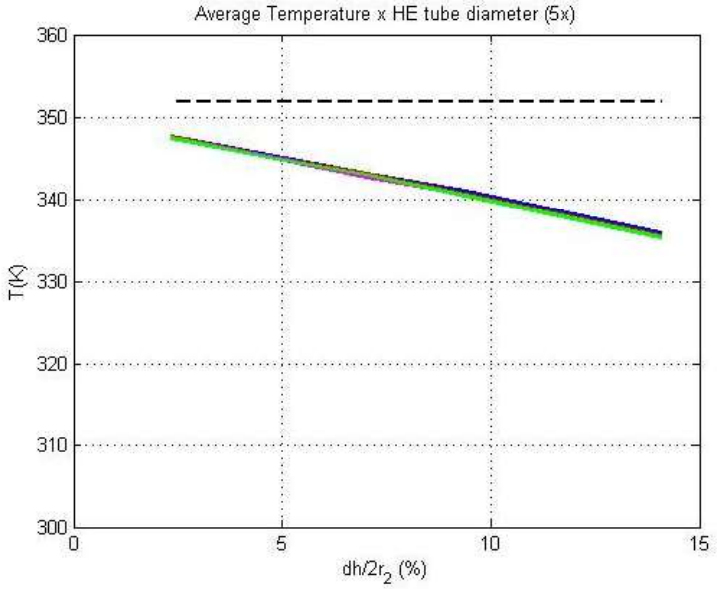


**Figure 4.50:** Results from scale factor $f = 5$. Average Temperature at 3.5 MPa versus of tubes diameter.

For $V/V$, the maximum value was 58.3 for $h = 5000\ W/m^2.K$ but for $h = 500\ W/m^2.K$, the value was 58.2 that seem to indicate that as larger as the tank, the less influence the value of $h$ has in the equipment performance.

The curve keeps the same behavior related to the growth of tubes diameter. Moreover, the curves of $V/V$ moved in terms of values of $f$.

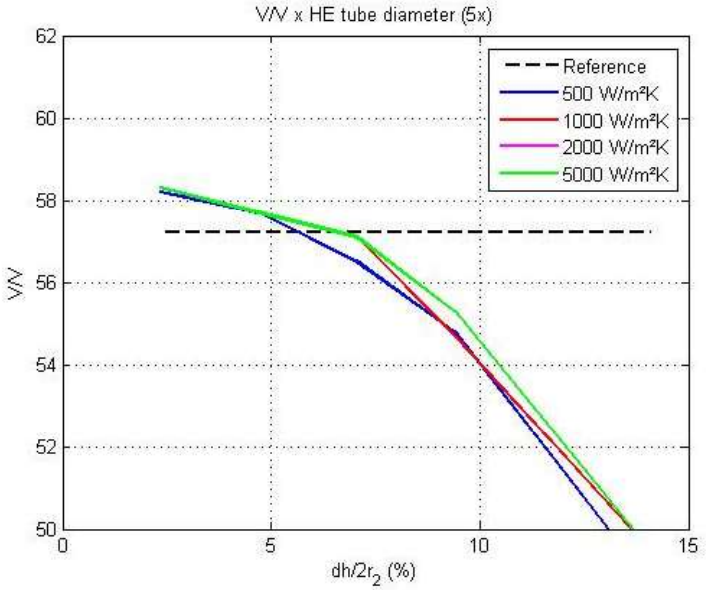


**Figure 4.51:** Results from scale factor $f = 5$. V/V at 3.5 MPa versus of tubes diameter.

By using the results for $h = 500\ W/m^2.K$, it is possible to see the growth of average temperature as we increases the tank size. On the other hand, the values of $V/V$ reduces in terms of $f$. Figs. 4.52 and 4.53 summarize this behavior:

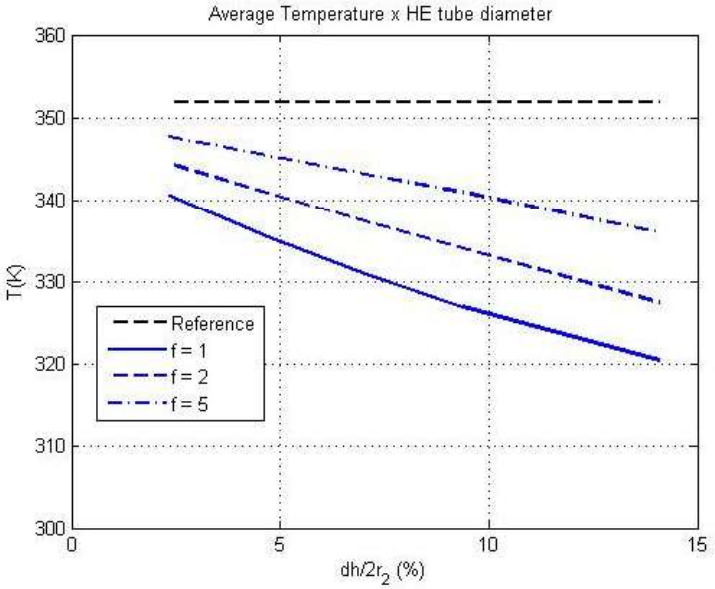


**Figure 4.52:** Results from scale factors. Average Temperature at 3.5 MPa versus of tubes diameter.($h = 500\ W/m^2.K$)

The conclusion of this analysis was that to make viable the large scale ANG systems, there is the need to design devices which maximize the heat transfer and overcome the scale problems.

Then, an optimization method to find those configurations is a requirement and not only to find an extrema of an objective function, but also there is a need

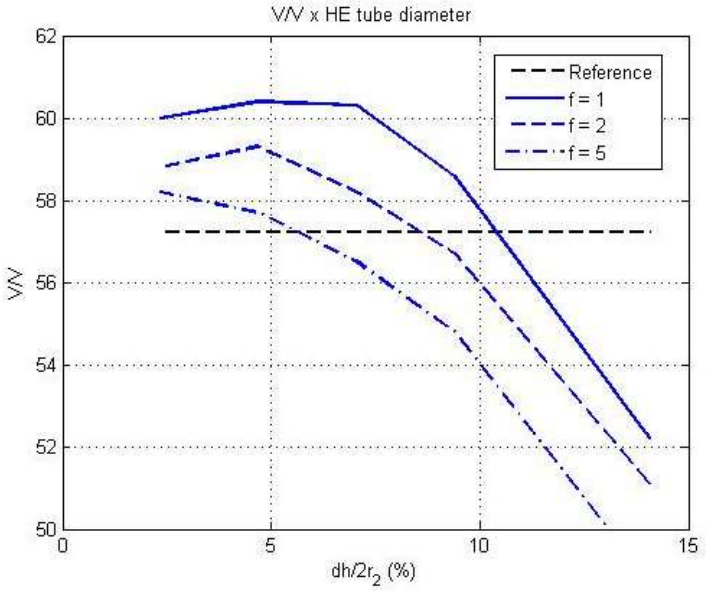


**Figure 4.53:** Results from scale factors. V/V at 3.5 MPa versus of tubes diameter. ($h = 500\ W/m^2.K$)

to be feasible when the number of design parameters were high. In this scenario, the Adjoint Method arises as an alternative and the application of this method in ANG systems is described in the next chapter.

# 5 Dual Problem - Adjoint Equations

This chapter presents a brief introduction to the Adjoint Method, the way it is discussed by Cacuci *et. all*, in a seminal paper. By using this concept, the Adjoint Equations based on the Primal Problem governing equations are deducted in the sequence.

## 5.1 Introduction

Historically, the Adjoint Method has evolved into two distinct approaches: discrete and continuous. In the former, a discrete adjoint operator is obtained on the basis of already discretized flow governing equations (Primal Problem). Whereas in the latter case, the adjoint equations are derived analytically from the equations that govern the physics, and only then they are discretized (GILES; PIERCE, 1997; GILES; PIERCE, 1998; GILES; PIERCE, 2000; GILES; PIERCE, 2001). Comparisons between the two approaches have also been drawn in the literature (JAMESON; SRIRAM; MARTINELLI, 2003; NADARAJAH; JAMESON, 2000; KIM; ALONSO; JAMENSON, 1999), and they do not indicate any sizable differences between them, in terms of optimization effectiveness.

This research intends to adopt the so–called continuous formulation of the Adjoint Method. For it is more directly in line with our approach to the adjoint boundary problem. As an additional result of this choice, the numerical methods that are used to integrate the primal problem are independent of those that are applied to the dual problem, thereby making the flow and adjoint solvers fully independent, as well.

In essence, the Adjoint Method is a powerful tool to compute the sensitivity of a given measure of merit, with respect to parameters that control the boundary conditions of a physical system. That system is assumed to be governed by a set of Partial Differential Equations (PDEs), and the measure of merit is taken to be

a functional— *i.e*, an objective functional, as it is also called. In our case, the flow represents the physical system and the objective functionals usually depend on flow variables and on the shape and location of the boundaries (JAMESON; PIERCE; MARTINELLI, 1998; JAMESON; SRIRAM; MARTINELLI, 2003). A few examples form the literature can illustrate the possibilities and are present in the eq. (5.1):

$$I = \oint_B \frac{(C_p - C_{pt})^2}{2}\,\mathrm{d}S \quad ; \quad K = \int_{\mathscr{D}} \frac{\rho u^2}{2}\,\mathrm{d}V \quad ; \quad \overline{C_f} = \frac{1}{T}\int_0^T \oint_B \frac{\mathbf{n}\cdot\boldsymbol{\sigma}\cdot\mathbf{e}}{q_\infty}\,\mathrm{d}S\mathrm{d}t \tag{5.1}$$

From left to right, the first integral is a measure of the mean square error of a pressure distribution, which is represented by $C_p$, with respect to a target distribution ($C_{pt}$), on a body surface ($B$)— it concerns inverse aerodynamic design applications. The second one represents the kinetic energy of the flow domain ($\mathscr{D}$). Whereas the third integral expresses a time average of the force the fluid exerts on the body surface $(\mathbf{n}\cdot\boldsymbol{\sigma})_B$, when it is projected onto a given direction ($\mathbf{e}$). Naturally, these are not the kind that suits our applications, where a target distribution of temperatures, the average internal energy or the wall heat transfer rate would be far more appropriate. Nonetheless, they show topics that have been explored.

In any case, the integration boundaries, and the boundary conditions, themselves, are controlled by a set of design parameters. For all practical purposes the set is assumed to be finite. Under these circumstances, a natural means of estimating the sensitivity of a functional to changes in flow parameters, would be to perturb each one of them individually, and then to compute the sensitivity gradient by finite differences.

The procedure clearly requires a converged flow solution for each parameter variation. As the number of design parameters increases, so does the the number of solutions, and the computational cost is bound to become prohibitive. Alternatively, by imposing the equations that govern the flow as constraints to the optimization problem, one precludes unrealizable solutions. That, in turn, eliminates the need for additional flow simulations. Therein lies the essence of the Adjoint Method. As a result of the simplification, the method offers an extremely attractive capability, which is to compute sensitivity gradients at a cost that is virtually independent of the number of design parameters.

As was mentioned above, a fairly general description of the Adjoint Method

is presented by Cacuci et al. (1980) , in the seminal work. In what follows, we present a brief account of that material, the reader is referred to the original paper for further details. We start by considering a measure of merit of a given physical system, *i. e.* an objective functional like those in eq. (5.1). In generic form, it may be written as the eq. (5.2):

$$R[\mathbf{X}, \alpha] = \int_{\mathscr{D}} F[\mathbf{X}(\kappa), \alpha(\kappa), \kappa] \mathrm{d}\rho \tag{5.2}$$

Where the vector $\mathbf{X}$ represents the coordinates of that system in state space. The vector $\kappa$ gives coordinates in phase space of the points in the domain of interest $\mathscr{D}$ — in the applications that are considered here, it corresponds to the physical space. Finally, vector $\alpha$ represents the set of parameters that control the system. In generic form, one would have

$$\begin{aligned} \mathbf{X}(\kappa) &= [X_1(\kappa), \ldots X_K(\kappa)] \\ \kappa &= (\kappa_1, \ldots, \kappa_J) \\ \alpha(\kappa) &= [\alpha_1(\kappa), \ldots, \alpha_I(\kappa)] \end{aligned}$$

The first Gâteaux variation (LUSTERNICK; SOBOLEV, 1961) of the functional (5.2) yields the eq. (5.3):

$$\delta R = \underbrace{\int_{\mathscr{D}} F'_X \delta\mathbf{X}(\kappa) \mathrm{d}\kappa}_{\delta R_X} + \underbrace{\int_{\mathscr{D}} F'_\alpha \delta\alpha(\kappa) \mathrm{d}\kappa}_{\delta R_\alpha} \tag{5.3}$$

Where the first term on the RHS, $\delta R_X$, represents the physical part of the total variation. Whereas the second, $\delta R_\alpha$, represents the parametric part, in the applications of interest here. In general, the term $F'_\alpha \delta\alpha(\kappa)$ is known in closed form and, thus, the variation $\delta R_\alpha$ can be evaluated analytically. The greatest difficulty in estimating $\delta R$ lies in the first term, $\delta R_X$, instead. For the variation $\delta\mathbf{X}(\kappa)$ is seldom known in closed form, even though $F'_X$, itself, may be. In effect, the mere presence of $\delta R_X$ in the total variation is indicative of the need for additional flow simulations, as the finite difference method requires.

As was mentioned above, the rationale behind the Adjoint Method requires the equations that govern the physics to be imposed on the variational problem, as realizability constraints. To that end, we assume that the system is governed by

a set $\mathbf{N}$ of $K$ nonlinear PDEs, which, in turn, are subject to a set $\mathbf{B}$ of boundary conditions. In terms of operators, one could write the expressions (5.4) and (5.5):

$$\mathbf{N}[\mathbf{X}(\kappa), \alpha] = \mathbf{Q}(\kappa, \alpha) \tag{5.4}$$

$$\mathbf{B}[\mathbf{X}(\kappa), \alpha]_s = 0 \tag{5.5}$$

Where the subscript $[\ ]_s$ naturally implies the conditions are imposed on the appropriate boundaries. It is also assumed that inner products can be defined in phase space and on the appropriate boundaries of the domain. They are of the form, presented in eq. (5.6), respectively:

$$\langle \Phi, \Psi \rangle \equiv \int_{\mathscr{D}} \Phi(\kappa) \cdot \Psi(\kappa)\, \mathrm{d}\rho \qquad \text{and} \qquad \langle \Phi, \Psi \rangle_s \equiv \int_{\partial\mathscr{D}} \Phi(\kappa) \cdot \Psi(\kappa)\, \mathrm{d}S \tag{5.6}$$

In principle, then, one can define an augmented functional in the eq. (5.7) that represents the constrained variational problem:

$$G(\mathbf{X}, \alpha, \Phi, \beta, a) = R[\mathbf{X}, \alpha] - \langle \Phi, \mathbf{N} - \mathbf{Q} \rangle - \langle \beta, \mathbf{B} \rangle_s - \langle \mathbf{a}, \alpha - \alpha_o \rangle \tag{5.7}$$

Usually non–holonomic, the constrains are introduced by the Lagrange multipliers $\Phi$, $\beta$ and $\mathbf{a}$, in the last three functionals of (5.7). The first of them imposes the governing equations, while the second enforces the corresponding boundary conditions. The third constraint ensures that the control parameters take on a given set of prescribed values $\alpha = \alpha_o$, which corresponds to a baseline configuration.

In order to determine the extrema of $G$ one must first compute its variation, $\delta G$. Then, the eq. (5.8)) presents the result of the variation:

$$\begin{aligned} \delta G = \underbrace{\delta R}_{\text{a}} - \underbrace{\langle \delta\Phi, \mathbf{N} - \mathbf{Q} \rangle}_{\text{b}} - \underbrace{\langle \Phi, \delta(\mathbf{N} - \mathbf{Q}) \rangle}_{\text{c}} - \underbrace{\langle \delta\beta, \mathbf{B} \rangle_s}_{\text{d}} - \underbrace{\langle \beta, \delta\mathbf{B} \rangle_s}_{\text{e}} \\ - \underbrace{\langle \delta\mathbf{a}, \alpha - \alpha_o \rangle}_{\text{f}} - \underbrace{\langle \mathbf{a}, \delta(\alpha - \alpha_o) \rangle}_{\text{g}} \end{aligned} \tag{5.8}$$

The term $a$ on the RHS of eq. (5.8) is just the functional of $R$, for which the first variation is given by eq. (5.3).

The terms $b$, $d$, $f$ and $g$ were kept in this form at the first moment and the terms $c$ and $e$ are the functional of the governing equations (5.4) and (5.5). Their Fréchet differentials are given by hte eq.(5.10:

$$\mathbf{L}\delta\mathbf{X} = \mathbf{S}\delta\alpha \tag{5.9}$$

$$\mathbf{B}'_X\delta\mathbf{X} = -\mathbf{B}'_\alpha\delta\alpha \tag{5.10}$$

Where the operators $\mathbf{L}$ and $\mathbf{S}$ are defined as $\mathbf{L} \equiv \mathbf{N}'_X$ and $\mathbf{S} \equiv \mathbf{Q}'_\alpha - \mathbf{N}'_\alpha$, respectively. The first of them represents the linearized form of the governing equations (Primal Problem), whereas the second one gathers the variations of control parameters.

Then, on making use of Gauss' theorem, we can transfer the differential operators from the state vector $\mathbf{X}$ to the Lagrange multiplier $\Phi$. That leads to the eq. (5.11):

$$\langle\Phi, \mathbf{L}\delta\mathbf{X}\rangle = P[\Phi, \delta\mathbf{X}]_s - \langle\mathbf{L}^*\Phi, \delta\mathbf{X}\rangle \tag{5.11}$$

Where the term $P[\Phi, \delta\mathbf{X}]_s$ is the bilinear concomitant the operation ensues (CACUCI et al., 1980; MORSE; FESHBACH, 1953). The subscript $[\ \ ]_s$ here has the same meaning as above. Furthermore, the first term on the RHS of (5.11) contains $\mathbf{L}^*$, which is the adjoint operator to $\mathbf{L}$.

Finally, by computing the Gâteax variations of the remaining functionals and on combining them with the above results, one obtains the first variation of the augmented functional, $\delta G$ in eq. (5.12):

$$\begin{aligned}\delta G = & -\langle\delta\Phi, \mathbf{N} - \mathbf{Q}\rangle - \langle\delta\beta, \mathbf{B}\rangle_s - \langle\delta a, \alpha - \alpha_o\rangle + \langle\mathbf{L}^*\Phi + F'_X, \delta\mathbf{X}\rangle + \\ & - \langle\beta, \mathbf{B}'_X\delta X\rangle_s - [\langle P_1(\Phi), \mathbf{B}'_X\delta\mathbf{X}\rangle_s + \langle\mathbf{B}^*(\Phi), \mathbf{A}\delta\mathbf{X}\rangle_s] + \langle\mathbf{F}'_\alpha, \delta\alpha\rangle + \\ & + \langle\Phi, \mathbf{S}\delta\alpha\rangle - \langle\mathbf{a}, \delta\alpha\rangle - \langle\beta, \mathbf{B}'_\alpha\delta\alpha\rangle_s\end{aligned} \tag{5.12}$$

Where $\delta R$ has already been replaced by eq. (5.3).

In addition to that, the bilinear concomitant $P[\Phi, \delta\mathbf{X}]_s$ of (5.11) has been decomposed into the two terms within square brackets. Both of them are inner products, only they must be computed over the appropriate boundaries. The first of those terms involves a $P_1(\Phi)$ and the linearized boundary operator $\mathbf{B}'_X\delta\mathbf{X}$.

While the second one involves a $\mathbf{B}^*(\Phi)$, which represents the adjoint boundary operator, and a term $\mathbf{A}\delta\mathbf{X}$. The decomposition of $P$ is **not** unique, and neither are the definitions of $P_1$ and $\mathbf{A}$. On the contrary, the only restriction that is actually imposed on the procedure is that the operator $\mathbf{A}$ be linearly independent of $\mathbf{B}'_X$. As a result of this, the very determination of the adjoint boundary problem hinges upon a non–unique decomposition, and it only makes sense that it should be this way. After all, there must be some leeway left to ensure the problem is well–posed.

The augmented functional $G$ realizes extrema upon the condition that (5.12) vanishes for arbitrary, albeit realizable, variations of its parameters:

$$\delta G = 0 \ \ \forall \ \ \{\delta\mathbf{X}, \delta\alpha, \delta\Phi, \delta\beta, \delta\mathbf{a}\} \ \ \in \ \ \{\text{locus of realizability}\}$$

That, in turn, requires that the following conditions be met:

I.- The equations that govern the physics (eq. 5.4) and their respective boundary conditions (eq. 5.5) are satisfied. In addition, the control parameters should take on the prescribed baseline values, $\alpha = \alpha_o$. These requirements imply that the first three terms of (5.12) are identically zero.

II.- On imposing the condition,

$$\beta = -P_1(\Phi) \ \ , \tag{5.13}$$

one drives to zero the sum of the fifth and sixth terms of eq. (5.12). This particular equation also solves the $\beta$ in terms of the $\Phi$.

III.- The vector $\Phi$ must satisfy the adjoint equation, which is given by eq. (5.14):

$$\mathbf{L}^*\Phi + F'_X = 0 \ \ , \tag{5.14}$$

as it appears in the fourth term of (5.12). The corresponding boundary conditions are given by the operator (5.15):

$$\mathbf{B}^*(\Phi) = 0 \ \ , \tag{5.15}$$

which comes from the seventh term in that equation. This eq. (5.15) should determine the $\Phi$ at the boundaries, along with the $\beta$ thereof.

IV.- The vector $\mathbf{a}$ is specified by the following condition presented in the eq. (5.16):

$$\langle \mathbf{a}, \delta\alpha \rangle = \langle \mathbf{F}'_\alpha, \delta\alpha \rangle + \langle \Phi, \mathbf{S}\delta\alpha \rangle - \langle \beta, \mathbf{B}'_\alpha \delta\alpha \rangle_s \tag{5.16}$$

which collects all the remaining terms when $\delta G = 0$. In fact, this is the realizable part of the sensitivity gradient, $\delta R$, as will be shown next.

To prove the above statement regarding the sensitivity gradient (CACUCI et al., 1980), suffices it to recognize that: If the governing equations, (5.4) and (5.5) are identically satisfied for a given variation $\Delta G$, of any size. Then, from the very definition of $G$ in (5.7), it comes that

$$\begin{aligned} &\Delta G = \Delta R - \langle \mathbf{a}, \Delta\alpha \rangle \\ &\text{for} \begin{cases} \Delta G \equiv G(X_2, \alpha_2; \Phi_2, \beta_2, a_2) - G(X_1, \alpha_1; \Phi_1, \beta_1, a_1) \\ \Delta R \equiv R(X_2, \alpha_2) - R(X_1, \alpha_1) \\ \Delta\alpha \equiv \alpha_2 - \alpha_1 \end{cases} \end{aligned} \tag{5.17}$$

In particular for an infinitesimal variation $\Delta G \to \delta G$, under the above conditions and where $\Phi$, $\alpha$ and $\beta$ fulfill the above requirements I–IV, there must correspond a stationary value of $G$. Therefore, one can write

$$\begin{aligned} \delta G &= \delta R - \langle \mathbf{a}, \delta\alpha \rangle = 0 \\ \delta R &= \langle \mathbf{a}, \delta\alpha \rangle \\ \delta R &= \langle \mathbf{F}'_\alpha, \delta\alpha \rangle + \langle \Phi, (\mathbf{Q}'_\alpha - \mathbf{N}'_\alpha)\, \delta\alpha \rangle + \langle P_1(\Phi), \mathbf{B}'_\alpha \delta\alpha \rangle_s \end{aligned} \tag{5.18}$$

Where the eqs. (5.13), (5.16) and the definition of $\mathbf{S}$ have been used. With the above expression (5.18), one can estimate the sensitivity gradient on the basis of the adjoint solution $\Phi$ and parameter variations $\delta\alpha$, alone.

It is worth noting here that all physical variations $\delta\mathbf{X}$ have been successfully removed from the gradient expression. Moreover, the first term on the RHS of (5.18) is precisely $\delta R_\alpha$, whereas the second measures the direct effects of $\delta\alpha$ on the governing equations, and the third does so with respect to their boundary conditions.

Despite the apparently simple conceptual foundations, there are some aspects of the adjoint problem, which should be approached with caution:

- The derivation of the adjoint operator $\mathbf{L}^*$ by analytical means may present some considerable difficulties, depending on the nature of the primal problem.

- As was mentioned above, the decomposition of the bilinear concomitant is not unique. In effect, it is problem–dependent and it plays a crucial role in ensuring that the adjoint equation is well–posed.

- One must account for the fact that the adjoint variables are purely mathematical entities. Hence one cannot always benefit from the knowledge of physics to formulate the adjoint problem.

With these considerations, we start the deduction of Adjoint problem applied to the governing equations of Adsorbed Natural Gas Storage Systems.

## 5.2 The Adjoint problem for Darcy Compressible Navier Stokes Flows

This section is dedicated to formulating the adjoint problem, as it applies to the particular class of flows that is of interest in this research. It discusses the derivation of the Adjoint equations, along with their boundary and time conditions. Throughout the deduction, we refer to the components of the eqs.(5.2) - (5.18) from in the previous section of this chapter.

In the applications that are considered here, the main objective is to find flow configurations that represent extrema of a given measure of merit. As previously mentioned, that measure is usually a functional of the flow variables and in some cases, a functional of the geometry parameters too. It could be either an integral over the flow domain (D) as a whole, or a surface integral over a boundary, such as the body surface (B), for instance. In this thesis, the integrals over the whole flow domain $\Omega$ are used and defined in eq.(5.19) :

$$R = \frac{1}{T}\int_0^T \oint_D F(X_i;\alpha_p)\mathrm{d}V\mathrm{d}t \tag{5.19}$$

Where $F$ could be any function of the state vector $X = (\rho, u, v, w, T)^T$ and the design control parameters $\alpha_p = (\alpha_1, \alpha_2, ..., \alpha_n)$. For convenience, the integral

was written as follows in the eq.(5.20):

$$\frac{1}{T}\int_0^T\!\!\oint_D (...)\mathrm{d}V\mathrm{d}t = \oint_\Omega (...)\mathrm{d}\Omega \tag{5.20}$$

To define the augmented functional, as in eq. (5.7), we present the flow governing equations in generalized form. As explained in the beginning of this chapter, the use of continuous formulation of the Adjoint Method allows one choose the more convenient form of the equations that defines the Primal problem. Then, the flow governing equations (5.21) used to Adjoint Equations deduction are presented as follows:

$$\begin{aligned}
\epsilon_t\partial_0\rho + (\rho u^i)|_i &= -\rho_b\partial_0 q \\
u^i + N_p P|^i &= 0 \\
\partial_0\Big[C_{eff}T - \epsilon_t\Big(\frac{\gamma-1}{\gamma}\Big)P\Big] + (T\rho u^i)|_i - \frac{1}{Pe}T|^i|_i &= \rho_b\frac{\Delta H}{M_g}\partial_0 q
\end{aligned} \tag{5.21}$$

Where $\partial_0 = \partial()/\partial t$ and the vertical bar with sub or superscripts represents the covariant derivative operators (Divergence, Gradient, Laplacian, etc). Now, we can make an analogy with eq.(5.7) and define Lagrange multipliers $\omega$, $\Psi$ and $\Theta$ to introduce the flow governing equations in the augmented functional. Defining the vectors $N$ and $Q$ in eqs.(5.22) and (5.23):

$$N = \left\{ \begin{array}{c} \epsilon_t\partial_0\rho + (\rho u^i)|_i \\ u^i + N_p P|^i \\ \partial_0[C_{eff}T - \epsilon_t(\frac{\gamma-1}{\gamma})P] + (T\rho u^i)|_i - \frac{1}{Pe}T|^i|_i \end{array} \right\} \quad \text{and} \tag{5.22}$$

$$Q = \left\{ \begin{array}{c} -\rho_b\partial_0 q \\ 0 \\ +\rho_b\frac{\Delta H}{M_g}\partial_0 q \end{array} \right\} \tag{5.23}$$

The augmented functional based on eq.(5.7) becomes the eq.(5.24):

$$\begin{aligned}
G &= R + \\
&+ \left\langle \omega, \epsilon_t\partial_0\rho + (\rho u^i)|_i + \rho_b\partial_0 q \right\rangle \\
&+ \left\langle \Psi_i, u^i + N_p P|^i \right\rangle \\
&+ \left\langle \Theta, \partial_0\Big[C_{eff}T - \epsilon_t\Big(\frac{\gamma-1}{\gamma}\Big)P\Big] + (T\rho u^i)|_i - \frac{1}{Pe}T|^i|_i - \rho_b\frac{\Delta H}{M_g}\partial_0 q \right\rangle \\
&+ \left\langle \beta, \mathbf{B} \right\rangle_s + \left\langle \mathbf{a}, \alpha - \alpha_o \right\rangle
\end{aligned} \tag{5.24}$$

On following the steps that were outlined in the previous sections, we need to introduce the terms that define the expression of the functional $\delta G$. First, we present the variations (5.25) and (5.26) of $N_X^{'}\delta X$, $N_\alpha^{'}\delta\alpha$, $Q_X^{'}\delta X$ and $Q_\alpha^{'}\delta\alpha$ that appear in term $c$ of the eq.(5.8):

$$\begin{aligned} N_X^{'}\delta X &= \left\{ \begin{array}{c} \epsilon_t\partial_0\delta\rho + (\rho\delta u^i + \delta\rho u^i)|_i \\ \delta u^i + N_p\delta P|^i \\ \partial_0[C_{eff}\delta T - \epsilon_t(\frac{\gamma-1}{\gamma})\delta P] + (\delta T\rho u^i + T\delta\rho u^i + T\rho\delta u^i)|_i - \frac{1}{Pe}\delta T|^i|_i \end{array} \right\} \text{and} \\ Q_X^{'}\delta X &= \left\{ \begin{array}{c} \rho_b\partial_0(\delta q) \\ 0 \\ -\rho_b\frac{\Delta H}{M_g}\partial_0\delta q \end{array} \right\} \end{aligned} \tag{5.25}$$

$$\begin{aligned} N_\alpha^{'}\delta\alpha &= \left\{ \begin{array}{c} \epsilon_t\partial_0\rho\delta J + \delta(J\beta^k_{q'})(\rho u^{q'})_k \\ \delta(J\beta^{j'}_{n'})(g^{r'n'})_j \\ \partial_0[C_{eff}T - \epsilon_t(\frac{\gamma-1}{\gamma})P]\delta J + \delta(J\beta^i_{j'})(T\rho u^{j'} - \frac{1}{Pe}g^{j'k'}T_k)|_i \end{array} \right\} \text{and} \\ Q_\alpha^{'}\delta\alpha &= 0 \end{aligned} \tag{5.26}$$

With this results, we can define the augmented functional variation $\delta G$. It becomes the eq.(5.27):

$$\begin{aligned} \delta G &= \delta R + \langle\delta\Phi, N - Q\rangle + \\ &+ \underbrace{\left\langle\omega, \epsilon_t\partial_0\delta\rho + (\rho\delta u^i + \delta\rho u^i)|_i + \partial_0(\rho_b\delta q)\right\rangle}_{\text{I}} \\ &+ \underbrace{\left\langle\Psi_i, \delta u^i + N_p\delta P|^i\right\rangle}_{\text{II}} \\ &+ \underbrace{< \Theta, \partial_0[C_{eff}\delta T - \epsilon_t(\frac{\gamma-1}{\gamma})\delta P] + (\delta T\rho u^i + T\delta\rho u^i + T\rho\delta u^i)|_i - \frac{1}{Pe}\delta T|^i|_i +}_{\text{III}} \\ &- \underbrace{\rho_b\frac{\Delta H}{M_g}\partial_0\delta q >}_{\text{III}} \\ &+ \langle\delta\beta, \mathbf{B}\rangle_s + \langle\beta, \delta\mathbf{B}\rangle_s + \langle\Phi, \mathbf{S}\delta\alpha\rangle + \langle\delta\mathbf{a}, \alpha - \alpha_o\rangle + \langle\mathbf{a}, \delta\alpha\rangle \end{aligned} \tag{5.27}$$

Where the order of the terms are in agreement of eq. (5.8) and the terms I,II and III are the expansion of term (c) in the same equation. Now, it is necessary to apply the Gauss' theorem to transfer the differential operators from the state vector $\mathbf{X}$ to the Lagrange multiplier $\Phi$. On starting from the convective term of mass equation, that leads to eq. (5.28):

$$\left\langle \omega, (\rho\delta u^i + \delta\rho u^i)|_i \right\rangle = \left\langle \omega, (\rho\delta u^i + \delta\rho u^i).n_i \right\rangle_s - \left\langle \omega|_i, (\rho\delta u^i + \delta\rho u^i) \right\rangle \tag{5.28}$$

Where the first term of the RHS is part of the bilinear concomitant and the second is the integral with transferred operator. The same approach pursued in the next terms, eqs. (5.29) to (5.32), presented as follows:

Gradient term in the momentum equation:

$$\left\langle \Psi_i, N_p\delta P|^i \right\rangle = \left\langle \Psi_i, N_p\delta P.n_i \right\rangle_s - \left\langle \psi_i|^i, N_p\delta P \right\rangle \tag{5.29}$$

Convective term in the energy equation:

$$\begin{aligned} < \Theta, (\delta T\rho u^i + T\delta\rho u^i + T\rho\delta u^i)|_i \; > \; &= \left\langle \Theta, (\delta T\rho u^i + T\delta\rho u^i + T\rho\delta u^i).n_i \right\rangle_s + \\ - \; < \; &\Theta|_i, (\delta T\rho u^i + T\delta\rho u^i + T\rho\delta u^i) > \end{aligned} \tag{5.30}$$

Diffusive term in the energy equation:

$$\left\langle \Theta, -\frac{1}{Pe}\delta T|^i|_i \right\rangle = \left\langle \Theta, -\frac{1}{Pe}\delta T|^i.n_i \right\rangle_s - \left\langle \Theta|_i, -\frac{1}{Pe}\delta T|^i \right\rangle \tag{5.31}$$

For Diffusion term it is necessary to apply the Gauss' theorem to second term of eq. (5.31), because only one of the differential operators was transferred. Repeating the approach:

$$\begin{aligned} \left\langle \Theta, -\frac{1}{Pe}\delta T|^i|_i \right\rangle &= \left\langle \Theta, -\frac{1}{Pe}\delta T|^i.n_i \right\rangle_s - \left\langle \Theta|_i, -\frac{1}{Pe}\delta T|^i \right\rangle = \\ &= \left\langle \Theta, -\frac{1}{Pe}\delta T|^i.n_i \right\rangle_s - \left\langle \Theta|_i.n^i, -\frac{1}{Pe}\delta T \right\rangle_s + \\ &+ \left\langle \Theta^i|_i, -\frac{1}{Pe}\delta T \right\rangle \end{aligned} \tag{5.32}$$

In addition, it is necessary to transfer the time derivative ($\partial_0$) in the mass and energy equations. To that end, we make use of the simple rule for differentiating a product. The term in the conservation of mass becomes the eq. (5.33):

$$\langle \omega, \epsilon_t\partial_0\delta\rho \rangle = \frac{1}{T}\int_0^T \oint_D \partial_0(\epsilon_t\omega\delta\rho)\mathrm{d}V\mathrm{d}t - \langle \partial_0\omega, \epsilon_t\delta\rho \rangle \tag{5.33}$$

The first integral can be solved in $t$ and it becomes the eq. (5.34):

$$\langle \omega, \epsilon_t\partial_0\delta\rho \rangle = \frac{1}{T}\Big[ \oint_D (\epsilon_t\omega\delta\rho)\mathrm{d}V \Big]_0^T - \langle \partial_0\omega, \epsilon_t\delta\rho \rangle \tag{5.34}$$

The term in the conservation of energy becomes the eq. (5.35):

$$\begin{aligned}\left\langle \Theta, \partial_0[C_{eff}\delta T - \epsilon_t(\frac{\gamma-1}{\gamma})\delta P]\right\rangle &= \frac{1}{T}\int_0^T\oint_D \partial_0(\Theta\Big[C_{eff}\delta T - \epsilon_t\Big(\frac{\gamma-1}{\gamma}\Big)\delta P\Big])\mathrm{d}V\mathrm{d}t + \\ &- \left\langle \partial_0\Theta, [C_{eff}\delta T - \epsilon_t(\frac{\gamma-1}{\gamma})\delta P]\right\rangle \end{aligned} \tag{5.35}$$

On perfoming the time integration of the first term on RHS of eq. (5.35), it becomes the eq. (5.36):

$$\begin{aligned}\left\langle \Theta, \partial_0[C_{eff}\delta T - \epsilon_t(\frac{\gamma-1}{\gamma})\delta P]\right\rangle &= \frac{1}{T}\Big[\oint_D (\Theta\Big[C_{eff}\delta T - \epsilon_t\Big(\frac{\gamma-1}{\gamma}\Big)\delta P\Big])\mathrm{d}V\Big]_0^T + \\ &- \left\langle \partial_0\Theta, [C_{eff}\delta T - \epsilon_t(\frac{\gamma-1}{\gamma})\delta P]\right\rangle \end{aligned} \tag{5.36}$$

The source terms were also modified by pursuing the same approach, thua forming the eqs. (5.38) and (5.40)

Mass source term becomes:

$$\langle \omega, \partial_0(\rho_b\delta q)\rangle = \int_0^T\oint_D \partial_0(\omega\rho_b\delta q)\mathrm{d}V\mathrm{d}t - \langle \partial_0\omega, (\rho_b\delta q)\rangle \tag{5.37}$$

On performing the time integration of the first term on RHS of eq. (5.37):

$$\langle \omega, \partial_0(\rho_b\delta q)\rangle = \frac{1}{T}\Big[\oint_D (\omega\rho_b\delta q)\mathrm{d}V\Big]_0^T - \langle \partial_0\omega, (\rho_b\delta q)\rangle \tag{5.38}$$

Energy source term becomes:

$$\left\langle \Theta, \frac{\Delta H}{M_g}\partial_0(\rho_b\delta q)\right\rangle = \int_0^T\oint_D \partial_0(\Theta\frac{\Delta H\rho_b}{M_g}\delta q)\mathrm{d}V\mathrm{d}t - \left\langle \partial_0\Theta, \frac{\Delta H\rho_b}{M_g}\delta q\right\rangle \tag{5.39}$$

On perfoming the time integration of the first term on RHS of eq. (5.39):

$$\left\langle \Theta, \frac{\Delta H}{M_g}\partial_0(\rho_b\delta q)\right\rangle = \frac{1}{T}\Big[\oint_D (\Theta\frac{\Delta H\rho_b}{M_g}\delta q)\mathrm{d}V\Big]_0^T - \left\langle \partial_0\Theta, \frac{\Delta H\rho_b}{M_g}\delta q\right\rangle \tag{5.40}$$

By considering the relations presented in the eqs. (5.41), one gets:

$$\begin{aligned}\delta P &= \delta\rho T + \rho\delta T \\ \delta q &= A_\rho\delta\rho + A_T\delta T\end{aligned} \tag{5.41}$$

And on substituting eqs. (5.28)-(5.30), (5.32), (5.34), (5.36), (5.38) and (5.40) into terms I,II and III of eq. (5.27), it yields the expanded augmented functional (5.42):

$$\begin{aligned}
\delta G &= \delta R + \langle \delta\Phi, N - Q\rangle + \\
&- \Big\langle (\epsilon_t + \rho_b A_\rho)\partial_0\omega + \Big[ -\epsilon_t\Big(\frac{\gamma-1}{\gamma}\Big)T + \frac{\rho_b \Delta H A_\rho}{M_g}\Big]\partial_0\Theta + \\
&+ N_P T\Psi_i\Big|^i + u^i\omega_i + u^i T\Theta\Big|_i, \delta\rho\Big\rangle \\
&- \Big\langle \rho\omega\Big|_i + \Psi_i + \rho T\Theta\Big|_i, \delta u^i\Big\rangle \\
&- \Big\langle (\rho_b A_T)\partial_0\omega + \Big[C_{eff} - \epsilon_t\Big(\frac{\gamma-1}{\gamma}\Big)\rho + \frac{\rho_b\Delta H A_T}{M_g}\Big]\partial_0\Theta + \\
&+ N_P\rho\Psi_i\Big|^i + \rho u^i\Theta\Big|_i + \frac{1}{Pe}\Theta\Big|^i\Big|_i, \delta T\Big\rangle \\
&+ \Big\langle \Big[\omega u^i.n_i + N_P T\Psi_i.n^i + \Theta T u^i.n_i\Big], \delta\rho\Big\rangle_s \\
&+ \Big\langle \Big(\omega\rho + \Theta\rho T\Big), \delta u^i.n_i\Big\rangle_s \\
&+ \Big\langle \Big[N_P\rho\Psi_i.n^i + \Theta\rho u^i.n_i - \frac{1}{Pe}(\Theta\Big|_i.n^i)\Big], \delta T\Big\rangle_s \\
&- \Big\langle \frac{\Theta}{Pe}, \delta T^i.n_i\Big\rangle_s \\
&+ \langle \delta\beta, \mathbf{B}\rangle_s + \langle \beta, \delta\mathbf{B}\rangle_s + \langle \Phi, \mathbf{S}\delta\alpha\rangle + \langle \delta\mathbf{a}, \alpha - \alpha_o\rangle + \langle \mathbf{a}, \delta\alpha\rangle \qquad (5.42)
\end{aligned}$$

Where the four terms $\Big[\oint_D (...)\mathrm{d}V\Big]_0^T$ which came from the transfer of the time derivative are driven to zero because at $t = 0$, the flow solution is known and its variations $\delta X$ are zero. Additionally, we impose a final condition on the adjoint problem, by assigning that they vanish ($\Phi = 0$) at $t = T$, i.e. homogeneous final adjoint conditions

On recalling that in Cacuci approach, we can expand $\delta R$ as showed in the eq. (5.43):

$$\delta R = \Big\langle F'_x, \delta X\Big\rangle + \Big\langle F'_\alpha, \delta\alpha\Big\rangle \qquad (5.43)$$

and by defining the integral with three terms $\langle L^*\Phi\rangle$, where:

$$L^*\Phi = \left\{ \begin{array}{lll}
(\epsilon_t + \rho_b A_\rho)\partial_0\omega & + & \Big[ -\epsilon_t\Big(\frac{\gamma-1}{\gamma}\Big)T + \frac{\rho_b\Delta H A_\rho}{M_g}\Big]\partial_0\Theta + \\
 & + & N_P T\Psi_i\Big|^i + u^i\omega_i + u^i T\Theta\Big|_i \\
\rho\omega\Big|_i + \Psi_i + \rho T\Theta\Big|_i & & \\
(\rho_b A_T)\partial_0\omega & + & \Big[C_{eff} - \epsilon_t\Big(\frac{\gamma-1}{\gamma}\Big)\rho + \frac{\rho_b\Delta H A_T}{M_g}\Big]\partial_0\Theta + \\
 & + & N_P\rho\Psi_i\Big|^i + \rho u^i\Theta\Big|_i + \frac{1}{Pe}\Theta\Big|^i\Big|_i
\end{array} \right\} \qquad (5.44)$$

The terms $F_x^{'}, \delta X$ and $\langle L^*\Phi \rangle$ are part of the Adjoint Equation, whereas the $F_\alpha^{'}, \delta\alpha$ become part of the sensitivity gradient.

### 5.2.1 Bilinear Concomitant and Adjoint Boundary Conditions

The next four terms in eq. (5.42) that are identified by subscript "s" form the bilinear concomitant. According to eq. (5.3), the term $P[\Phi, \delta X]_s$ was divided into parts, where $P_1(\Phi)$ are related to the linearized boundary conditions $B_X^{'}\delta X$ and $B^*(\Phi)$, which represents the adjoint boundary conditions.

On combining the parts in a unique integral, and on rearranging its terms, one gets the eq. (5.45):

$$\begin{aligned}
&\Big\langle \Big[\omega u^i.n_i + N_P T\Psi_i.n^i + \Theta T u^i.n_i\Big], \delta\rho \Big\rangle_s + \Big\langle \Big(\omega\rho + \Theta\rho T\Big), \delta u^i.n_i \Big\rangle_s \\
&+\Big\langle \Big[N_P\rho\Psi_i.n^i + \Theta\rho u^i.n_i - \frac{1}{Pe}(\Theta|_i.n^i)\Big], \delta T \Big\rangle_s - \Big\langle \frac{\Theta}{Pe}, \delta T^i.n_i \Big\rangle_s = \\
&\qquad = \int_{\delta\Omega} (\omega + \Theta T)(\delta\rho u^i + \rho\delta u^i).n_i + (\delta\rho N_P T + \delta T N_P\rho)\Psi_i.n^i \\
&\qquad\qquad +\Big( - \frac{\delta T^i.n_i}{Pe}\Big)\Theta + \delta T\Big[(\rho u^i.n_i)\Theta - \frac{1}{Pe}\Theta|_i.n^i\Big] dSdt
\end{aligned} \tag{5.45}$$

### 5.2.2 Proposal for a new arrangement of the Adjoint Equations

As previously mentioned, the decomposition of bilinear concomitant is **not** unique. To make the derivation simpler, we define the Adjoint pressure variable, $\sigma$, with the followed relation:

$$\sigma = \omega + \Theta T \quad \Rightarrow \quad \omega = \sigma - \Theta T \tag{5.46}$$

By preparing the relations to substitute in the Adjoint Equations, we get:

$$\partial_0\omega = \partial_0\sigma - T\partial_0(\Theta) - \Theta\partial_0(T) \tag{5.47}$$

$$\omega\Big|_i = \sigma\Big|_i - T\Big(\Theta\Big|_i\Big) - \Theta\Big(T\Big|_i\Big) \tag{5.48}$$

Where the terms $\partial_0(T)$ and $T\Big|_i$ are evaluated in the flow solution. By substituting the eqs. (5.46) to (5.48) in the eq. (5.44), we get the new proposal of the Adjoint Equations:

$$L^*\Phi = \left\{ \begin{array}{l} (\epsilon_t + \rho_b A_\rho)\partial_0\sigma - \Big[\epsilon_t\Big(\frac{\gamma-1}{\gamma}\Big)T + \rho_b A_\rho \frac{\Delta H}{M_g}\Big]\partial_0\Theta + N_P T\Psi_i\Big|^i \\ +u^i\sigma\Big|_i - \Big[(\epsilon_t + \rho_b A_\rho)\partial_0 T + u^i T\Big|_i\Big]\Theta \\ -\Psi_i + \rho\sigma\Big|_i - \Big(\rho T\Big|_i\Big)\Theta \\ (\rho_b A_T)\partial_0\sigma + \Big[C_{eff} - \epsilon_t\Big(\frac{\gamma-1}{\gamma}\Big)\rho - \rho_b A_T \frac{\Delta H}{M_g}\Big]\partial_0\Theta + N_P\rho\Psi_i\Big|^i \\ +\rho u^i\Theta\Big|_i - \frac{1}{Pe}\Theta\Big|^i\Big|_i \end{array} \right\} \quad (5.49)$$

The Bilinear Concomitant has one change in the first term, and it becomes:

$$\begin{aligned} &\int_{\delta\Omega} (\delta\rho u^i + \rho\delta u^i.n_i)\sigma + N_P(\delta\rho T + \delta T\rho)\Psi_i.n_i + \\ &+\Big(\rho u^i.n_i\delta T - \frac{\delta T^i.n_i}{Pe}\Big)\Theta + \delta T\Big[\frac{1}{Pe}\Theta|_i.n^i\Big]dSdt \end{aligned} \quad (5.50)$$

### 5.2.3 Adjoint Boundary Conditions

Basically, the ANG flow problem involves four relevant types of boundary conditions: Inflow, Outflow, Solid Wall (Tank and Heat Transfer) and symmetry (for axisymmetric geometries). We consider each one of them separately to extract the terms that compose the two parts of the bilinear concomitant.

#### 5.2.3.1 Inflow

As presented in chapter 4, the inflow boundary condition ($B$) consists in an specific mass flux vector profile, and a Dirichlet condition for the temperature. They are presented in the eq.(5.51)

$$\begin{aligned} \rho u^i - f^i(X, t, \alpha^T) &= 0 \\ T - \alpha_{Td} &= 0 \end{aligned} \quad (5.51)$$

Where $f$ could be any function that describes the mass flux vector, $\alpha^T$ is the control parameters vector and $\alpha_{Td}$ is the value of the temperature that is imposed on that boundary (We use $\alpha_{..}$ to indicate a control parameter). The linearized

form $\delta B = B'_X + B'_\alpha$ of the boundary condition becomes:

$$\begin{aligned}(\delta\rho u^i + \rho\delta u^i) - \frac{\delta f}{\delta\alpha^T}\delta\alpha^T = 0\\ \delta T - \delta\alpha_{Td} = 0\end{aligned} \tag{5.52}$$

In the eq. (5.52), the second term of the first and second equations become part of the sensitivity gradient $\langle\beta, B'_\alpha\delta\alpha\rangle$. By decomposing the linear concomitant (5.50) for the inflow condition, we get:

$$\begin{aligned}&\underbrace{\int_{\delta\Omega}\sigma(\delta\rho u^i + \rho\delta u^i).n_i}_{1} + \underbrace{(\delta\rho N_P T + \delta T N_P\rho)\Psi_i.n_i}_{2}\\ &+\underbrace{\Big(-\frac{\delta T^i.n_i}{Pe}\Big)\Theta}_{3} - \underbrace{\delta T\Big[(\rho u^i.n_i)\Theta - \frac{1}{Pe}\Theta|_i.n^i\Big]}_{4}\,dSdt\end{aligned} \tag{5.53}$$

Where terms 1 and 4 compose the term $\langle P_1(\Phi), B'_X\rangle_s$, presented in the eq. (5.54), because they have the Primal problem linearized boundary conditions $(\delta\rho u^i + \rho\delta u^i)$ and $(\delta T)$ respectively:

$$\Big\langle P_1(\Phi), B'_X\Big\rangle_s = \Big(\sigma, (\rho u^i.n_i)\Theta - \frac{\Theta|_i.n^i}{Pe}\Big).(\delta\rho u^i + \rho\delta u^i, \delta T) \tag{5.54}$$

The remaining terms 2 and 3 yield the corresponding Adjoint boundary conditions (5.55):

$$B^*(\Phi) \;=\; (\Psi_i.n^i, \Theta) = (0,0) \tag{5.55}$$

As consequence, the term $A\delta X$ which multiplies the adjoint boundary condition is:

$$A\delta X \;=\; (TN_P\delta\rho + \rho N_P\delta T, -\frac{\delta T|^i.n_i}{Pe}) \tag{5.56}$$

It is important to point that the terms $A\delta X$ in the eq.(5.56) and $B'_X\delta X$ are linearly independent, according to Cacuci' approach.

#### 5.2.3.2 Outflow

The outflow boundary condition needs the information about the pressure and heat transfer, presented in eq.(5.57):

$$\begin{aligned} P - \alpha_{Pd} &= 0 \\ T|^i.n_i &= 0 \end{aligned} \tag{5.57}$$

On recalling the non-dimensional ideal gas law $P = \rho T$, the linearized outflow boundary condition becomes the eq. (5.58):

$$\begin{aligned} \delta\rho T + \rho\delta T - \delta\alpha_{Pd} &= 0 \\ \delta T|^i.n_i &= 0 \end{aligned} \tag{5.58}$$

Where the term $\delta\alpha_{Pd}$ becomes part of the sensitivity gradient $\left\langle \beta, B'_\alpha \delta\alpha \right\rangle$. By decomposing the linear concomitant (5.50) to outflow condition:

$$\underbrace{\int_{\delta\Omega} \sigma(\delta\rho u^i + \rho\delta u^i).n_i}_{1} + \underbrace{(\delta\rho N_P T + \delta T N_P \rho)\Psi_i.n_i}_{2}$$
$$+ \underbrace{\big(-\frac{\delta T^i.n_i}{Pe}\big)\Theta}_{3} - \underbrace{\delta T[(\rho u^i.n_i)\Theta - \frac{1}{Pe}\Theta|_i.n^i]}_{4}\, dSdt$$

Where term 2 and part of 3 compose the term $\left\langle P_1(\Phi), B'_X \delta X \right\rangle_s$, presented in the eq. (5.59):

$$\left\langle P_1(\Phi), B'_X \right\rangle_s = \left\langle (N_P \Psi_i.n^i, -\frac{\Theta}{Pe}), (\delta\rho T + \rho\delta T, \delta T|^i.n_i) \right\rangle \tag{5.59}$$

The term 1, the other part of 3 and 4 yield the corresponding Adjoint boundary conditions, presented in the eq. (5.60):

$$B^*(\Phi) \;=\; (\sigma, Pe(\rho u^i.n_i)\Theta - \Theta|^i.n_i) = (0,0) \tag{5.60}$$

As a consequence, the term $A\delta X$ which multiply the adjoint boundary condition is presented in the eq. (5.61):

$$A\delta X \;=\; ((\delta\rho u^i + \rho\delta u^i).n_i, \delta T) \tag{5.61}$$

#### 5.2.3.3 Solid Wall

The boundary conditions that are imposed on solid walls are described in the eqs. (5.62):

$$\begin{aligned} \rho u^i &= 0 \\ T|^i.n_i + \alpha_{Tw1}(T - \alpha_{Tw2}) &= 0 \end{aligned} \tag{5.62}$$

The first condition $\rho u^i = 0$ reffers to no-slip boundary condition, following by a Robin condition related to heat transfer in the boundary. The coefficients $\alpha_{Tw1}$, $\alpha_{Tw2}$ ,$\alpha_{Tw3}$ represent the generic form of the heat transfer boundary condition. To recover the BC used in the eq.(4.31), the values of the coefficients are $\alpha_{Tw1} = Nu$ and $\alpha_{Tw2} = T_\infty$. Then, the linearized form becomes the eqs.(5.63):

$$\begin{aligned} \delta\rho u^i + \rho\delta u^i &= 0 \\ \delta T|^i.n_i + \delta\alpha_{Tw1}(T - \alpha_{Tw2}) + \alpha_{Tw1}\delta T - \alpha_{Tw1}\delta\alpha_{Tw2} &= 0 \end{aligned} \tag{5.63}$$

Where the terms $\delta\alpha_{Tw1}(T - \alpha_{Tw2})$, and $-\alpha_{Tw1}\delta\alpha_{Tw2}$ become part of the sensitivity gradient $\langle \beta, B'_\alpha \delta\alpha \rangle$. By decomposing the linear concomitant (5.50) for the solid wall conditions, it yields:

$$\begin{aligned} &\underbrace{\int_{\delta\Omega} \sigma(\delta\rho u^i + \rho\delta u^i).n_i}_{1} + \underbrace{(\delta\rho N_P T + \delta T N_P \rho)\Psi_i.n_i}_{2} \\ &+ \underbrace{\big(-\frac{\delta T^i.n_i}{Pe}\big)\Theta}_{3} - \underbrace{\delta T[(\rho u^i.n_i)\Theta - \frac{1}{Pe}\Theta|_i.n^i]}_{4}\, dSdt \end{aligned} \tag{5.64}$$

Where term 1 and part of term 4 (-$\delta T\rho u^i.n_i\Theta$) vanish, because of the no-slip condition. The remaining part of term 4 and the term 3 are manipulated as follows in eq. (5.65):

$$\begin{aligned} -\frac{1}{Pe}\Big(\delta T|^i.n_i\Theta + \delta T\Theta|_i.n^i\Big) &= \\ -\frac{1}{Pe}\Big(\delta T|^i.n_i\Theta + \delta T\Theta|_i.n^i &+ \Theta\alpha_{Tw1}\delta T - \Theta\alpha_{Tw1}\delta T\Big) \end{aligned} \tag{5.65}$$

On collecting the first and third terms and the second and fourth terms, it

yields the eq.(5.66):

$$\begin{aligned} - & \frac{1}{Pe}\Big(\delta T|^{i}.n_i\Theta + \delta T\Theta|_i.n^i\Big) = \\ - & \frac{1}{Pe}\Big[\delta T(\Theta|^{i}.n_i - \alpha_{Tw1}\Theta) + \Theta(\delta T|^{i}.n_i + \alpha_{Tw1}\delta T)\Big] \end{aligned} \tag{5.66}$$

The first part of the eq.(5.66) consist in an Adjoint Boundary condition $B^{*}_{\Phi}$. The second part consists in a linearized flow boundary condition $B^{'}_{X}$:

$$\Big\langle P_1(\Phi), B^{'}_{X}\Big\rangle_s = \Big(\sigma, -\frac{\Theta}{Pe}\Big).((\delta\rho u^i + \rho\delta u^i).n_i, \delta T|^{i}.n_i + \alpha_{Tw1}\delta T) \tag{5.67}$$

$$B^{*}\Phi \;=\; \Big(\Psi_i.n^i, \Theta|_i.n^i - \alpha_{Tw1}\Theta\Big) = (0,0) \tag{5.68}$$

As a consequence, the term $A\delta X$ becomes the eq. (5.69):

$$A\delta X \;=\; \Big(\delta\rho N_P T + \rho N_P\delta T, -\frac{\delta T}{Pe}\Big) \tag{5.69}$$

#### 5.2.3.4 Symmetry

The symmetry boundary condition applied to $2D$ assisymmetric model is presented in the chapter 4 as follows in the eqs. (5.70):

$$\begin{aligned} \rho u^i.n_i &= 0 \\ T|^{i}.n_i &= 0 \end{aligned} \tag{5.70}$$

The linearized form yields the eqs. (5.71):

$$\begin{aligned} (\delta\rho u^i + \rho\delta u^i).n_i &= 0 \\ \delta T|^{i}.n_i &= 0 \end{aligned} \tag{5.71}$$

By decomposing the linear concomitant (5.50) for the this condition, one gets:

$$\begin{aligned} &\underbrace{\int_{\delta\Omega}\sigma(\delta\rho u^i + \rho\delta u^i).n_i}_{1} + \underbrace{(\delta\rho N_P T + \delta T N_P\rho)\Psi_i.n_i}_{2} \\ &+ \underbrace{\big(-\frac{\delta T^i.n_i}{Pe}\big)\Theta}_{3} - \underbrace{\delta T[(\rho u^i.n_i)\Theta - \frac{1}{Pe}\Theta|_i.n^i]}_{4}\,dSdt \end{aligned} \tag{5.72}$$

Where term 1, 3 and part of term 4, $\delta T \rho u^i.n_i$ compose the term $\left\langle P_1(\Phi), B'_X \right\rangle_s$, presented in the eq. (5.73). This terms vanish because of the symmetry condition.

$$\left\langle P_1(\Phi), B'_X \right\rangle_s = \left(\sigma, -\frac{\Theta}{Pe}\right).((\delta\rho u^i + \rho\delta u^i).n_i, T|^i.n_i) \tag{5.73}$$

Term 2 and the remaining part of term 4 becomes the Adjoint boundary condition, as presented in the eq. (5.74):

$$B^*(\Phi) \;=\; (\Psi_i.n^i, \Theta|_i.n^i) = (0,0) \tag{5.74}$$

As consequence, the term $A\delta X$ becomes the eq. (5.75):

$$A\delta X \;=\; (\delta\rho N_P T + \rho N_P \delta T, -\frac{1}{Pe}) \tag{5.75}$$

It is important to make it clear that all the boundary conditions have terms $A\delta X$ and $B'_X\delta X$ linearly independents, according to Cacuci' approach.

#### 5.2.3.5 Summary of Boundary Conditions

The summary of the boundary conditions are presented in the table (5.1):

**Table 5.1:** Summary of the Boundary Conditions

| BC | Primal Problem | Dual Problem |
|---|---|---|
| Inflow | $\rho u^i - f^i(X,t,\alpha^T) = 0$<br>$T - \alpha_{Td} = 0$ | $\Psi_i.n^i = 0$<br>$\Theta = 0$ |
| Outflow | $P - \alpha_{Pd} = 0$<br>$T\|^i.n_i = 0$ | $\sigma = 0$<br>$Pe(\rho u^i.n_i)\Theta - \Theta\|^i.n_i = 0$ |
| Wall | $\rho u^i = 0$<br>$T\|^i.n_i + \alpha_{Tw1}(T - \alpha_{Tw2}) = 0$ | $\Psi_i.n^i = 0$<br>$\Theta\|_i.n^i - \alpha_{Tw1}\Theta = 0$ |
| Symmetry | $\rho u^i.n_i = 0$<br>$T\|^i.n_i = 0$ | $\Psi_i.n^i = 0$<br>$\Theta_i.n^i = 0$ |

### 5.2.4 Sensitivity Gradient

Remembering the eq. (5.18) which describes a general expression of sensitivity gradient:

$$\delta R = \langle \mathbf{F}'_\alpha, \delta\alpha \rangle + \langle \Phi, (\mathbf{Q}'_\alpha - \mathbf{N}'_\alpha)\,\delta\alpha \rangle + \langle P_1(\Phi), \mathbf{B}'_\alpha \delta\alpha \rangle_s \tag{5.76}$$

The first term represents the variation of the Objective function in terms of the control parameters and it is determined when the measure of merit is chosen to find the sensitivities. The second represents the variations of primal problem (flow governing equations) in terms of the same control parameters.

The main interest of the thesis is focused on the third term. It represents the sensitivity of the parameters which control the boundary conditions. After concluded the review of the approach of the boundary conditions described previously, and remembering that $\mathbf{B}'_X \delta\mathbf{X} = -\mathbf{B}'_\alpha \delta\alpha$ presented in eq.(5.10), we found the expression of the sensitivity gradient of these parameters $\alpha_j$, using eqs.(5.52),(5.58) and (5.63):

$$\begin{aligned} \left\langle P_1(\Phi), B'_\alpha \delta\alpha \right\rangle &= -\left\langle \sigma, \frac{\partial f^i}{\partial \alpha^T} \delta\alpha^T . n_i \right\rangle - \left\langle \frac{(\rho u^i)\Theta - \Theta|^i . n_i}{Pe}, \delta\alpha_{T_{Td}} \right\rangle \\ -\left\langle N_P \Psi^i . n_i, \delta\alpha_{P_{Pd}} \right\rangle &- \left\langle -\frac{\Theta}{Pe}, -(T - \alpha_{Tw2})\delta\alpha_{Tw1} \right\rangle - \left\langle -\frac{\Theta}{Pe}, \alpha_{Tw1}\delta\alpha_{Tw2} \right\rangle \end{aligned} \tag{5.77}$$

The five terms represent the sensitivity of each parameter individually. After we determine the expression of $f$ in the first term, we can able to find the quantity of parameters of the vector $\alpha^T$.

The second term is related to control the inlet gas temperature. The third term controls the outflow pressure, followed by the fourth term which controls the heat transfer at the tank wall, based on the Nusselt Number.

Finally the fifth term, it controls the external temperature sensibility. The next section expands this general expression to particular cases, defining not only the function $f$ of the first term, but also some examples of the objetive functions.

# 6 Dual Problem - Numerical Results

## 6.1 Introduction

The previous chapter presented considerations on the Adjoint Method, with simplifications and its general expressions. Now, the work will consider particular applications to specific objective functions and control parameters.

The CFD implementation has also used the $FREEFEM++$ platform. The advantage of the continuous Adjoint Method, which treates the primal and dual problem separately, is now showed.Because the solver methods are independent.

## 6.2 Mathematical Considerations

We start by recalling the set of dual problem equations that have been derived in the previous chapter with the composition of the term $L^*\Phi$ and the forced terms:

$$\begin{aligned} \Gamma_{11}\partial_0\sigma + \Gamma_{12}\partial_0\Theta + \Gamma_{13}\sigma|^i + \Gamma_{14}\Psi^i|_i + \Gamma_{15}\Theta &= F'_\rho \\ \Gamma_{21}\Psi^i + \Gamma_{22}\sigma|^i + \Gamma_{23}\Theta &= F'_{u^i} \\ \Gamma_{31}\partial_0\sigma + \Gamma_{22}\partial_0\Theta + \Gamma_{33}\Theta|^i + \Gamma_{34}\Psi^i|_i + \Gamma_{35}\Theta|^i|_i &= F'_T \end{aligned} \tag{6.1}$$

Where, in eqs.(6.1), $F'_X = (F'_\rho, F'_{u^i}, F'_T)$ is the vector of the variations of the objetive function in terms of the state vector $X = (\rho, u^i, T)$. These values will be defined in the next pages. Additionally, the next table presents the values of the coefficients $\Gamma_{ij}$ which depends only of the primal problem solution.

The table (6.1) presents information which are obtained by the set of data used in the primal problem and its numerical result. The terms $A_\rho$ and $A_T$ are defined in the variation of Adsorption model.

**Table 6.1:** Coefficients of the dual problem

| | | |
|---|---|---|
| $\Gamma_{11} = (\epsilon_t + \rho_b A_\rho)$ | $\Gamma_{12} = -\Big[\epsilon_t\Big(\frac{\gamma-1}{\gamma}\Big)T + \frac{\Delta H}{M_g}\rho_b A_\rho\Big]$ | $\Gamma_{13} = u^i$ |
| $\Gamma_{14} = N_P T$ | $\Gamma_{15} = -[(\epsilon_t + \rho_b A_\rho)\partial_0 T + u^i T\vert_i]$ | |
| $\Gamma_{21} = -1$ | $\Gamma_{22} = \rho$ | $\Gamma_{23} = -\rho T\vert_i$ |
| $\Gamma_{31} = \rho_b A_T$ | $\Gamma_{32} = \Big[C_{eff} - \epsilon_t\Big(\frac{\gamma-1}{\gamma}\Big)\rho - \frac{\Delta H}{M_g}\rho_b A_T\Big]$ | $\Gamma_{33} = \rho u^i$ |
| $\Gamma_{34} = N_P \rho$ | $\Gamma_{35} = -\frac{1}{Pe}$ | |

#### 6.2.0.1 Adsorption Model Coefficients

Combining eqs. (3.47),(3.48),(3.49) and (3.50), it yields the eq. (6.2):

$$q = W_0 \frac{\bar{\rho_{ads}}}{exp[\alpha_e(T - T_b)]} exp\Big[-\Big(\frac{RT.ln\Big(\frac{P_{cr}(\frac{T}{T_{cr}})^2}{p}\Big)}{\beta.E_0}\Big)^n\Big] \tag{6.2}$$

By naming the constants $C_1$ to $C_4$ in the eqs.(6.3), it reads:

$$\begin{aligned} C_1 &= W_0 \bar{\rho_{ads}} \\ C_2 &= -\Big(\frac{R}{\beta E_0}\Big)^n \\ C_3 &= \frac{P_{cr}}{T_{cr}^2} \\ C_4 &= -\alpha_e \end{aligned} \tag{6.3}$$

Then, the model yields the eq. (6.4):

$$q = C_1.exp\Big[C_2\Big[T.ln\Big(C_3\frac{T^2}{p}\Big)^n + C_4(T - T_b)\Big]\Big] \tag{6.4}$$

Now, by evaluating the variation of q in terms of $p$ and $T$, we produce the eq. (6.5):

$$\delta q = \underbrace{C_1 exp\Big[C_2\Big[T.ln\Big(C_3\frac{T^2}{p}\Big)^n + C_4(T - T_b)\Big]\Big]}_{\text{I}} . \Big[C_2 n\Big[T.ln\Big(C_3\frac{T^2}{p}\Big)\Big]\Big]^{n-1} .$$
$$. \Big[ln\Big(C_3\frac{T^2}{p}\delta T\Big) + T\Big(\frac{p}{C_3 T^2}\Big)\Big(\frac{C_3(2pT\delta T - T^2\delta p)}{p^2}\Big) - C_4\delta T\Big] \tag{6.5}$$

The term $I$ is exactly the expression of $q$ in the eq. (6.4) due to exponential variation. By naming two other relations, $D_1$ and $D_2$ presented in eqs. (6.6):

$$D_1 = \Big[T.ln\Big(C_3\frac{T^2}{p}\Big)\Big]^{n-1}$$
$$D_2 = ln\Big(C_3\frac{T^2}{p}\Big) \tag{6.6}$$

It yields the eq. (6.7):

$$\delta q = q\Big[C_2 n D_1\Big[D_2\delta T + 2\delta T - \frac{T}{p}\delta p\Big] - C_4\delta T\Big] \tag{6.7}$$

On using the state equation ($p = \rho T$), we produce the eq. (6.8):

$$\delta q = q\Big[C_2 n D_1\Big[D_2\delta T + 2\delta T - \frac{1}{\rho}(\delta\rho T + \rho\delta T)\Big] - C_4\delta T\Big] \tag{6.8}$$

By collecting the terms with $\delta\rho$ and $\delta T$, the previous equation becomes the eq. (6.9):

$$\delta q = q\Big[-\frac{C_2 n D_1 T}{\rho}\delta\rho + (C_2 n D_1(D_2+1) - C_4)\delta T\Big] \tag{6.9}$$

With this result, it is possible to determine $A_\rho$ and $A_T$, presented in the eqs. (6.10):

$$\begin{aligned} A_\rho &= -q\Big[C_2 n D_1\frac{T}{\rho}\Big] \\ A_T &= q[C_2 n D_1(D_2+1) - C_4] \end{aligned} \tag{6.10}$$

## 6.3 Numerical Discretization

### 6.3.1 Weak Formulation and Spatial Discretizations

The Equations (6.1) and the respective boundary conditions presented in the table 5.1 must be implemented into the FREEFEM++ platform, in the weak form.

By defining a inner product $< f, g >= \int_\Omega f \cdot g dV$ and the generic weight functions for Adjoint equations (ow,p1,p2 and tw), one can apply the volume integration to the eqs. (6.11):

$$\begin{aligned}\Big\langle \Gamma_{11}\partial_0\sigma + \Gamma_{12}\partial_0\Theta + \Gamma_{13}\sigma|^i + \Gamma_{14}\Psi^i|_i + \Gamma_{15}\Theta - F'_\rho, ow\Big\rangle &= 0\\ \Big\langle \Gamma_{21}\Psi^i + \Gamma_{22}\sigma|^i + \Gamma_{23}\Theta - F'_{u^i}, pi\Big\rangle &= 0\\ \Big\langle \Gamma_{31}\partial_0\sigma + \Gamma_{22}\partial_0\Theta + \Gamma_{33}\Theta|^i + \Gamma_{34}\Psi^i|_i + \Gamma_{35}\Theta|^i|_i - F'_T, tw\Big\rangle &= 0 \qquad (6.11)\end{aligned}$$

Remembering the primal problem implementation, the FREEFEM++ has hard coded algorithms to evaluate the partial derivatives of first order. Therefore, the operators $\frac{\partial}{\partial 1}$ (axial direction) and $\frac{\partial}{\partial 2}$ (radial direction) do not require any special discretization.

The diffusive term in the third equation in the set (6.11) was treated by using integration by parts:

$$\int_\Omega \Gamma_{35}.\Theta|^i|_i.twdV = \Gamma_{35}\int_{\partial\Omega}(\Theta|^i.n_i.tw)d\partial\Omega + \Gamma_{35}\int_\Omega \Theta|^i.tw|^i d\Omega \qquad (6.12)$$

Where the first term represents a Neumman boundary condition, as applied to the boundary $\partial\Omega$. The second term has only partial derivatives with respect to axial and radial directions.

The equations do not have non-linear terms. Then, it is not necessary the use of auxiliary variables, presented in the primal problem.

### 6.3.2 Time Discretization

The time-dependent terms are discretized by using backward differetiation multistep method, eq. (4.42) (GUNZBURGER, 1989). Finally, on apllying the above considerations to the Adjoint equations, we have obtained the following set of eqs. (6.13), which we have implemented into the FREEFEM++ platform:

$$\begin{aligned}\int_\Omega \Big(\Gamma_{11}\Big(\frac{3\sigma - 4\sigma_{m-1} + \sigma_{m-2}}{2dt}\Big) + \Gamma_{12}\Big(\frac{3\Theta - 4\Theta_{m-1} + \Theta_{m-2}}{2dt}\Big) + \Gamma_{13}\sigma|^i \quad +\\ \Gamma_{14}\Psi^i|_i + \Gamma_{15}\Theta - F'_\rho\Big).ow \quad +\\ \Big(\Gamma_{21}\Psi^i + \Gamma_{22}\sigma|^i + \Gamma_{23}\Theta - F'_{u^i}\Big).p_i \quad +\\ \Big(\Gamma_{31}\Big(\frac{3\sigma - 4\sigma_{m-1} + \sigma_{m-2}}{2dt}\Big) + \Gamma_{22}\Big(\frac{3\Theta - 4\Theta_{m-1} + \Theta_{m-2}}{2dt}\Big) + \Gamma_{33}\Theta|^i + \Gamma_{34}\Psi^i|_i \quad +\\ +\Gamma_{35}\Theta|^i.tw|^i - F'_T\Big).twd\Omega = 0 \qquad (6.13)\end{aligned}$$

## 6.4 Setup of Numerical Simulations

After the equations were implemented into FREFEEM++, we have carried out validation tests of the dual problem. However, there is no reference about the Adjoint solutions in the literature. Then, one way to check the numerical results is evaluating a sensitivity gradient using its solution and then to compare the results with another method to estimate derivatives.

The reference method used was the centered finite differences, which is considered as the one of simplest methods to evaluate sensitivities. The expression of this method is presented in the eq.(6.14):

$$\frac{\partial R}{\partial \alpha_i} = \frac{R(\alpha_1, \alpha_2, ..., \alpha_i + \delta\alpha_i, ..., \alpha_n) - R(\alpha_1, \alpha_2, ..., \alpha_i - \delta\alpha_i, ..., \alpha_n)}{2\delta\alpha_i} \tag{6.14}$$

Where $R(\alpha_1, \alpha_2, ..., \alpha_i + \delta\alpha_i, ..., \alpha_n)$ and $R(\alpha_1, \alpha_2, ..., \alpha_i - \delta\alpha_i, ..., \alpha_n)$ are the objetive function evaluated with positive $(+\delta\alpha_i)$ and negative $(-\delta\alpha_i)$ pertubation of the design parameter $\alpha_i$. These terms are evaluated using the primal problem code implemented at FREEFEM++.

By using the sensitivity gradient expression, we choose three terms of eq. (5.77) to find the sensitivity gradient: First, Fourth and Fifth. The last two are defined and have only one design parameter. The first needs the definition of the function $f$ and we use the same expression of the primal problem validation:

$$f(G_z, G_r) = \begin{cases} \left(2.G_m \frac{t}{t_{ac}}.\left(1 - \frac{r^2}{r_i^2}\right), 0\right) & t \leq t_{ac} \\ \left(2.G_m.\left(1 - \frac{r^2}{r_i^2}\right), 0\right) & t > t_{ac} \end{cases} \tag{6.15}$$

The eq. (6.15) has two design parameters: The nominal average mass flux, $G_m$ and the time when flow grows linearly until the nominal value $t_{ac}$. By evaluating the variation of this equations, it becomes the eq. (6.16):

$$\delta f(G_z, G_r) = \begin{cases} \left(2\frac{t}{t_{ac}}.\left(1 - \frac{r^2}{r_i^2}\right), 0\right)\delta G_m + \left(-2.G_m \frac{t}{t_{ac}^2}.\left(1 - \frac{r^2}{r_i^2}\right), 0\right)\delta t_{ac} & t \leq t_{ac} \\ \left(2.\left(1 - \frac{r^2}{r_i^2}\right), 0\right)\delta G_m + \left(0, 0\right)\delta t_{ac} & t > t_{ac} \end{cases} \tag{6.16}$$

Substituting eq. (6.16) into the first term of eq. (5.77) and driving to zero

the second and third terms which we do not use as control parameters, we find the gradient expression that was used in dual problem validation. For each component, we consider that a single $\delta a_k \neq 0$

$$\begin{aligned}
\Big\langle P_1(\Phi), B'_\alpha \delta\alpha \Big\rangle &= -\Big\langle \sigma, 2\frac{t}{t_{ac}}.\Big(1-\frac{r^2}{r_i^2}\Big)\delta G_m \Big\rangle \\
&- \Big\langle \sigma, -2.G_m \frac{t}{t_{ac}^2}.\Big(1-\frac{r^2}{r_i^2}\Big)\delta t_{ac} \Big\rangle \\
&- \Big\langle -\frac{\Theta}{Pe}, -(T-\alpha_{Tw2})\delta\alpha_{Tw1} \Big\rangle \\
&- \Big\langle -\frac{\Theta}{Pe}, \alpha_{Tw1}\delta\alpha_{Tw2} \Big\rangle
\end{aligned} \tag{6.17}$$

As is evident in the eq. (6.14), two solutions are required for each design parameter. With the eq. (6.17), we determined 4 control parameters: Average Mass Flux ($G_m$), time span for the flow to achieved the nominal value ($t_{ac}$), the Nusselt Number $\alpha_{Tw1} = Nu$ and the external temperature $\alpha_{Tw2} = T_\infty$. All of this parameters are operational and control the boundary conditions.

Then, given a objective function $R$, for estimate the 4 derivatives in terms of the control parameters, there is necessary 8 primal problem solutions if the central finite difference is used. The other objetive of the valiation tests is to compute this components of sensitivity gradient using the Adjoint Method and compare the computational costs in relation to Finite Difference

### 6.4.1 Mesh Geometry, Simulation setup and Initial Conditions

The mesh geometry, fig. 4.2, and the simulation setup are the same of the primal problem, which were in tables 4.2 and 4.3. The adjoint initial conditions are set to zero, was mentioned in the previous chapter. The only change is in the value of the volumetric flow rate where we set $15L/min$ which represents $G_m = 5.5615kg/m^2s$.

### 6.4.2 Objetive Functions

On considering the Adjoint Equations (6.1), it is necessary to define an Objective Function. The tests were done using 4 different expressions: Mass, Pressure, Temperature and Density of Adsorption. The following section presenting the results of each of them with respective derivation of forced terms presented in the

Adjoint Equations.

## 6.5 Numerical Results

This section presents the estimation of sensitivity gradient using the numerical results of the dual problem (Adjoint Equations). The objective functions and control parameters were described in the previous section. Morever, the computational cost of Adjoint Method was compared to Finite Difference Method, which we call "FD" in this section, and the results are presented as follows.

The filling flow was set to 15 LPM (liters per minute) at STP. The total time of simulations was $210s$ and the sensitivity gradient was obtained in 6 different times: $60s$, $90s$, $120s$, $150s$, $180s$ and $210s$ to see the values along the filling time. Natural convection was considered.

### 6.5.1 R = Mass

For the mass, the expression of the Objetive function is presented in the eq.(6.18):

$$R = \frac{1}{T}\int_0^T \oint_D (\epsilon_t \rho + \rho_b q) \mathrm{d}V \mathrm{d}t \tag{6.18}$$

By evaluating the variation of Objetive Function $\partial R$, it yields the eq.(6.19):

$$\partial R = \frac{1}{T}\int_0^T \oint_D [(\epsilon_t + \rho_b A_\rho)\delta\rho + \rho_b A_T \delta T] \mathrm{d}V \mathrm{d}t \tag{6.19}$$

Where $\delta q$ was expanded using the eq. (5.41).The values of $F'_\rho$, $F'_{u^i}$ and $F'_T$ that used as forced terms in the Adjoint Equations are presented in eq.(6.20):

$$\begin{cases} F'_\rho &= \epsilon_t + \rho_b A_\rho \\ F'_{u^i} &= 0 \\ F'_T &= \rho_b A_T \end{cases} \tag{6.20}$$

Then, the following figures present the behavior of the gradient components along the filling time.

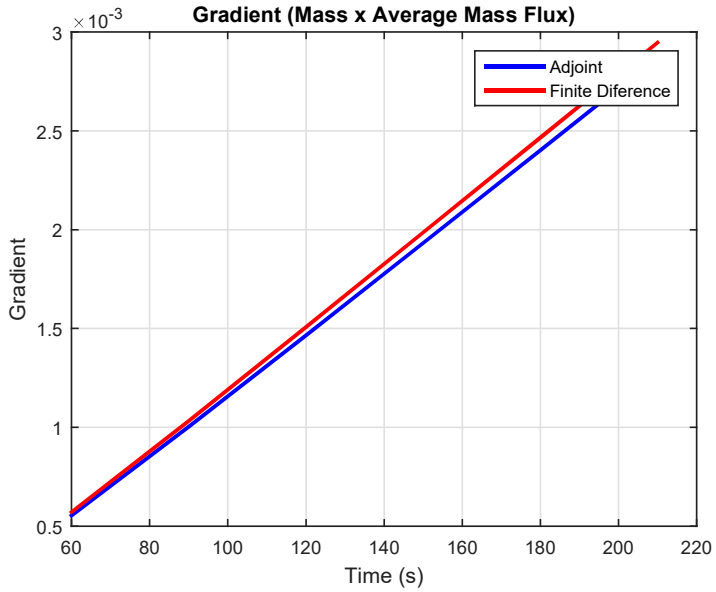


**Figure 6.1:** $\frac{\partial M}{\partial G_m}$ from $15LPM$ along the filling time - Blue: Adjoint; Red: FD.

At fig. 6.1, the magnitude of the difference between Adjoint and FD increases along the filling time. The value grows from $1.7.10^{-5}$ at $60s$ to $7.4.10^{-5}$ at $210s$. However, the relative error was decreased due to magnitude of the gradient. At $60s$, the absolute error was 3.0% , while at $210s$, was 2.5%.

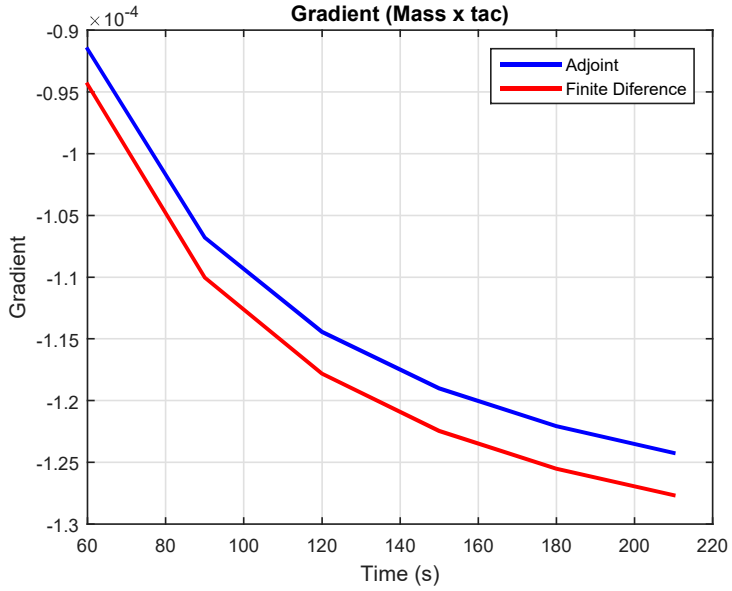


**Figure 6.2:** $\frac{\partial M}{\partial t_{ac}}$ from $15LPM$ along the filling time - Blue: Adjoint; Red: FD.

Observing the fig. 6.2, the magnitude of the difference between Adjoint and FD has the same behavior of the previous control parameter and increase along the filling time. The value grows from $2.8.10^{-6}$ at $60s$ to $3.4.10^{-6}$ at $210s$. On the other hand, the relative error was decreased due to magnitude of the gradient. At $60s$, the absolute error was 3.0% while at $210s$, the value was 2.7%.

The similarity of the error along the time could be explained by the fact that the two components have the dependence of the same Adjoint variable, $\sigma$. The next figures present the gradient of the two other parameters, which depends of the Adjoint variable $\Theta$.

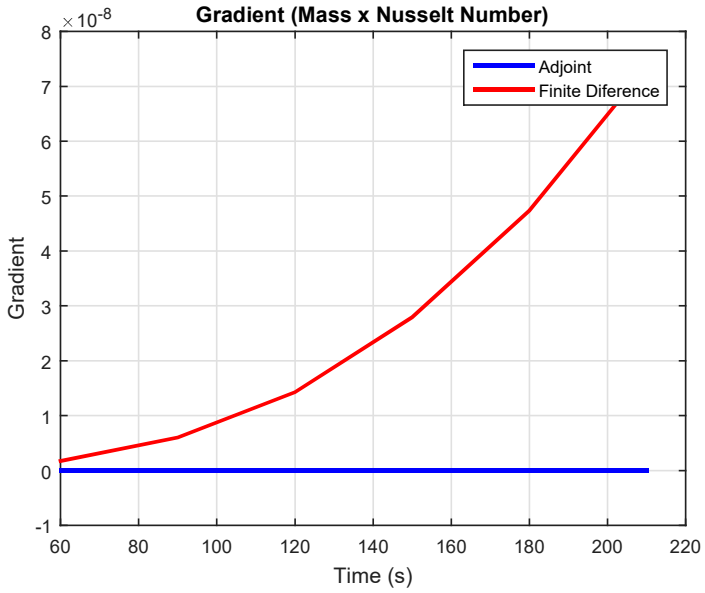


**Figure 6.3:** $\frac{\partial M}{\partial Nu}$ from $15LPM$ along the filling time - Blue: Adjoint; Red: FD.

The result of $Nu$ presented in fig.6.3 shows that the gradient by Adjoint Method was zero, while the value by FD was small, but not zero. Observing the Adjoint solution for this case, the value of $\Theta$ is zero and then, the gradient vanishes. For the same reason, the results for $T_\infty$ indicates the gradient zero using Adjoint Method. The fig. (6.4) shows a non zero value using FD.

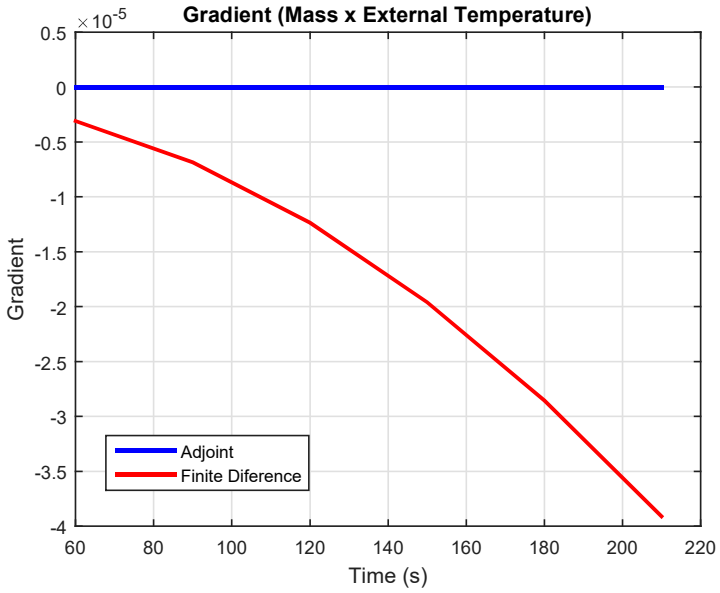


**Figure 6.4:** $\frac{\partial M}{\partial T_\infty}$ from $15LPM$ along the filling time - Blue: Adjoint; Red: FD.

### 6.5.2 R = Volume Averaged Pressure

For the volumetric average pressure, the expression of the Objective function is presented in eq.(6.21):

$$R = \frac{1}{T}\int_0^T \oint_D \left(\frac{p}{V_t}\right) \mathrm{d}V\,\mathrm{d}t \tag{6.21}$$

Where $V_t$ is the internal volume of the ANG tank. By evaluating the variation of Objetive Function $\partial R$, it yields the eq. (6.22):

$$\partial R = \frac{1}{T}\int_0^T \oint_D \frac{1}{V_t}\Big(\delta p\Big) \mathrm{d}V\,\mathrm{d}t \tag{6.22}$$

By using the variation of gas state equation ($\delta p = \delta\rho T + \rho\delta T$), we form the eq.(6.23):

$$\partial R = \frac{1}{T}\int_0^T \oint_D \frac{1}{V_t}\Big(\delta\rho T + \rho\delta T\Big) \mathrm{d}V\,\mathrm{d}t \tag{6.23}$$

Then, the values of $F'_\rho$, $F'_{u^i}$ and $F'_T$ are presented in the eq. (6.24):

$$\begin{cases} F'_\rho &= \frac{T}{V_t} \\ F'_{u^i} &= 0 \\ F'_T &= \frac{\rho}{V_t} \end{cases} \tag{6.24}$$

It is important to know that for each Objective function defined, it is necessary to find its variation and consequently the expressions that defined the forced terms of the Adjoint Equations. The LHS of those equations, $L^*(\Phi)$, which has the differential operators are kept without changes.

By keeping the same gradient expressions, the following figures present the comparison between the sensitivity gradient obtained by Adjoint Method and FD method.

The fig. 6.5 shows the great proximity of the gradient results. The value obtained by Adjoint Method grows from $4.0.10^{-2}$ at $60s$ to $6.0.10^{-1}$ at $210s$. The relative error was smaler due to magnitude of the gradient. At $60s$, the absolute

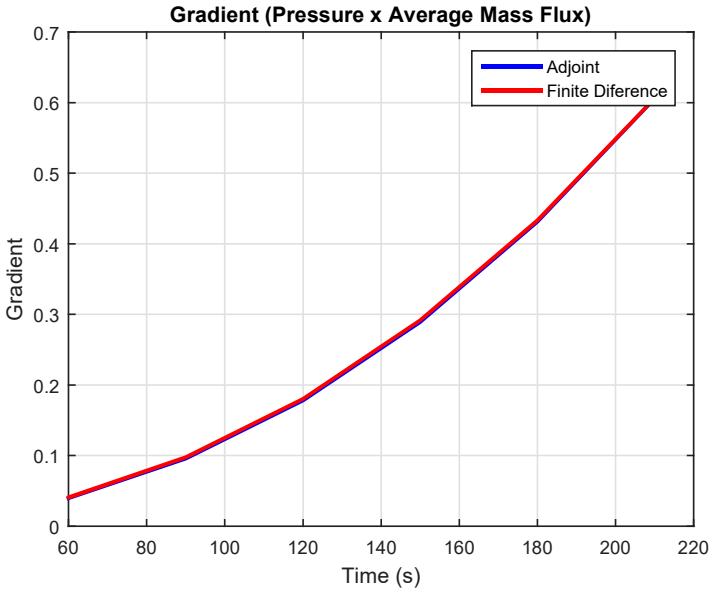


**Figure 6.5:** $\frac{\partial p}{\partial G_m}$ from $15LPM$ along the filling time - Blue: Adjoint; Red: FD.

error was 2.5% , while at $210s$, was 0.04%.

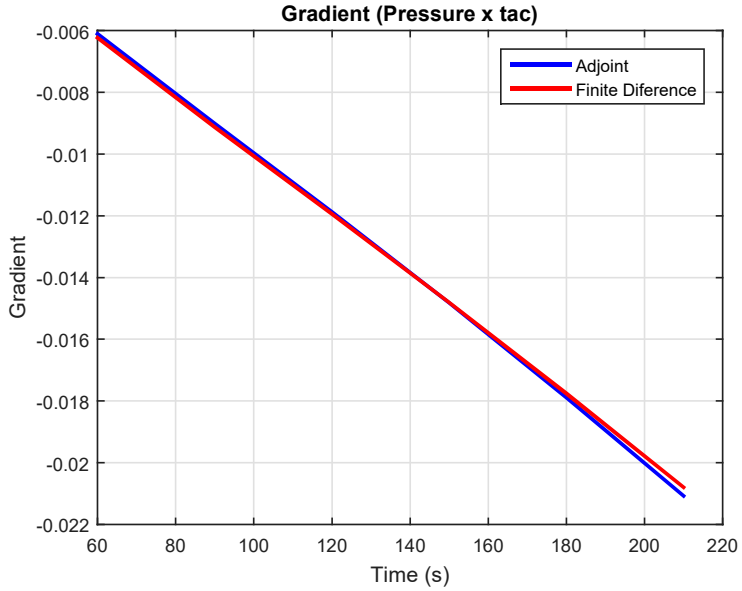


**Figure 6.6:** $\frac{\partial p}{\partial t_{ac}}$ from $15LPM$ along the filling time - Blue: Adjoint; Red: FD.

The results from $t_{ac}$ show a good accuracy as the values from $G_m$ as can be seen in the fig.(6.6). The value obtained by Adjoint Method decreases from $-6.1.10^{-3}$ at $60s$ to $-2.1.10^{-2}$ at $210s$. The relative error changes the signal with time. At $60s$, the error was $-2.0\%$ , while at $210s$, the error was $+1.3\%$.

For gradient terms which depend of on the adjoint variable $\Theta$, results were more accurate. The component related to $Nu$ varied from $-6.3.10^{-5}$ at $60s$ to $-2.5.10^{-3}$ at $210s$ according to fig. 6.7. The relative error presented small values, but the value increases along time. At $60s$, the error was 0.3% while at $210s$, the

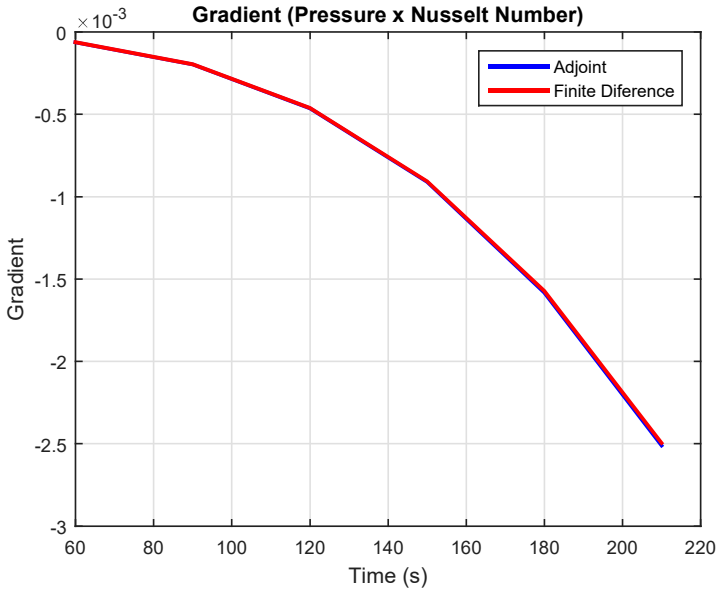


**Figure 6.7:** $\frac{\partial p}{\partial Nu}$ from $15LPM$ along the filling time - Blue: Adjoint; Red: FD.

value was 0.6%.

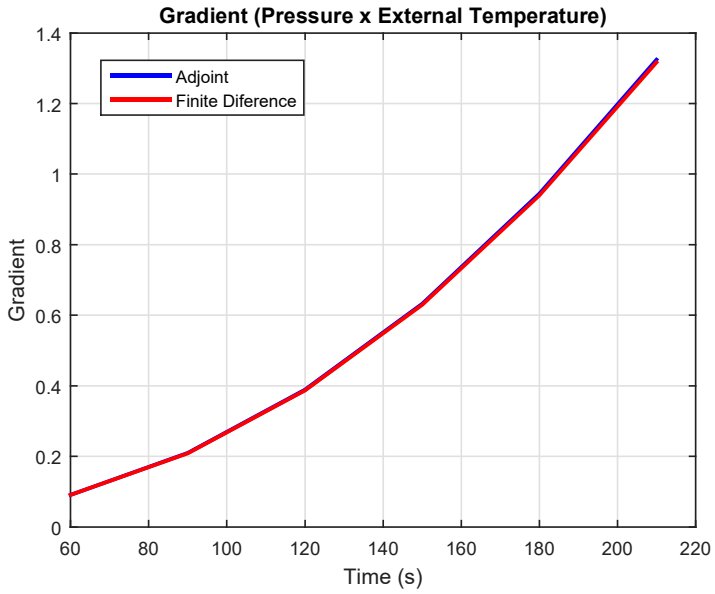


**Figure 6.8:** $\frac{\partial p}{\partial T_\infty}$ from $15LPM$ along the filling time - Blue: Adjoint; Red: FD.

The same behavior was found in the component related to $T_\infty$ and it can be seen in fig. 6.8. The gradient value varied from $9.1.10^{-2}$ at $60s$ to $1.3.10^{0}$ at $210s$. The relative error also presented small values, with the same growing of gradient related to $Nu$. At $60s$, the error was 0.2% while at $210s$, the value was 0.6%.

### 6.5.3 R = Volume Averaged Temperature

For the volumetric average temperature, the expression of the objetive function is presented as follows in the eq.(6.25):

$$R = \frac{1}{T}\int_0^T \oint_D \left(\frac{T}{V_t}\right) \mathrm{d}V\,\mathrm{d}t \tag{6.25}$$

Where $V_t$ is the internal volume of the ANG tank. By evaluating the variation of the objetive function, it yields the eq. (6.26):

$$R = \frac{1}{T}\int_0^T \oint_D \left(\frac{\delta T}{V_t}\right) \mathrm{d}V\,\mathrm{d}t \tag{6.26}$$

The values of $F'_\rho$, $F'_{u^i}$ and $F'_T$ are presented in the eq. (6.27):

$$\begin{cases} F'_\rho &= 0 \\ F'_{u^i} &= 0 \\ F'_T &= \frac{1}{V_t} \end{cases} \tag{6.27}$$

Again, by keeping the same gradient expressions, the following figures present the compassion between the sensitivity gradient obtained by Adjoint Method and FD method.

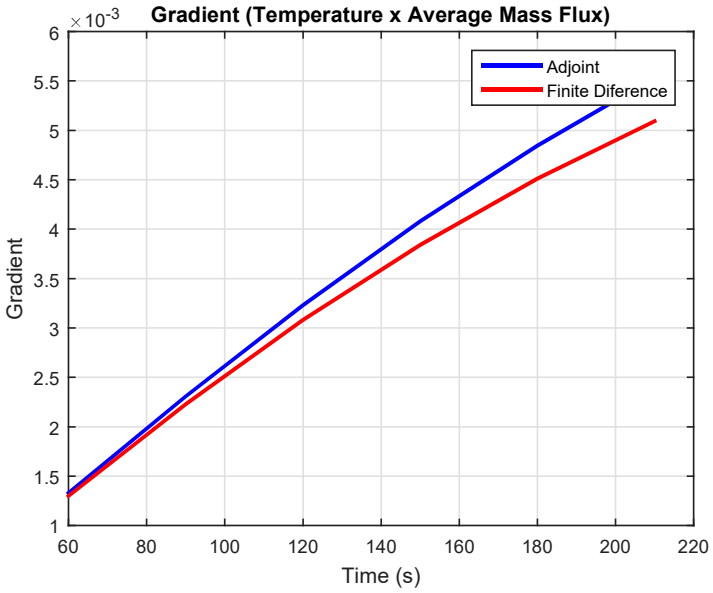


**Figure 6.9:** $\frac{\partial T}{\partial G_m}$ from $15LPM$ along the filling time - Blue: Adjoint; Red: FD.

The fig. 6.9 shows good proximity of the gradient results, but not the same precision when the pressure was the objective function. The value obtained by Adjoint Method grows from $1.3.10^{-3}$ at $60s$ to $5.5.10^{-3}$ at $210s$. The relative error was increased due to magnitude of the gradient. At $60s$, the error was 2.2% , while at $210s$, the error was 8.6%.

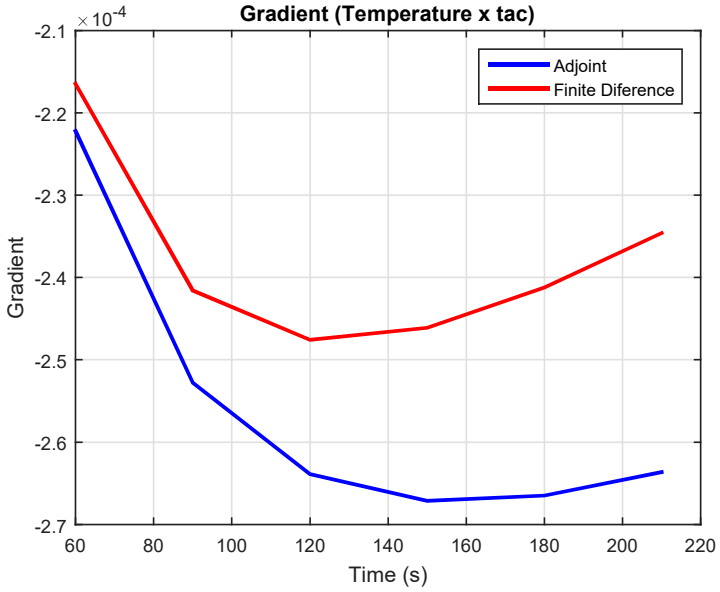


**Figure 6.10:** $\frac{\partial T}{\partial t_{ac}}$ from $15LPM$ along the filling time - Blue: Adjoint; Red: FD.

The results for $t_{ac}$ show a decrease in accuracy as the values for $G_m$ and can be seen in the fig. 6.10. The value obtained by Adjoint Method changes slowly from $-2.2.10^{-4}$ at $60s$ to $-2.6.10^{-4}$ at $210s$. The relative error grows faster than in the previous result. At $60s$, the error was 2.6% , while at $210s$, the error was 12.4%. Again, the gradient components which depends from $\sigma$ presented the worst results.

On the other hand, the results of gradient components which depend on the adjoint variable $\Theta$ keeps the good precision. The component related to $Nu$ varied from $-1.3.10^{-5}$ at $60s$ to $-9.6.10^{-3}$ at $210s$ according to fig.(6.11). The relative error presented small values, but the value increases with time. At $60s$, the error was 0.1% while at $210s$, the value was 0.2%.

The behavior of the component related to $T_\infty$ was better than the component related to $Nu$ and it can be seen in fig.(6.12). The gradient value varied from $2.0.10^{-2}$ at $60s$ to $5.8.10^{0}$ at $210s$. The relative error also presented small values. At $60s$, the error was 0.02% while at $210s$, the value was 0.1%.

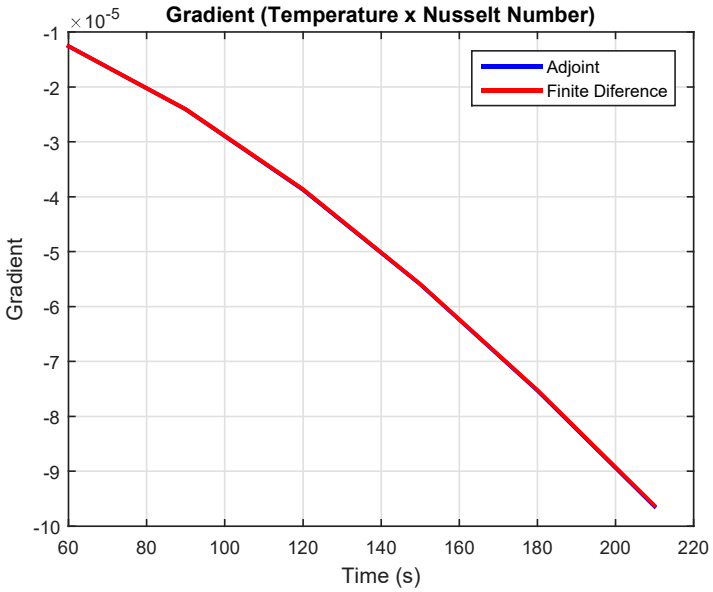


**Figure 6.11:** $\frac{\partial T}{\partial Nu}$ from $15LPM$ along the filling time - Blue: Adjoint; Red: FD.

### 6.5.4 R = Volume Averaged Density of Adsorption

For the volumetric average density of adsorption, the expression of the Objective function is presented in eq. (6.28):

$$R = \frac{1}{T}\int_0^T \oint_D \left(\frac{q}{V_t}\right) \mathrm{d}V\mathrm{d}t \tag{6.28}$$

Where $V_t$ is the internal volume of the ANG tank. By evaluating the variation of Objective Function $\partial R$, it yields the eq.(6.29):

$$R = \frac{1}{T}\int_0^T \oint_D \left(\frac{\delta q}{V_t}\right) \mathrm{d}V\mathrm{d}t \tag{6.29}$$

Where $\delta q$ was expanded using the eq. (5.41), forming the eq.(6.30):

$$R = \frac{1}{T}\int_0^T \oint_D \left(\frac{A_\rho \delta\rho + A_T \delta T}{V_t}\right) \mathrm{d}V\mathrm{d}t \tag{6.30}$$

The values of $F'_\rho$, $F'_{u^i}$ and $F'_T$ are presented below, in the eq.(6.31)

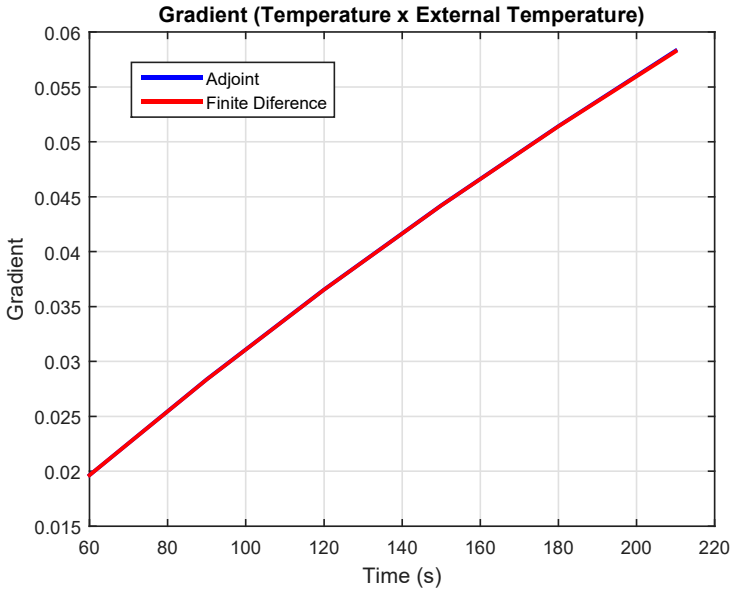


**Figure 6.12:** $\frac{\partial T}{\partial T_\infty}$ from $15LPM$ along the filling time - Blue: Adjoint; Red: FD.

$$\begin{cases} F'_\rho &= \rho_b A_\rho \\ F'_{u^i} &= 0 \\ F'_T &= \rho_b A_T \end{cases} \tag{6.31}$$

The following figures present the comparison between the sensitivity gradient obtained by Adjoint Method and FD method.

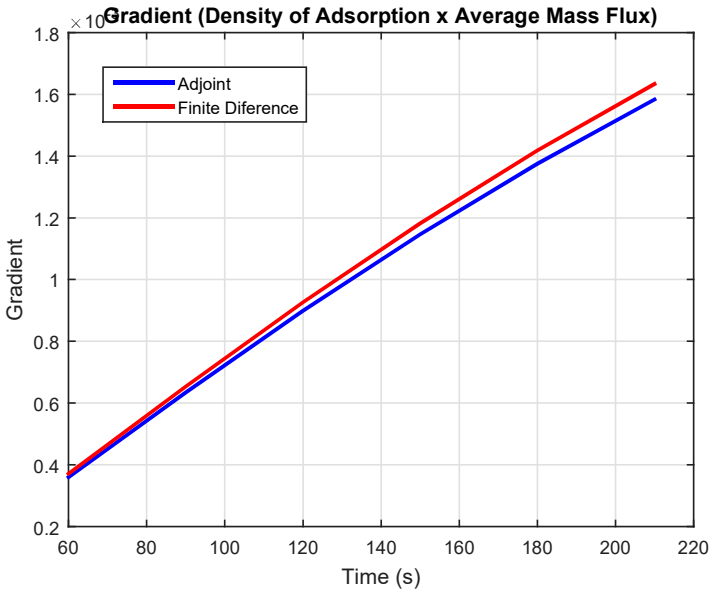


**Figure 6.13:** $\frac{\partial q}{\partial G_m}$ from $15LPM$ along the filling time - Blue: Adjoint; Red: FD.

Figure 6.13 shows better proximity of the gradient results in comparison be-

tween the results using the temperature as measure of merit, but not the same precision when the pressure was the objective function. The value obtained by the adjoint Method grows from $3.6.10^{-4}$ at $60s$ to $1.6.10^{-3}$ at $210s$. The relative error had small oscilation due to magnitude of the gradient. At $60s$, the error was $-3.0\%$ , while at $210s$, the error was $-3.1\%$.

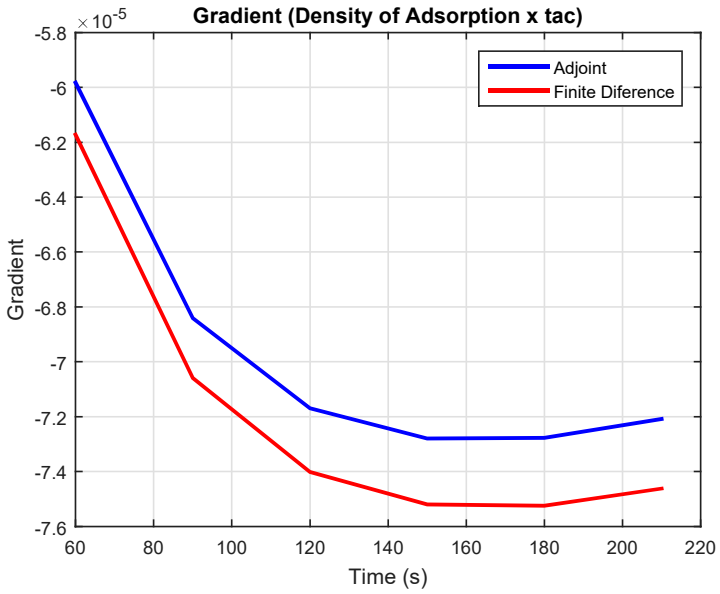


**Figure 6.14:** $\frac{\partial q}{\partial t_{ac}}$ from $15LPM$ along the filling time - Blue: Adjoint; Red: FD.

The results from $t_{ac}$ show the same precision as the values from $G_m$ as can be seen in the fig.(6.14). The value obtained by Adjoint Method changes from $-6.0.10^{-5}$ at $60s$ to $-7.2.10^{-5}$ at $210s$. The relative error keeps the same behavior of previous result. At $60s$, the error was $-3.1\%$ , while at $210s$, the error was $-3.4\%$.

The results of gradient components that depend on Adjoint variable $\Theta$ keep the same precision of the components in terms of $\sigma$. The component related to $Nu$ varied from $4.4.10^{-8}$ at $60s$ to $1.6.10^{-6}$ at $210s$ according to fig.(6.15). At $60s$, the relative error was $-2.9\%$ while at $210s$, the value was $-2.5\%$.

The behavior of the component related to $T_\infty$ was the same as the component related to $Nu$ and it can be seen in fig.(6.16). The gradient value varied from $-6.5.10^{-5}$ at $60s$ to $-8.3.10^{-4}$ at $210s$. At $60s$, the absolute error was $3.0\%$ while at $210s$, was $2.5\%$.

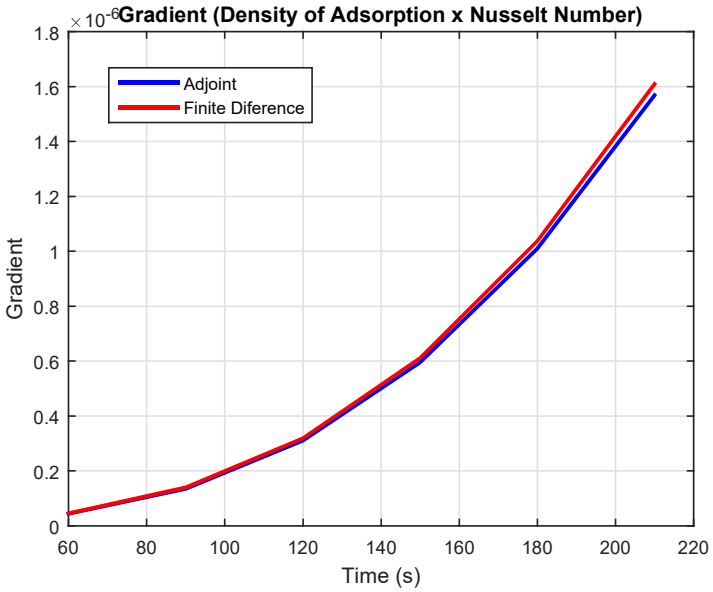


**Figure 6.15:** $\frac{\partial q}{\partial Nu}$ from $15LPM$ along the filling time - Blue: Adjoint; Red: FD.

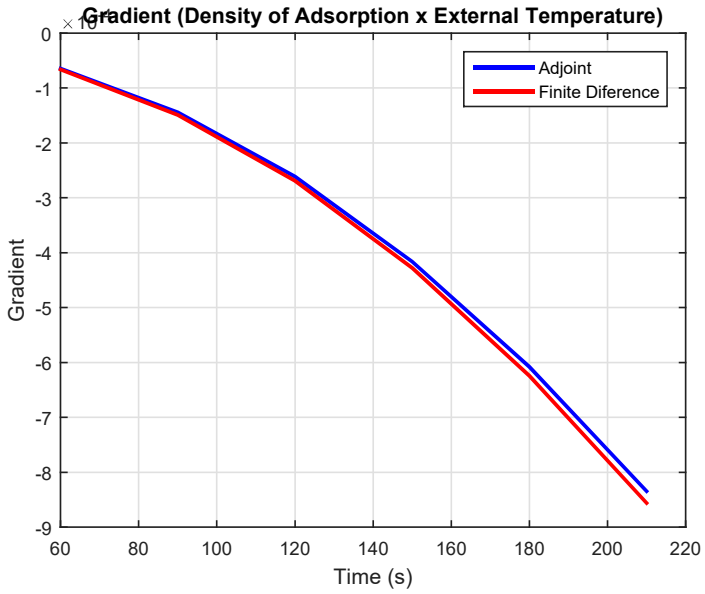


**Figure 6.16:** $\frac{\partial q}{\partial T_\infty}$ from $15LPM$ along the filling time - Blue: Adjoint; Red: FD.

# 7 Optimization Algorithm

The previous chapters presented the parts of the Optimization Loop Algorithm ($OLA$) and their individual validations, which prove the consistency of the primal/dual equations and the sensitivity gradient expressions. Now, this chapter presents the integration of these parts, the validation tests and an example of an engineering application that can be used in the industry.

As the parts of the algorithm were written in different *.*edp* files (*.*edp* is the source code extension read in FREEFEM++), we prefer to keep the codes separated and create text files to transport the information along the $OLA$. The fig. 7.1 presents the basic scheme of the programming logic:

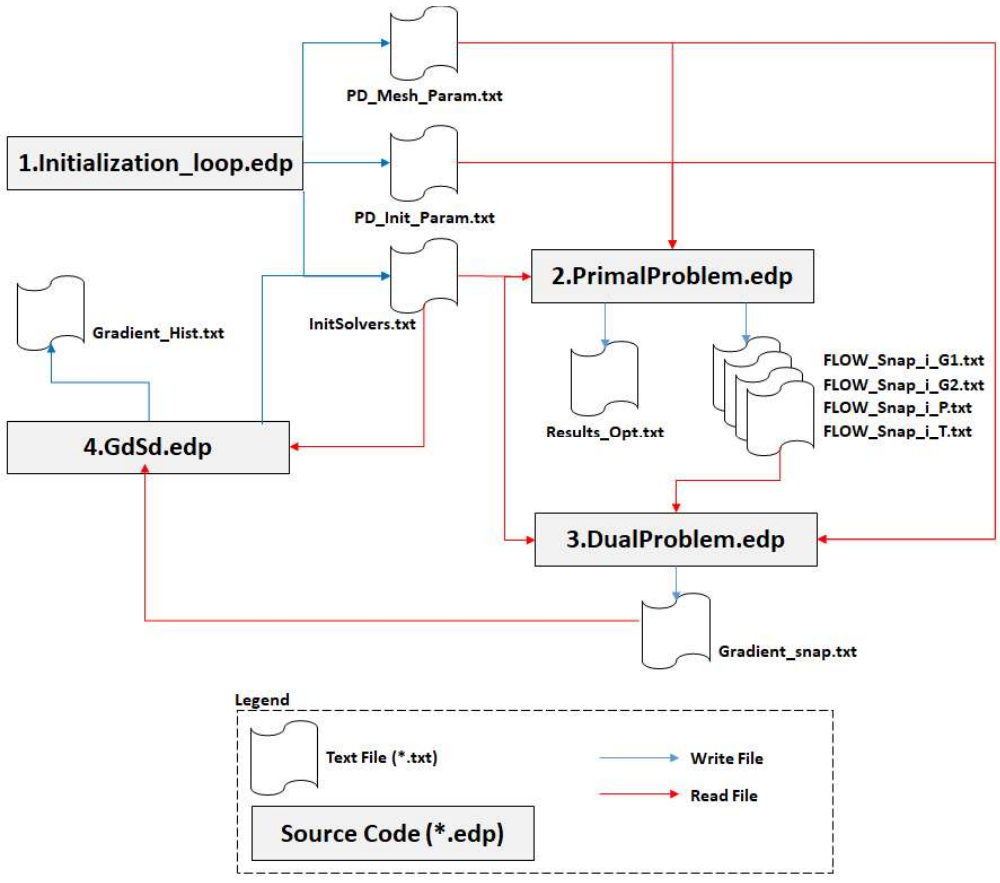


**Figure 7.1:** Information way along the $OLA$

The *OLA* has four source codes which are described below:

- **initialization_loop.edp**: The first source code is the setup of the *OLA*. The values of design parameters, mesh geometry, constant properties and simulation data are listed here and distributed in three different files:

  *PD_Mesh_Param.txt* which has the information of the mesh geometry;

  *PD_Init_Param.txt* which has the constant properties of the flow, such as the thermal parameters of the gas and adsorbent, D-A adsorption model constants, reference state to the non-dimensional equations, etc;

  *InitSolvers.txt* which has the values of the design parameters and their respective numerical maximum variation allowed. This file has also the values of the total time of the simulation, the time step and *OLA* control parameters, such as the number of the cycles performed.

- **PrimalProblem.edp**: This source code has the flow governing equations, described in the chapters 3 and 4, and the evaluation of the Objective function. It reads the files written by the **initialization_loop.edp** in the first optimization cycle or by **GdSd.edp** in the other cycles. The results of this code are the record of the previous and current cycles (*Results_Opt.txt*) and the snapshots of the flow simulation which are used to solve the Adjoint Equations *FLOW_snap_i_....txt*).

- **DualProblem.edp**: The Adjoint Equations and gradient expressions described in the chapters 5 and 6 were implemented in this source code. It reads, not only the data used in Primal Problem, but also the snapshots written during the processing of the flow governing equations. The output is the file *Gradient_snap.txt* which contains the values of the sensitivity gradient in each time step.

- **GdSd.edp**: The last source code of the *OLA* is responsible for the integration of the sensitivity gradient which gives the search direction of all design parameters. With this direction, the values of the parameters are changed using a steepest decent method and the file *InitSolvers.txt* is rewritten, starting a new optimization cycle. Also, a record of the values of sensitivity gradient was registered in the file *Gradient_Hist.txt*.

## 7.1 Validation Tests Setup

With the programming of the $OLA$, validation tests were performed to test the integration of the whole source codes. We choose the inflow boundary condition as the test, changing the parametrization of the flow curve, based on the eq. (6.15):

$$f(G_z, G_r) = \left(2.\eta G_m.\left(1 - \frac{r^2}{r_i^2}\right), 0\right) \tag{7.1}$$

In the eq. (7.1), $G_m$ was considered constant and $\eta$ represents a function, described by the design parameters and dependent on time. In the other words, $\eta$ is a factor that multiplies the nominal average mass flux $G_m$.

The objective function was determined by considering the monitoring of the $OLA$ answer. The idea is the inverse design application, where we use a known distribution of the density of adsorption inside the tank, that we call *target*. Then, we impose an volumetric ($V_t$) average quadratic error between the currently distribution and the target as measure of merit, presented in the eq.(7.2):

$$R = \frac{1}{T.V_t} \int_0^T \oint\!\!\oint_D \frac{(q - q_t)^2}{2} \mathrm{d}V\,\mathrm{d}t \tag{7.2}$$

Where $q_t$ is the known distribution (target) and $q$ is the density of adsorption distribution evaluated in the optimization cycle. By evaluating the variation of objective function $\partial R$, it yields the eq. (7.3):

$$R = \frac{1}{T.V_t} \int_0^T \oint\!\!\oint_D (q - q_t)\delta q \mathrm{d}V\,\mathrm{d}t \tag{7.3}$$

By considering the relation of $\delta q$ and the state variables, eq. (5.41), we determine the forced terms that are used in the dual problem:

$$\begin{cases} F'_{\rho} &= \frac{(q-q_t)A_{\rho}}{V_t} \\ F'_{u^i} &= 0 \\ F'_{T} &= \frac{(q-q_t)A_{T}}{V_t} \end{cases} \tag{7.4}$$

For the following tests, the mesh geometry, fig. 4.2 and the simulation setup are the same as those of the primal and dual problem validations which are presented in tables 4.2 and 4.3. We use the same value of the volumetric flow rate that was used in the dual problem validation: $15L/min$ which represents $G_m = 5.5615\ kg/m^2s$.

It is good practice in the OLA validations, to use a smaller set of design parameters in the first tests. The simplest case is the use of one parameter which implies in a linear function $\eta = a.t$, where $a$ is the linear slope and the design parameter also. The gradient expression used in the $OLA$ was derived using the first term in RHS of eq.(5.77), presented in the eq.(7.5):

$$\Big\langle P_1(\Phi), B'_\alpha \delta\alpha \Big\rangle \;=\; -\Big\langle \sigma, 2.\Big(\frac{\partial \eta}{\partial a}\Big).G_m.\Big(1 - \frac{r^2}{r_i^2}\Big)\delta a \Big\rangle \tag{7.5}$$

The derivative of $\eta$ in terms of $a$ is easily found:

$$\frac{\partial \eta}{\partial a} = t \tag{7.6}$$

Finally, by substituting the eq.(7.6) in the eq.(7.5), we have the gradient expression 7.7, used in the tests with $\eta$ as a linear function:

$$\Big\langle P_1(\Phi), B'_\alpha \delta\alpha \Big\rangle \;=\; -\Big\langle \sigma, 2.t.G_m.\Big(1 - \frac{r^2}{r_i^2}\Big)\delta a \Big\rangle \tag{7.7}$$

The *target* distribution was evaluated by using the Primal Problem code and the value of the design parameter was $a = 0.5$. A stop criterion interrupt the cycles when the value of objective function becomes below of $10^{-9}$.

Additionally, the maximum variation of the design parameter after a gradient estimation was reduced by 50% when the search direction changed its signal, which means the proximity of the optimal value. Then, it is a good strategy a reduction of the variation.

The first test was started with $a = 0.3$ and the expected result is the $OLA$, during the optimization cycles, changing $a$ until values close to 0.5. The fig. 7.2 presents the results during the cycles:

The $OLA$ spent 5 cycles to find $a = 0.505628$ which results in $R = 1.41685.10^{-10}$.

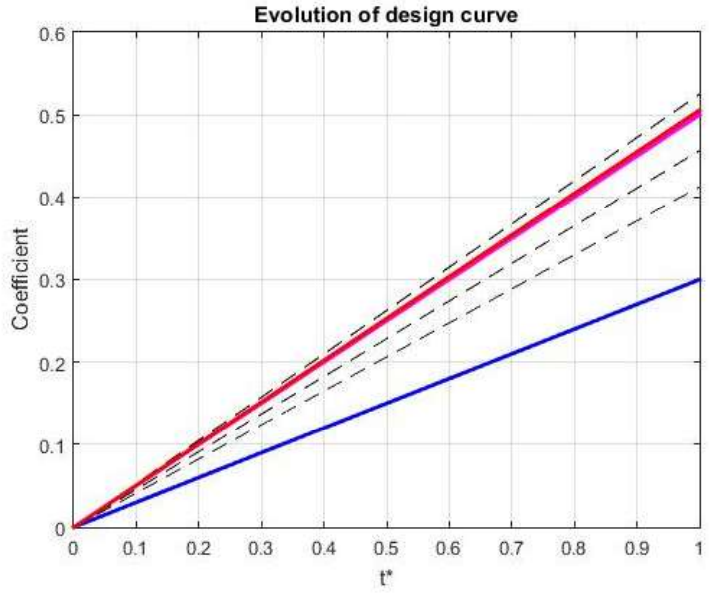


**Figure 7.2:** Optimization Results of the Test 1: Magenta: Target Curve; Blue: First Cycle; Dashed Black: Intermediate cycles; Red: Last Cycle

The behavior of the codes was satisfactory with the correct search directions estimation and the respective changes when the signal inversion occurred. Basically, the $OLA$ succeded in recovering the correct value of $a$ that represents the target density of adsorption distribution.

The fig.(7.3) presents the evolution of sensitivity gradient along the cycles.

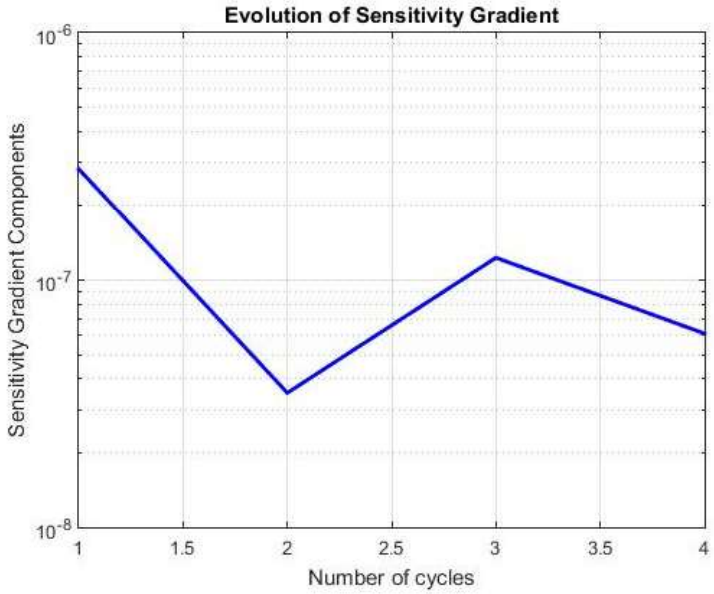


**Figure 7.3:** Sensitivity Gradient of the Test 1

It is important to see that oscillations of the absolute value of sensitivity gradient are expected, considering the possibility of the signal inversion during the cycles. The test 2 uses the same setup as first test, but changing the initial value of $a$ to 0.7. The fig. 7.4 presents the results during the cycles:

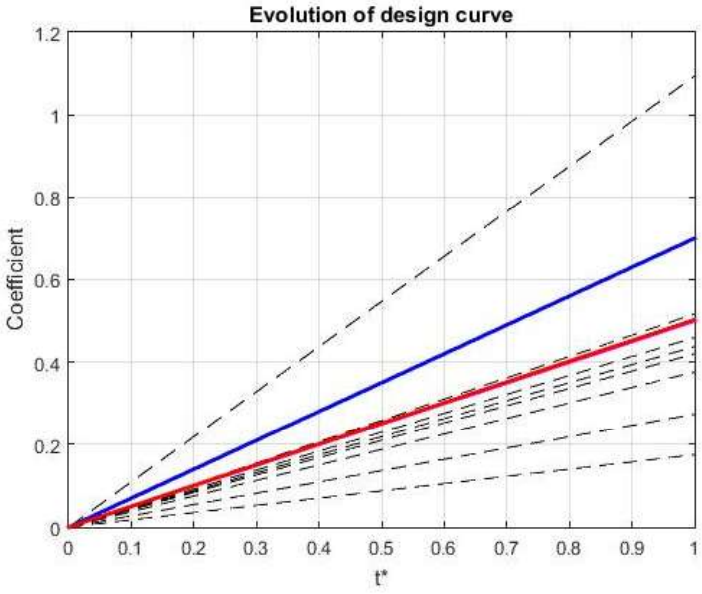


**Figure 7.4:** Optimization Results of the Test 2: Magenta: Target Curve; Blue: First Cycle; Dashed Black: Intermediate cycles; Red: Last Cycle

In this test, the $OLA$ spent 10 cycles to find $a = 0.502489$. The objective function achieved $R = 2.77035.10^{-11}$. However, the cycles presented a big oscillation of the value of $a$. The reason is the maximum variation allowed for the design parameter. We set this variation to 75% of the current parameter value. By reducing this variation to 50%, test 3 are presented in the fig. 7.5:

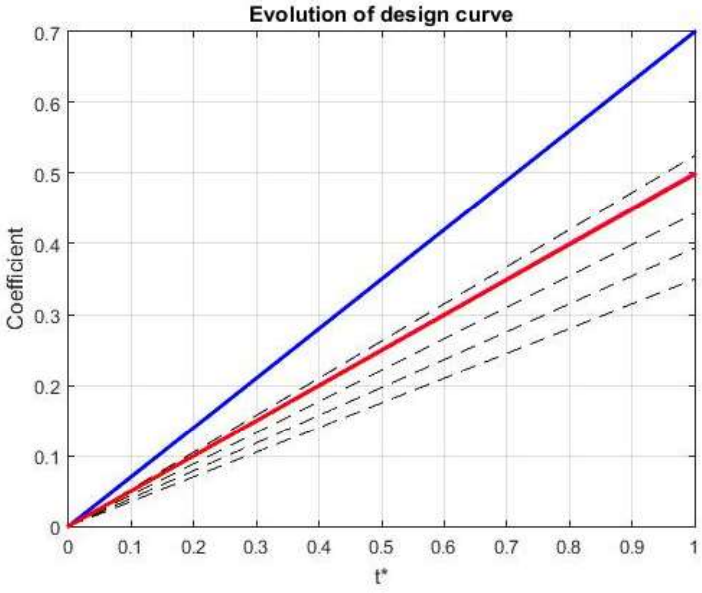


**Figure 7.5:** Optimization Results of the Test 3: Magenta: Target Curve; Blue: First Cycle; Dashed Black: Intermediate cycles; Red: Last Cycle

The test 3 spent 6 cycles, less than the test 2, to achieve $a = 0.49834$ which represents a $R = 1.23416.10^{-11}$. With a smaller variation than the previous test, the $OLA$ could find the optimal value faster than test 2. That is an important

consideration in gradient estimation. Because not only the initial solution but also the variation of the parameters affect the number of cycles needed to find the best solution.

As the linear function presented good results during the optimization, we step up the target function to see the behavior of the $OLA$. The test 4 changed the target distribution, by using a parabola flow curve $\eta = 0.3t^2 + 0.2t$. We kept one design parameter in the $OLA$, $(\eta = b.t)$, so the expected curve is the value of $b$ which represents the best approximation of the target distribution. Also, the simulation totaltime increase to $60s$. The fig. 7.6 presents the results, considering a initial value of design parameter in $b = 0.25$:

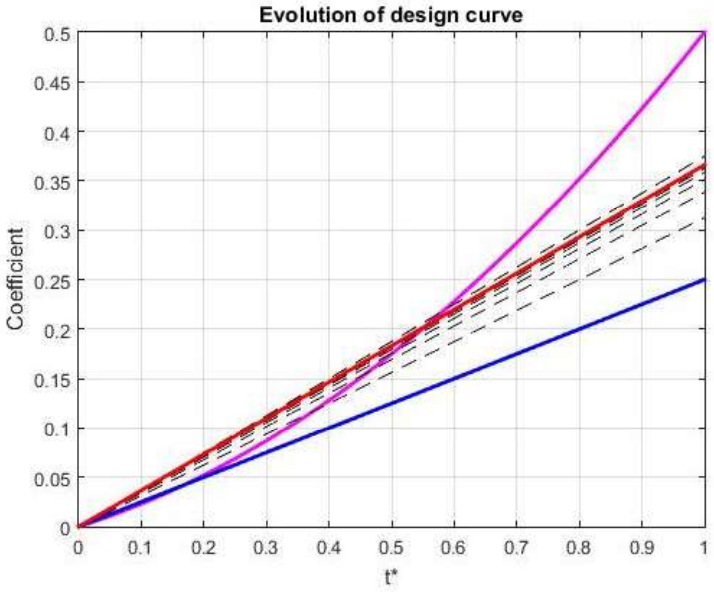


**Figure 7.6:** Optimization Results of the Test 4: Magenta: Target Curve; Blue: First Cycle; Dashed Black: Intermediate cycles; Red: Last Cycle

The $OLA$ spent 11 cycles to achieve the best result. It is important to mention that we introduce another stop criterion beyond the value of the objective function. The $OLA$ will stop if the maximum variation of the design parameter reduces to values below $10^{-2}$. The reason for this implementation is the observation of small variations in the value of the Objective function when the design parameter variation is below $10^{-2}$. As seen in the test 4, the value of objective function becomes to $R = 5.6318.10^{-8}$, above the $10^{-9}$ imposed as stop criteria. The $OLA$ stops due the criteria of the maximum variation and find the value of design parameter $b = 0.366241$. Figure 7.7 presents the evolution of the sensitivity gradient:

With the second stop criterion, the value of sensitivity gradient reduced more than the other tests, due the smaller variations of the design parameters which

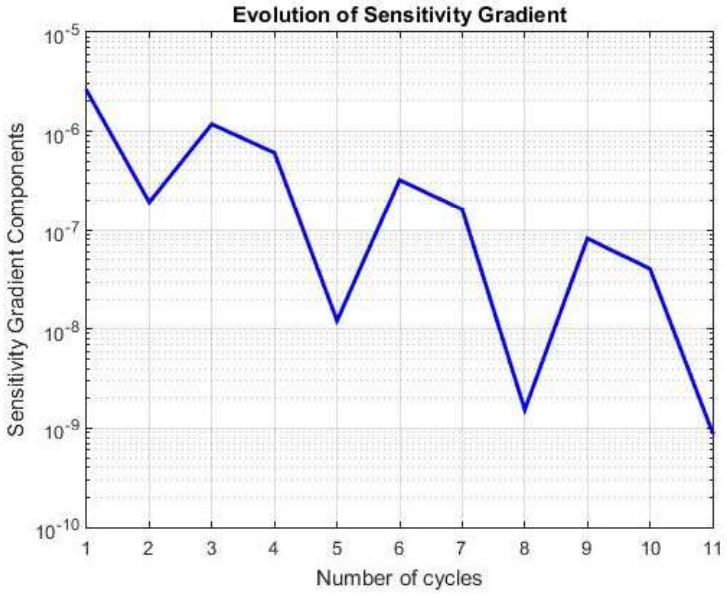


**Figure 7.7:** Sensitivity Gradient of the Test 4

allows more precision in the result of the design parameter. In the next test, we change the target to negative concavity parabola: $\eta = -0.5t^2 + 0.8t$. The fig. 7.8 presents the evolution of the solution:

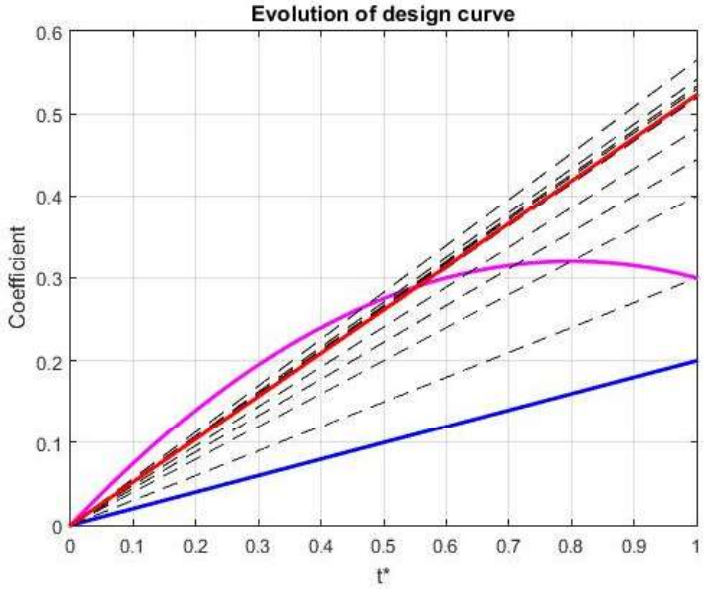


**Figure 7.8:** Optimization Results of the Test 5: Magenta: Target Curve; Blue: First Cycle; Dashed Black: Intermediate cycles; Red: Last Cycle

The $OLA$ spent 16 cycles to stop, due the maximum variation criteria. The value of the design parameter started in $b = 0.2$ and achieved $b = 0.522848$ which represents a objective function value: $R = 1.54947.10^{-7}$. The sensitivity gradient achieved an absolute value $8.27.10^{-9}$ and its evolution is presented in the fig. 7.9.

The next two tests change the parametrization of the flow curve, introducing a second design parameter, so that curve becomes a parabola: $\eta = at^2 + bt$. The

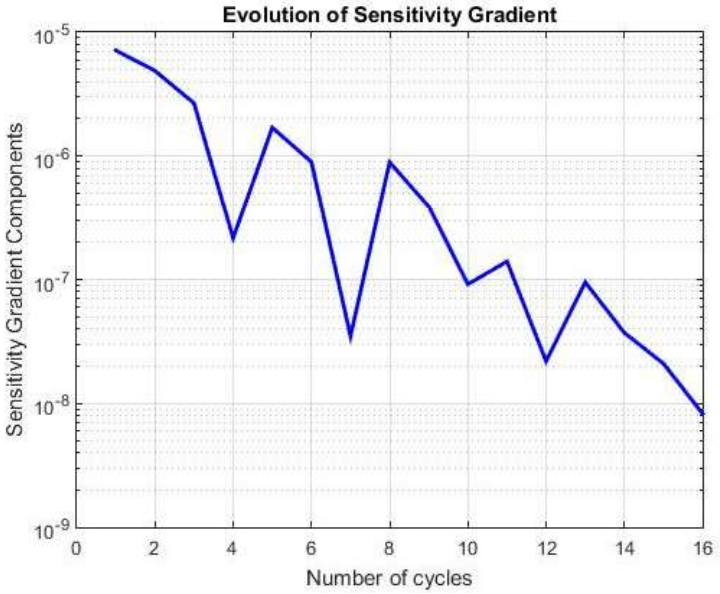


**Figure 7.9:** Sensitivity Gradient of the Test 5

test 6 using as target the density of adsorption distribution generated by the parabola $\eta = -0.5t^2 + 0.8t$ and the expected result is $a = -0.5$ e $b = 0.8$. As initial values, the design parameters were $a = -0.3$ and $b = 0.5$. The fig. 7.10 present the results:

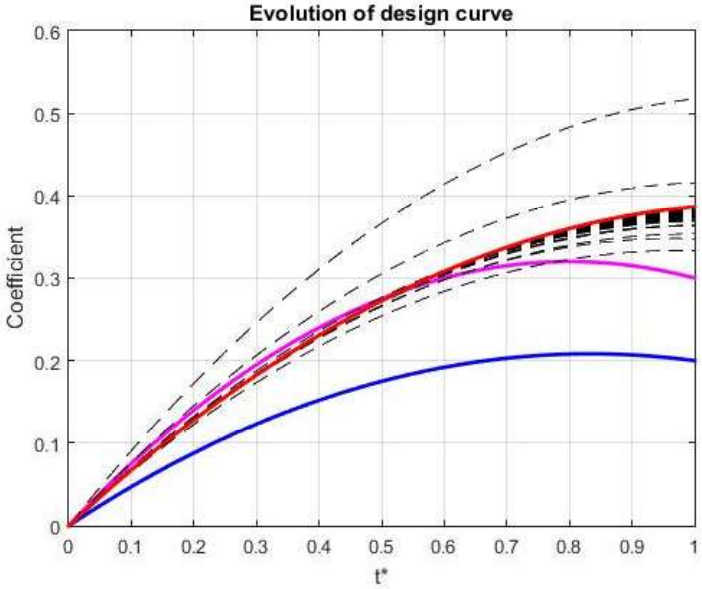


**Figure 7.10:** Optimization Results of the Test 6: Magenta: Target Curve; Blue: First Cycle; Dashed Black: Intermediate cycles; Red: Last Cycle

The results did not present the expected behavior, and do not the target values of the design parameters. The $OLA$ stops due the maximum variation criteria and found $a = -0.316832$ and $b = 0.70355$ with the objective function in $R = 2.26149.10^{-8}$. By observing the behavior in the intermediate cycles, when a design parameter changes, the whole curve is modified and the consequence is an

interference in the other design parameter. The $OLA$ can not read the changes separately and it is a limitation of this kind of parametrization.

To prove this argument, we did the test 7, using an initial solution $a = 0.2$ and $b = 0.4$, keeping the same target distribution of the text 6. The fig. 7.11 present the results:

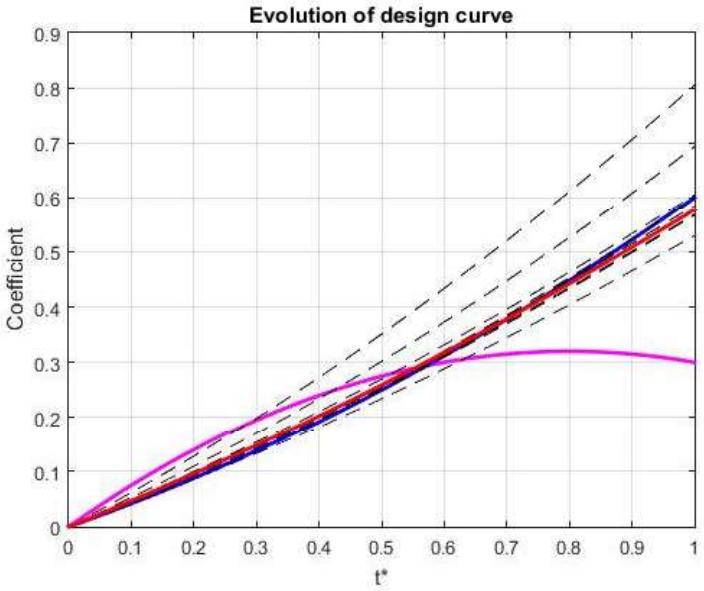


**Figure 7.11:** Optimization Results of the Test 7: Magenta: Target Curve; Blue: First Cycle; Dashed Black: Intermediate cycles; Red: Last Cycle

As can be seen in the test 6, the $OLA$ can not recover the curve that generates the target distribution. In addition, the algorithm did not change the signal of the design parameter $a$ which represents the parabola concavity. After 10 cycles, the values found were $a = 0.119043$ and $b = 0.457844$ and the objective function achieved $R = 2.37555.10^{-7}$. Then, a simple polynomial parametrization has limitations during the optimizations cycles.

To solve this problem, we propose a new parametrization, based on the research group experience, the Bernstein polynomials (KULFAN; BUSSOLETTI, 2006). Originally developed to describe geometrical shapes, the definition of these polynomials are presented in eq.(7.8):

$$S_n = \sum_{k=0}^{n} b_k C_{n,k} x^k (1-x)^{(n-k)} \tag{7.8}$$

Where $b_k$ represent the actual control parameters, which are evaluated by means of the Adjoint method. The variable $x$ is limited to values between 0 and 1. This is easily programmed in the $OLA$ defining $x = t/totaltime$. The

coefficients $C_{n,k}$ are Newton binomial coefficients, defined as:

$$C_{n,k} = \frac{n!}{k!(n-k)!} \tag{7.9}$$

As an example, if we defined a second degree Bernstein polynomials by $\eta(t)$, they get the eq. (7.10):

$$\eta(t) = b_0 C_{2,0} x^0 (1-x)^{(2-0)} + b_1 C_{2,1} x^1 (1-x)^{(2-1)} + b_2 C_{2,2} x^2 (1-x)^{(2-2)} \tag{7.10}$$

By evaluating the binomials and simplifying the exponents, we get the eq. (7.11):

$$S_2 = \underbrace{b_0(1-x)^2}_{I} + \underbrace{b_1[2x(1-x)]}_{II} + \underbrace{b_2 x^2}_{III} \tag{7.11}$$

To show the advantage of the Bernstein polynomials parametrizations, fig. 7.12 presents curves generated by three terms of the second-degree polynomials, considering the control parameters $b_k = 1$ (KULFAN; BUSSOLETTI, 2006):

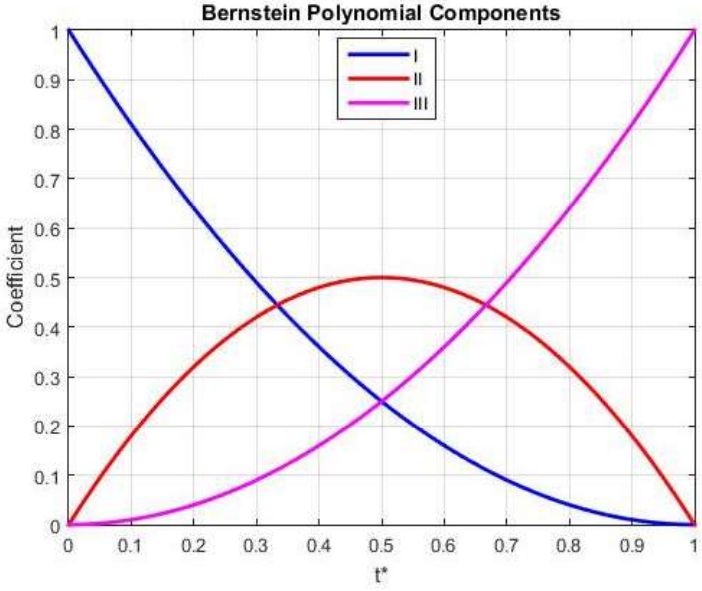


**Figure 7.12:** Individual components of the second-degree Bernstein polynomials

The figure shows the interval between 0 and 1 where the polynomials have influence. The polynomial $I$ is the only responsible for the curve when $x = 0$. The polynomial $II$ has the maximum influence when $x = 0.5$ and the third, is the

responsible for the value when $x = 1$. Then, the interval is divided in influence zones of the polynomials and each of them can change one part of the whole curve.

Another example, the eq.(7.13) presents the five-degree Bernstein polynomials:

$$S_5 = \underbrace{b_0(1-x)^5}_{I} + \underbrace{b_1[5x(1-x)^4]}_{II} + \underbrace{b_2[10x^2(1-x)^3]}_{III} + \underbrace{b_3[10x^3(1-x)^2]}_{IV} + \underbrace{b_4[5x^4(1-x)^1]}_{V} + \underbrace{b_5x^5}_{VI} \tag{7.12}$$

As the degree of the Bernstein polynomials increase, the zones of influence grows also. Fig. 7.13 presents the curves generated by six terms of the fifth-degree polynomials, considering the control parameters $b_k = 1$ (KULFAN; BUSSOLETTI, 2006):

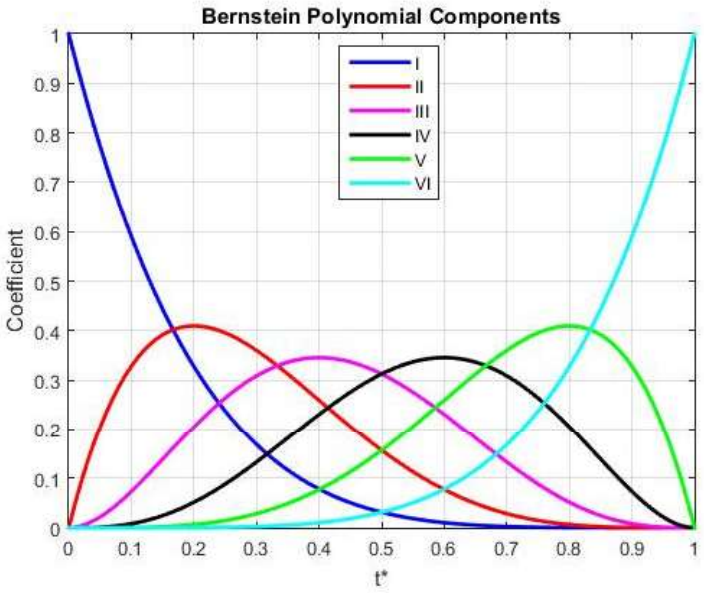


**Figure 7.13:** Individual components of the fifth-degree Bernstein polynomials

For the fifth degree polynomials, the first term ($I$) has the maximum (and unique) influence when $x = 0$. The intermediates ($II$ to $V$) have maximum influence when $x = 0.2$,$x = 0.4$,$x = 0.6$ and $x = 0.8$ respectively. The last polynomial ($VI$) has the maximum influence at $x = 1$ and determine the value at this point.

After the introduction of this parametrization, we present the next tests. Test 8 keeps the same target distribution, generated by the parabola $\eta = -0.5t^2 + 0.8t$ and uses the Bernstein polynomials presented in the eq. 7.11. The value of $b_0$ is

kept in zero to have $\eta(0) = 0$. Then, we have only two free parameters, $b_1$ and $b_2$, with initial value set in $b_1 = 0.1$ and $b_2 = 0.5$. The fig.(7.14) presents the results:

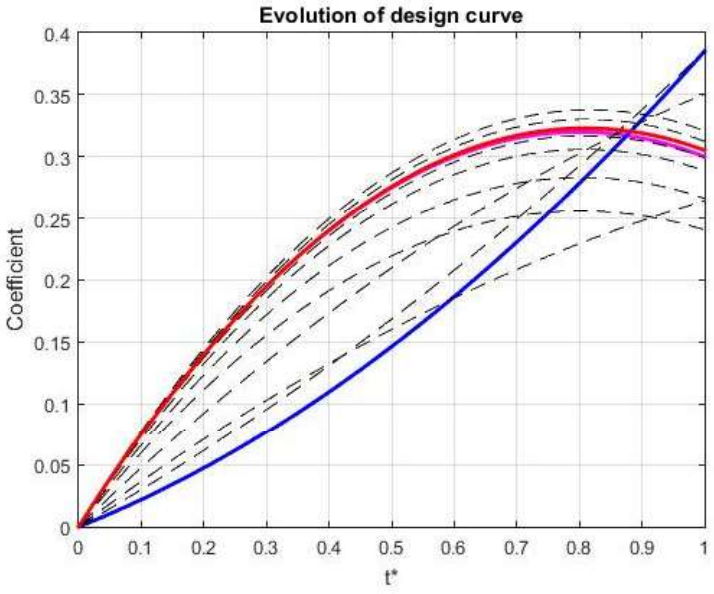


**Figure 7.14:** Optimization Results of the Test 8: Magenta: Target Curve; Blue: First Cycle; Dashed Black: Intermediate cycles; Red: Last Cycle

After 11 cycles, the $OLA$ stops due the value of the objective function ($R = 2.95228.10^{-10}$). The values found for $b_1$ and $b_2$ were 0.398971 and 0.305161 respectively, recovering the parabola that generates the target function. The new parametrization shows more flexibility when the parameters were changed and allows a suitable precision in the results. The fig. 7.15 presents the evolution of the sensitivity gradient along the cycles:

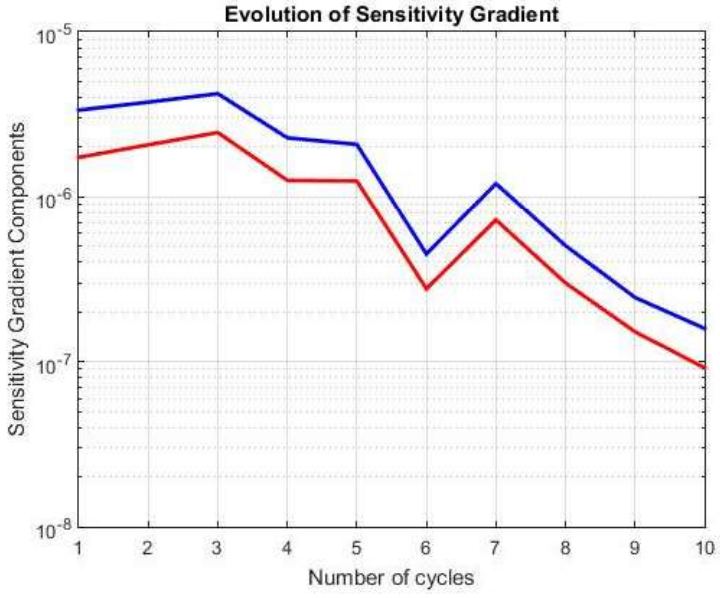


**Figure 7.15:** Sensitivity Gradient of the Test 8; Blue: Gradient component of $b_1$;Red:Gradient component of $b_2$

The sensitivity gradient oscillated but reduces until $10^{-7}$ for the two parameters. The expectation is the gradient decreasing and it happens. Test 9 changed the target distribution, using another parabola: $\eta = -4t^2 + 4t$ and increasing the total filling time to $120s$. The $OLA$ started with $b_1 = 1.2$ and $b_2 = 1.0$ and the results of the optimization are presented in the fig.(7.16):

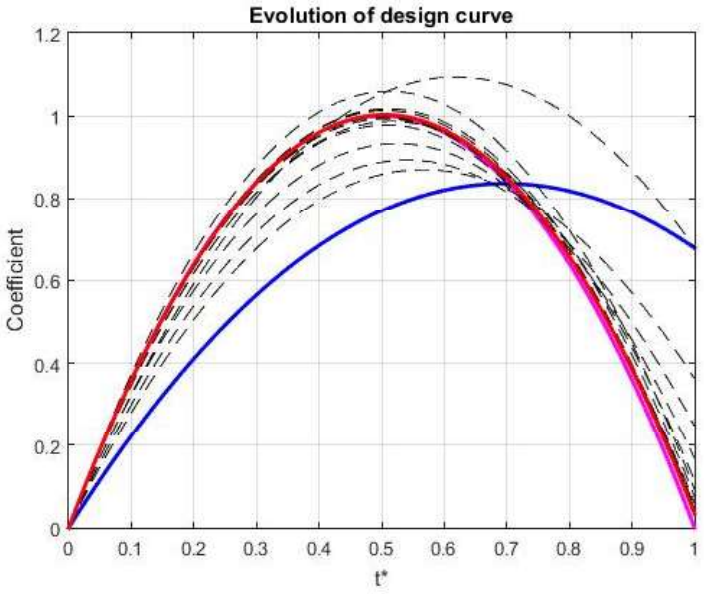


**Figure 7.16:** Optimization Results of the Test 9: Magenta: Target Curve; Blue: First Cycle; Dashed Black: Intermediate cycles; Red: Last Cycle

The $OLA$ stopped due the maximum variation criteria and spent 15 cycles to find $b_1 = 1.98894$ and $b_2 = 0.0335734$. The expected result was $b_1 = 2.0$ and $b_2 = 0$ in agreement of the target curve. If the maximum criteria had not have been executed, the $OLA$ could have recovered the value with more precision. The gradient magnitude getting close to $10^{-7}$ for both design parameters.

Test 10 had the objective to check the behavior of an approximation of the target curve generated by a parabola using a fifth-degree Bernstein polynomial. The parametrization curve changed to eq.(7.13, keeping $b_0$ fixed in zero. The fig. 7.17 presents the results:

The $OLA$ starts with $b_1 = 0.4$, $b_2 = 1.4$, $b_3 = 0.9$, $b_4 = 1.4$ and $b_5 = 0.7$. After 35 cycles, the $OLA$ stops due maximum variation criteria, with the values changed to $b_1 = 0.762011$, $b_2 = 1.28003$, $b_3 = 1.12153$, $b_4 = 0.781715$ and $b_5 = 0.0475444$ and the objective function coming to $R = 2.82846.10^{-8}$. The recovering of the target curve were suitable, regardless of the difference in degree between the target and the current parametrization. The sensitivity gradient component achieved values between $10^{-8}$ and $10^{-9}$.

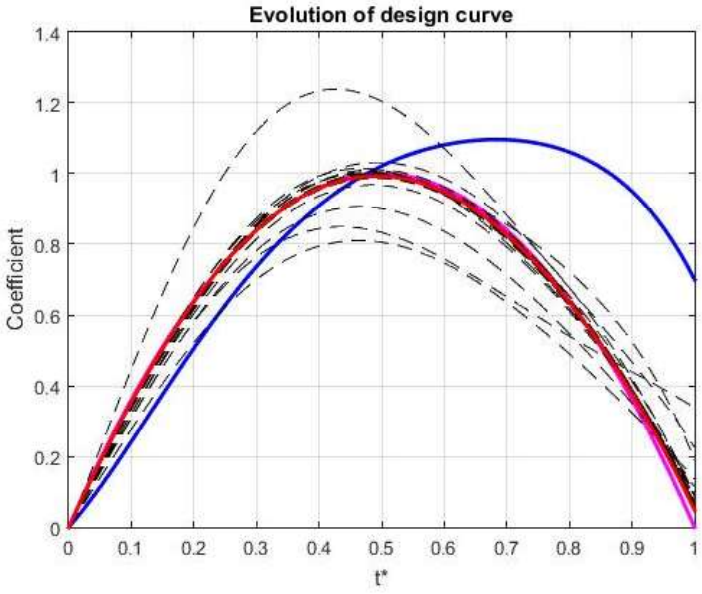


**Figure 7.17:** Optimization Results of the Test 10: Magenta: Target Curve; Blue: First Cycle; Dashed Black: Intermediate cycles; Red: Last Cycle

## 7.2 Engineering Application

The validation tests presented the OLA capacity to change the filling flow curves to achieve the extreme of a given objective function. Now, to conclude this thesis, we present an application that can be used in storage facilities. The chapter 2 showed the ample evidence in the literature, to the effect that maximum adsorption capacity is attained under isothermal conditions. Whence comes the need for heat transfer, to counteract the exothermic character the adsorption process exhibits. On the other hand, adsorption rates also depend on the thermodynamic state, *i.e.* $(P, T)$ distributions, as the DA model eqs. (3.47)–(3.50) indicate. It is under such conditions that the search for an optimum filling curve must take place.

An attempt is made to generate a target distribution for the adsorption density $q_t$, which corresponds to an isothermal process. A fixed value of temperature, $T = 300K$, is introduced into the foregoing eq. (3.47)–(3.50), while pressure is linearly increased from $20kPa$ to $200kPa$. The corresponding values of $q$, thus obtained, are then uniformly distributed over the time–span of the filling process, and the resulting distribution is assigned to $q_t$.

The optimization was performed with the same tank dimensions using in the validation tests, the initial pressure and temperature setted in $20kPa$ and $300K$ respectively and the time of filling in 30 seconds. The initial filling flow curve $\eta(t)$ was impose as a fifth degree Bernstein polynomial with following values:

$b_0 = 0.0$, $b_1 = 1.0$, $b_2 = 1.0$, $b_3 = 1.0$, $b_4 = 1.0$, $b_5 = 1.0$. The average mass flux was $G_m = 11.123\ kg/m^2s$ which corresponds a volumetric flow of the $30LPM$.

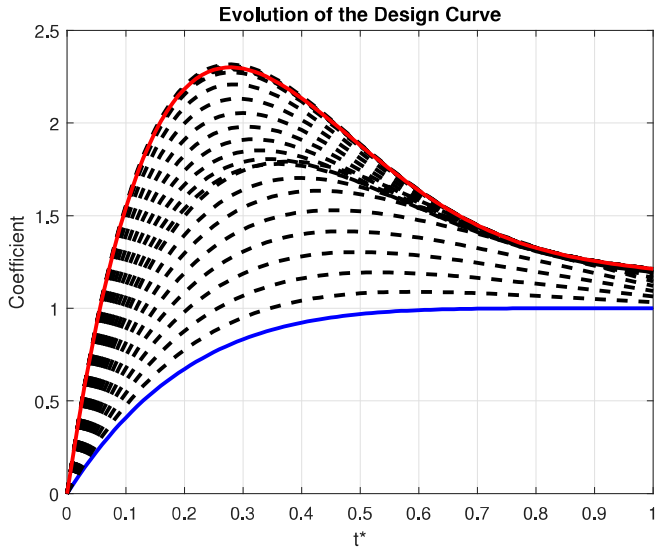


**Figure 7.18:** Evolution of the filling flow curve during the optimization

After 19 cycles, the OLA finds the curve presented in the fig. (7.18). The value of the objective function was $8.8.10^{-3}$ in the first cycle and reduced to $8.70.10^{-4}$ in the last one. The geometry of the function $\eta(t)$ is not intuitive, corroborating with the justification of the use of a systematic optimization method. The components of the sensitivity gradient is presented in the fig. 7.19.

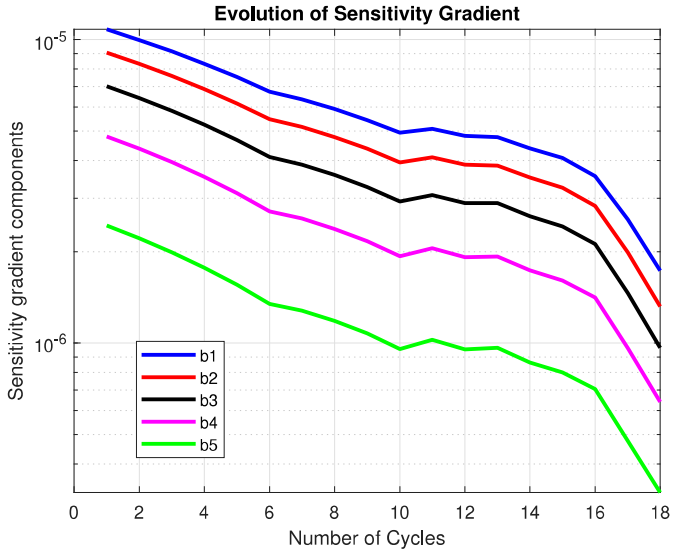


**Figure 7.19:** Evolution of the sensitivity gradient during the optimization

By using this result, a new optimization was implemented with the objective to checking whether by changing the isotherm temperature, for example to $310K$, affects the result. A new target density of adsorption was generated and the OLA was setted with the same parameters of the previous test. The fig. 7.20 presents

the evolution of the design curves.

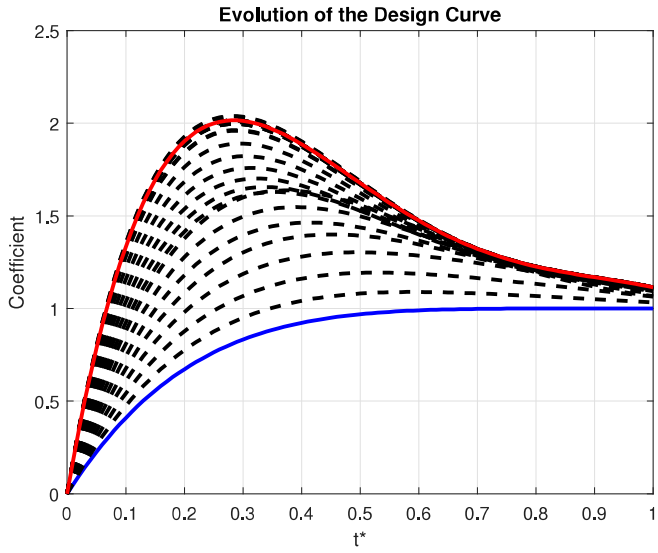


**Figure 7.20:** Evolution of the filling flow curve during the optimization

The Objective function comes from $4.34.10^{-3}$ to $2.00.10^{-4}$ in the $19th$ cycle. The values of the parameters in the last cycle were: $b_0 = 0.0$, $b_1 = 3.68351$, $b_2 = 1.58019$, $b_3 = 1.21113$, $b_4 = 1.24194$, $b_5 = 1.1146$. The result is similar to the first test and the fig.(7.21) presents both curves. It is important to note the similarity of the geometries that implies in the temperature dependence of the gas quantity can be stored. The shape of the filling curve does not change and the justification is the imposition of the same growing pressure.

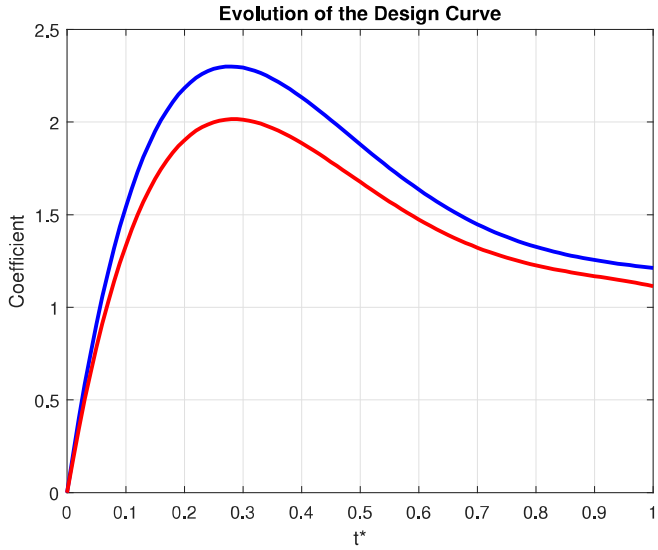


**Figure 7.21:** Parallelism of the results of the two tests. Blue: First Test (300K - 30s); Red:Second Test (310K - 30s)

The fig. (7.22) presents the evolution of the sensitivity gradient of the design parameters.

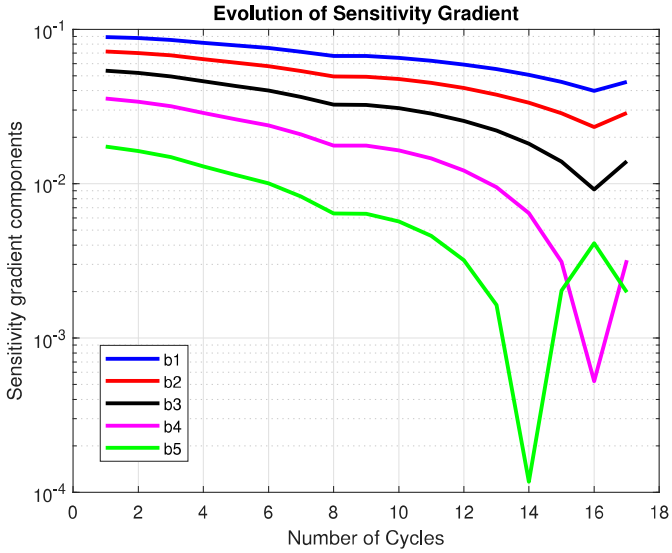


**Figure 7.22:** Evolution of the sensitivity gradient during the optimization

The similarity of the design curves prompts a new test, that is, to verify whether by changing the filling time to 60 seconds, while keeping the final pressure at $200kPa$, the design curve will still have the same optimized shape. A new target distribution was generated and the fig.(7.23) presents the evolution of the design curves.

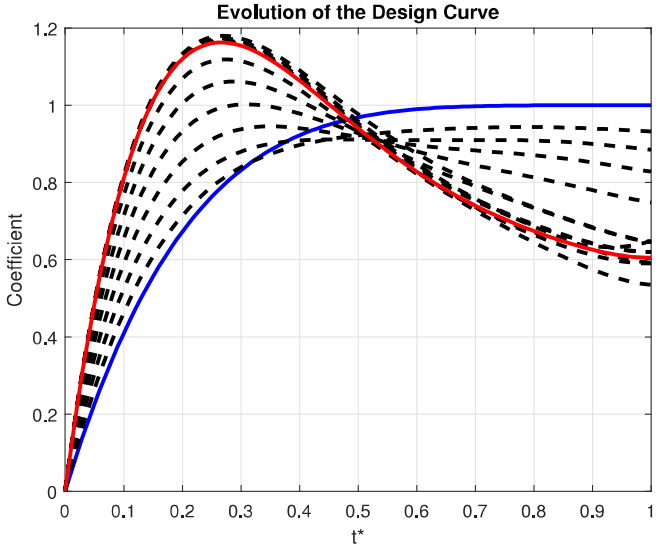


**Figure 7.23:** Evolution of the filling flow curve during the optimization

After only 14 cycles, the objective function reduces from $2.86.10^{-3}$ to $8.40.10^{-4}$. The initial solution was already close to the optimal result, which justifies de low reduction of the measure of merit. The coefficients of the last cycle were $b_0 = 0.0$, $b_1 = 2.32025$, $b_2 = 0.585112$, $b_3 = 0.90412$, $b_4 = 0.599167$, $b_5 = 0.60558$.

In the last optimization, we keep the filling time in 60 seconds and change the pressure evolution, starting in $20kPa$ and growing up to $380kPa$ which represents

the same slope as the first optimization. The fig.(7.24) presents the optimization of the filling flow curve.

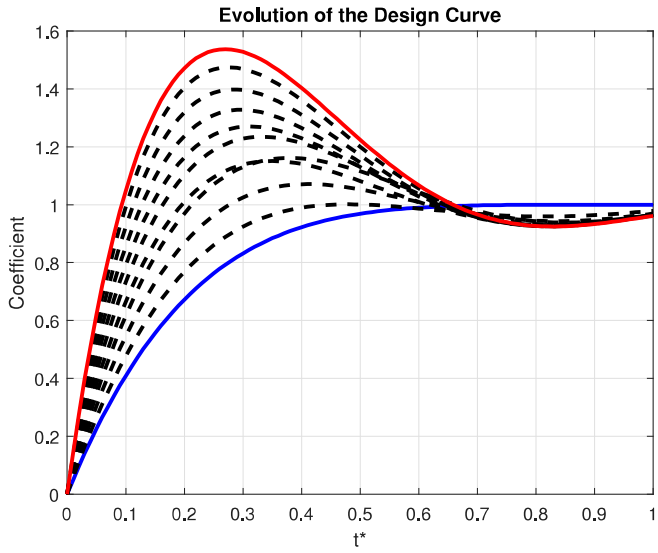


**Figure 7.24:** Evolution of the filling flow curve during the optimization

The objective function starts from $4.85.10^{-3}$ and reduces to $8.97.10^{-3}$ after 11 cycles. The values of optimized parameters were: $b_0 = 0.0$, $b_1 = 2.93497$, $b_2 = 1.08278$, $b_3 = 0.820881$, $b_4 = 0.901602$, $b_5 = 0.961276$. The components of the sensitivity gradient are presented in the fig.(7.25).

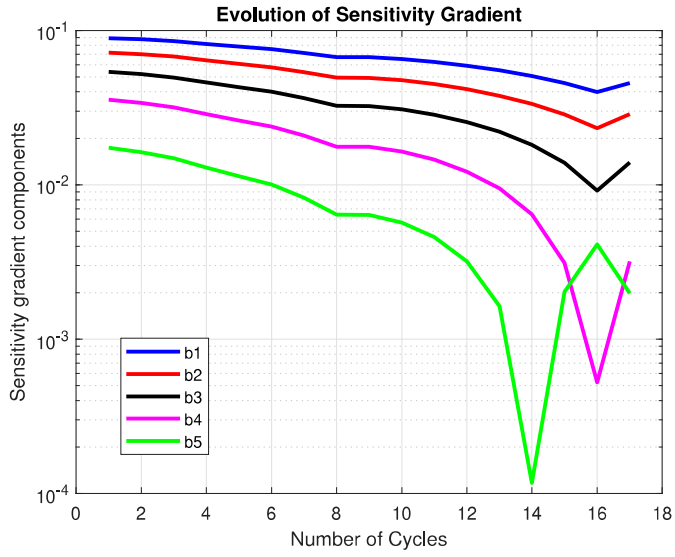


**Figure 7.25:** Evolution of the sensitivity gradient during the optimization

As the final result, the fig.(7.26) presents the optimized curves of the four tests.

The compassion of the fig.(7.26) presented an important conclusion of the optimization of the filling flow curve. This application can control the behavior of the pressure but it is not suitable for the temperature management. The two

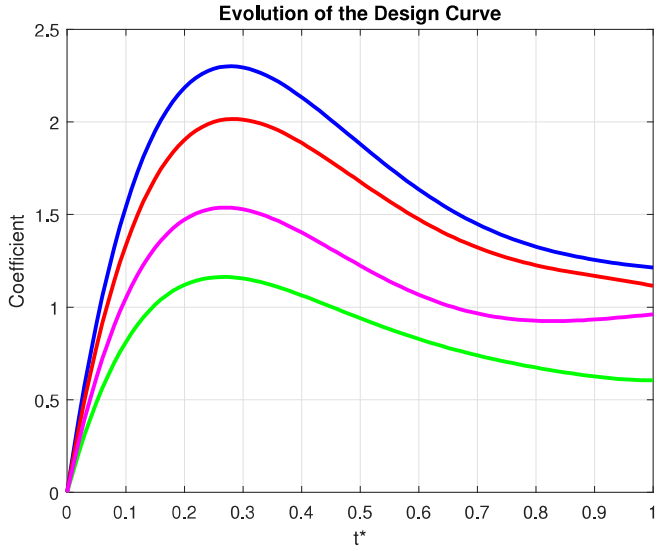


**Figure 7.26:** Parallelism of the results of the two tests. Blue: First Test (300K - 30s - 20kPa to 200kPa); Red:Second Test (310K - 30s - 20kPa to 200kPa); Green: Third Test (300K - 60s - 20kPa to 200kPa); Magenta: Fourth Test (300K - 60s - 20kPa to 380kPa)

properties changed the quantity of gas adsorbed and it is appropriate to control both.

For the continuity of the research, the temperature management will be developed, not only using no geometric sensitivities, but also with a geometric optimization of the tank, including heat fins and heat exchangers, presented briefly in the chapter 4.

# 8 Conclusions

The research has achieved the goal which was the development of a optimization loop algorithm (OLA) based on the Adjoint Method. The parts of the OLA were discussed separately as follows.

## 8.1 Problem Description

In our literature survey, we have found many studies about ANG systems. From them, we can surmise they have tackled simple cases and limited their simulations to one or two parameters variations. Now, the developed OLA is able to analyze a large number of parameters without addition of computational cost and keeping the high fidelity to the physics. That opens up the possibility of innovation for high performance ANG systems.

One of the possibilites consists in storing the boil-off gas, which may be lost in LNG systems. The estimation of losses is about 0.1% per day for a LNG carrier trip. When we consider the high volume stored and the duration of the trips, the quantity of lost gas is relevant. The first studies show that ANG systems increase the performance as the inlet gas temperature decreases. So, we could use this advantage to maximize de gas density inside the ANG tank and this proposal was forwarded to future research projects.

Other important consideration is about the development of new materials for the adsorption process. In the survey, most researchers are studying new adsorbents, increasing the interaction between gas molecules and the solid. With the OLA, one may search for optimum configurations for these new adsorbents and this is an important advantage of the algorithm, it can follow the advances of adsorption technology.

Besides, as mentioned in the beginning of this thesis, the OLA is not specific for ANG systems and it can be applied in a study of adsorption to a Carbon Capture and Storage (CCS). There is an early stage project in the RCGI that aims

to evaluate the feasibility of implementing the carbon geological storage (CGS) technology in unconventional petroleum reservoirs in order to contribute to CO2 abatement in the southeast region of Brazil, which concentrates the major carbon emission sources within the country. The Project deals with the hypothesis that shales, rich in organic matter, can adsorb significant amounts of CO2 at the same time as gas and / or oil production would occur and that turbidites and oil reservoir rocks can also adsorb CO2 in capacity compatible with the quantity released in the pre-salt gas and oil production activities. The OLA can contribute in the modeling of the adsorption phenomena and find the relevant sensitivities to optimize.

## 8.2 Mathematical Model and Numerical Results

The mathematical model of the flow physics was thoroughly tested and the equations are consistent. The implementation in *FREEFEM* was a success. The preliminary tests were consistent with the literature (SAHOO; JOHN, 2011) and the exploratory simulations show which parameters affect most the storage capacity.

Morevover, the study of the tank size influence in the adsorption process shows the displacement of the optimal solutions, considering for example, the maximization of the methane mass inside the tank. In large scale, optimal solutions are more significant than for small tanks. Because the quantity of energy the involved is considerable and its management is required.

As development of the Adjoint Method in a $2D$ model is already big step in the innovation of the ANG optimization, we had decided to postpone the update of the solver source code to a $3D$ model during the research. We have chosen to end the whole axisymmetric loop because this algorithm has already a significant number of prospective engineering applications, considering a circular cylinder tank. The results found after this decision showed that the choice was correct.

## 8.3 Adjoint Method

We have derived the Adjoint Equations, their boundary conditions and some expressions for the sensitivity gradient to given objetive functions. The augmented functional was defined and it follows the Cacuci formulation (CACUCI et al., 1980).

As the decomposition of the bilinear concomitant is not unique, the challenge

to make a well-posed problem is one of the most important parts of the research and now we are exactly at this point. We propose and present the first approach in this report but this question is still open for future analysis.

Again, it is important to highlight the Adjoint Method main advantages: It allows an exceptional reduction in the computational costs and it makes for a more efficient analysis of design alternatives, without compromising the results accuracy. During the validation of the sensitivity gradient, a cycle of the Adjoint method with four design parameters, consisting of solution to the primal and dual problems, spent an average of 33.0% processing time of the finite difference method that needs 8 primal problem solution to find the same four design parameters sensitivities (????).

## 8.4 Optimization Algorithm - OLA

The OLA code base has been developed and the FREEFEM ++ software allows for easy editing and enhancement. We present an important engineering application where the filling flow curve was controlled based on the desired density of adsorption distribution. However, the temperature is not controlled by this curve, being required a heat transfer parameters, as Nusselt Number, inflow and external temperatures. The geometric sensitivities gradient is a next step of the research, where we can combine this parameters to optimize active heat control management devices, such as heat fins and internal heat exchangers, as seen in the chapter 4 and published by the research group (??).

## 8.5 Suggestions for continuity of the Research

For the continuity of the research, there is some projects with different graduation levels that can be developed and they are present as follows:

- Analysis with different adsorbed materials: For undergraduted students, the primal problem code can be used to verify the influence of the materials properties in the adsorption process, introducing the basic concepts of the CFD for the young researcher.
- Sensitivities of the adsorption properties: For a mastering level, the primal and dual code can be used to find sensitivities of the adsorbed bed properties and guide the studies of new adsorbed materials, verifying the most important properties that have influence in the adsorption performance. The

researcher should develop new gradient expressions and implement them in the *FREEFEM++* code.

- Implementation of geometric sensitivities: For a PHD level, the researcher should expand the basic expressions presented in the chapter 5 and derive the gradient expressions for the basic tank dimensions and some internal devices, such as heat fins or tubes that make a heat exchanger. This work needs the same procedure made in this report: a series of validation tests and then an engineering application to to show where code can be employed.

# References


BASUMATARY, R.; DUTTA, e. a. Themal modeling of activated carbon based adsorptive natural gas storage system. *Carbon 43*, 2005.

CACUCI, D. G.; WEBER; F., C.; M., O. E.; MARABLE, J. H. Sensitivity theory for general systems of non–linear equations. *Nuclear Science and Engineering*, v. 75, p. 88–110, 1980.

CIA. *CIA The World Factbook - https://www.cia.gov/library/publications/the-world-factbook/rankorder/2253rank.html*. [S.l.]: US Goverment, 2016.

FREEFEM. *Users Manual*. [S.l.: s.n.], 2011.

GILES, M.; PIERCE, N. Adjoint equations in cfd: Duality, boundary conditions and solution behavior. AIAA Paper 97–1850. 1997.

GILES, M.; PIERCE, N. On the properties of solutions of the adjoint Euler equations. In: *Numerical Methods for Fluid Dynamics VI. ICFD*. [S.l.: s.n.], 1998.

GILES, M.; PIERCE, N. An introduction to the adjoint approach to design. *Flow, Turbulence and Control*, v. 65, p. 393–415, 2000.

GILES, M.; PIERCE, N. Analytic adjoint solutions for the quasi–1d Euler equations. *Journal of Fluid Mechanics*, v. 426, p. 327–345, 2001.

GUNZBURGER, M. *Finite Element Methods for Viscous Incompressible Flows*. London: Academic Press, INC., 1989.

HAYASHI, M. *Cálculo de sensibilidades nao-geométricas em escoamentos modelados pelas equacões de Euler compressíveis utilizando o Método Adjunto*. Tese (Doutorado) — Escola Politécnica da USP, 2016.

HAYASHI, M.; CEZE, M.; VOLPE, E. Characteristics-based boundary conditions for the Euler adjoint problem. *Int. J. Numer. Meth. Fluids*, v. 71, p. 1297–1321, 2013.

HAYASHI, M.; LIMA, J.; CHIEREGATTI, B.; VOLPE, E. Non–geometric sensitivities using the adjoint method. In: *ICAAA2016*. [S.l.: s.n.], 2016. v. 10, p. 155–163.

HECHT, F. New development in freefem++. *Journal of Numerical Matematics, no 3-4, 251-265*, 2012.

HIMENO, S.; KOMATSU, T. e. a. High pressure adorption equilibra of methane and carbon dioxide on several activated carbons. *J. Chem*, 2005.


HIMENO, S.; KOMATSU, T. e. a. High pressure adorption equilibra of methane and carbon dioxide on several activated carbons. *J. Chem*, 2005.

HIRATA, S.; COUTO, P. e. a. Modeling and hybrid simulation of slow discharge process of adsorbed methane tanks. *International Journal of Thermal Sciences*, 2009.

JAMESON, A.; MARTINELLI, L. An adjoint method for design optimization of ship hulls. In: *9th International Conference on Numerical Ship Hydrodynamics*. [S.l.: s.n.], 2007.

JAMESON, A.; PIERCE, N.; MARTINELLI, L. Optimum aerodynamic design using the Navier-Stokes equations. In: *35th Aerospace Sciences Meeting & Exhibit*. [S.l.: s.n.], 1997.

JAMESON, A.; PIERCE, N.; MARTINELLI, L. Optimum aerodynamic design using the Navier-Stokes equations. *Theoretical and Computational Fluid Dynamics*, v. 1, p. 213–237, 1998.

JAMESON, A.; SRIRAM, A.; MARTINELLI, L. A continuous adjoint method for unstructured grids. In: *AIAA Computational Fluid Dynamics Conference*. [S.l.]: AIAA 2003–3955, 2003.

J.C., S.; MARCONDES, F. e. a. Performance analysis of a new tank configuration applied to the natural gas storage systems by adsorption. *Applied Thermal Engineering 29*, 2009.

JUDD, R. W.; GLADDDING, R. e. a. The use of adsorbed natural gas technology for large scale storage. *BG Technology, Gas research and Technology Centre.*, 1998.

KAVIANY, M. *Principles of Heat Transfer in Porous Media*. USA: Springer, 1995.

KIM, S.; ALONSO, J.; JAMENSON, A. A gradient accuracy study for the adjoint–based Navier–Stokes design method. In: *AIAA Computational Fluid Dynamics Conference*. [S.l.: s.n.], 1999.

KULFAN, B.; BUSSOLETTI, J. Fundamental parametric geometry representations for aircraft component shapes. *11th Multidisciplinary Analysis and Optimization Conference*, 2006.

LIMA, J. *Cálculo de sensibilidades geométricas e não-geométricas para escoamentos viscosos incompressíveis utilizando o Método Adjunto*. Tese (Doutorado) — Escola Politécnica da USP, 2017.

LIMA, J.; ISLER, J.; VOLPE, E.; MAO, X.; CARMO, B.; CESTARI, I. Computation of sensitivity derivatives for pediatric ventricular assist device using the adjoint method. In: *VI International Conference on Computational Bioengineering – ICCB 2015*. [S.l.: s.n.], 2015.

LUSTERNICK, L.; SOBOLEV, V. *Elements of Functional Analysis*. Delhi: Hindustan Pub. Co., 1961.

MATRANGA, K. R.; MYERS, A. e. a. Storage of natural gas by adsorption on activated carbon. *Chemical Engineering Science*, v. 47, 1992.

MENON, V. C.; KOMARNENI, S. Porous adsorbents for vehicular natural gas storage: A review. *Journal of Porous Materials*, 1998.

MONTEIRO, J. F.; SILVA, J. da. *Gás Natural Aplicado à Industria e ao Grande Comércio*. São Paulo, SP, Brasil: Blucher, 2010.

MORSE, P.; FESHBACH, H. *Methods of Theoretical Physics*. [S.l.]: MacGraw–Hill, 1953.

MOTA, J. Impact of gas composition on natural gas storage by adsorption. *AIChE Journal*, 1999.

MOTA, J.; SAATDJIAN, E. e. a. A simulation model of high capacity methane adsorptive storage system. *Adsorption 1*, 1995.

NADARAJAH, S. K.; JAMESON, A. A comparison of the continuous and discrete adjoint approach to automatic aerodynamic optimization. In: *AIAA 38th Aerospace Sciences Meeting and Exhibit*. [S.l.]: AIAA 2000–0667, 2000.

NIELD, D.; BEJAN, A. *Convection in Porous Media*. USA: Springer, 2006.

NOUH, S.; LAU, K. e. a. Modeling and simulation of fixed bed adsorption column using integrated cfd approach. *Journal of Applied Sciences*, 2010.

PUPIER, O.; GOETZ, V.; FISCAL, R. Effect of cycling operations on an adsorbed natural gas storage. *Chemical Engineering and Processing*, 2005.

RAHMAN, K. *Experimental and Theoretical Studies on Adsorbed Natural Gas Storage System using Activated Carbons*. Tese (Doutorado) — National University of Singapore, 2011.

ROQUEROL F., S. K.; J., R. *Adsorption by powders and Porous Solids*. France: Academic Press, 1994.

SAHOO, P.; JOHN, M. e. a. Simulation of methane adsorption in ang storage system. *Comsol Conference, India*, v. 1, 2010.

SAHOO, P.; JOHN, M. e. a. Filling characteristics for an activated carbon based adsorbed natural gas storage system. *I & EC research*, 2011.

SOLAR C., B. A. e. a. Adsorption of methane in porous materials as the basis for the storage of natural gas. *In-Tech*, Laboratorio de Sólidos Porosos - Instituto de Física Aplicada - CONICET - Universidad de San Luis - Argentina, 2010.

SUZUKI, M. *Adsorption Engineering*. New York: El Sevier, 1990.

TBG. *TBG Company - www.tbg.com.br*. [S.l.]: TBG, 2016.

VOLPE, E. Continuous formulation of the adjoint problem for unsteady incompressible Navier–Stokes flows. 2013.

WHITAKER, S. Diffusion and dispersion in porous media. *AIChE Journal*, v. 13, p. 420–427, 1967.

WHITAKER, S. The species mass jump condition at a singular surface. *Chemical Engineering Science*, v. 47, p. 1677–1685, 1992.

WHITAKER, S. *The Method of Volume Averaging*. London, UK: "Kluwer Academic Publishers, 1996.

WHITAKER, S. *Fluid Transport in Porous Media*. Southampton, UK: Computational Mechanics Publications, 1997.

WIKIPEDIA. *Wikipedia, the free encyclopedia - www.wikipedia.com*. [S.l.]: Free, 2016.

XIAO, J.; PENG, R. e. a. Cfd model for charge and discharge cycle of adsorptive hydrogen storage on activated carbon. *International Journal of Hydrogen Energy*, 2013.

XIAO, J.; TONG, L. e. a. Cfd simulation for charge and discharge cycle of cryo-adsorptive hydrogen storage on activated carbon. *International Journal of Hydrogen Energy*, 2012.

YANG, X.; ZHENG, Q. e. a. Experimental studies of the performance of adsorbed natural gas storage system during discharge. *Applied Thermal Engineering*, 2005.